UNIVERSITÀ DEGLI STUDI DI BARI ALDO MORO

DIPARTIMENTO INTERATENEO DI FISICA "M. MERLIN"

Dottorato di ricerca in FISICA – Ciclo XXXII

Settore Scientifico Disciplinare: FIS/03

# Femtosecond laser-based procedures for the rapid prototyping of polymeric Lab-On-a-Chip devices

**Dottorando:**

Udith Krishnan Vadakkum Vadukkal

**Supervisori:**

Dott. Antonio Ancona

Dott. Ing. Francesco Ferrara

**Coordinatore:**

Ch.mo Prof. Giuseppe Iaselli

ESAME FINALE 2020

**“To the relentless warriors fighting an incessant battle,**
**To those who dream of ushering in a better world,**
**To my dearest Comrades.”**

# Contents

# List of abbreviations

| | |
|---|---|
| µCP | Micro Contact Print |
| µEDM | Micro Discharge Machining |
| µTM | Micro Transfer Molding |
| ATC | Automatic Tool Changer |
| CAD | Computer Aided Design |
| CAM | Computer Aided Modelling |
| CI | Confidence Interval |
| CMD | Compartmentalized Microfluidic Device |
| CNC | Computer Numerical Control |
| CNS | Central Nervous System |
| COC | Cyclic Olefin Copolymer |
| CPA | Chirped Pulse Amplification |
| CTC | Circulating Tumour Cell |
| DEP | Dielectrophoresis |
| DES | Drug Eluting Stents |
| DLD | Deterministic Lateral Displacement |
| DoE | Design of Experiment |
| EpCAM | Epithelial Cell Adhesion Molecule |
| FACS | Fluorescence Activated Cell Sorting |
| FEA | Finite Element Analysis |
| GEDI | Geometrically Enhanced Differential Immunocapture |
| HTMSU | High Throughput Micro Sampling Unit |
| IPA | Isopropyl alcohol |
| LOC | Lab-On-a-Chip |
| MACS | Magnetic Activated Cell Sorting |
| MIMIC | Micro Molding in Capillaries |
| OOC | Organs-On-Chip |
| P2P | Plate-to-Plate |
| PC | Polycarbonate |

PCL Polycaprolactone

PDMS Polydimethylsiloxane

PE Polyethylene

PEEK Polyether ether ketone

PEI Poly (etherimide)

PET Polyethylene terephthalate

PFF Pinched Flow Fractionation

PI Prediction Interval

PLGA Poly (lactic-co-glycolic acid)

PLO Poly-l-ornithine

PMMA Poly (methyl methacrylate)

PP Polypropylene

PS Polystyrene

PTFE Polytetrafluoroethylene

PU Polyurethane

PVA Poly (vinyl alcohol)

PVC Polyvinyl chloride

PVDF Polyvinylidene fluoride

R2P Roll-to-Plate

R2R Roll-to-Roll

RBC Red Blood Cell

REM Replica Mold

RIE Reactive Ion Etching

SAM Self Assembled Monolayers

SAMIM Solvent Assisted Micro Molding

SEM Scanning electron microscope

TTM Two Temperature Model

# Abstract

Lab-on-a-chip (LOC) is a microfluidic device integrating multiple functions in a chip of a few square centimeters. Transparent polymers are becoming the materials of choice for the fabrication of inexpensive and disposable devices. Among the polymers PMMA was selected for this thesis work because of its optical, mechanical and chemical characteristics, such as transparency, rigidity, good thermal stability, chemical inertness and high hydrophobicity.

Different micro-manufacturing technologies are being used nowadays. Ultrafast laser technology, thanks to its intrinsic flexibility and the ability of femtosecond pulses to produce "cold" ablation of the irradiated volume with negligible collateral damage to the surroundings, is particularly suitable for rapid prototyping and high precision micromachining of LOC devices with complex microfluidic channel networks. However, parametrization of femtosecond laser processes is often based on a trial and error approach, which requires a lot of expensive experimental efforts.

In order to avoid a time-consuming trial and error approach for the laser microfabrication, an accurate statistical Design of Experiment (DoE) procedure was defined to estimate the influence of the laser repetition rate, pulse energy, scanning speed, and hatch distance on the femtosecond laser micro milled depth of the microstructures. The Factorial design indicated that the pulse energy and its interaction with the other variables are the main factors affecting the depth. Once it was found the model describing the relationship between the response variable depth and the main laser parameters, as the outcome of the research, two different prototypes of polymeric LOCs were fabricated.

The Circulating tumour cell (CTC) capturing device was realized by a smart microfabrication procedure by combining femtosecond laser technology and mechanical micro milling. The serpentine microchannel with micrometric precision was fabricated by femtosecond laser milling with negligible collateral damage of the surrounding material. While the inlet/outlet holes, which do not require high level of precision, were fabricated using mechanical micro milling. The device was assembled and sealed by using a facile and low-cost isopropanol assisted thermal bonding method. The bonding was established for two PMMA-PMMA slices at low temperature and pressure, which brought

strong adhesion and robust device without affecting the shape of the fabricated microchannels. The functionality of the device was tested to capture human Oral Squamous Carcinoma Cells from spiked suspension of OECM-1 cell culture medium.

The LOCs for neuronal cell culturing were fabricated by exploiting two microfabrication methods, in particular femtosecond laser ablation and hot embossing. A compartmentalized design was chosen for the device in order to understand the communication between peripheral neurons and non-neuronal tissues. Communication between neurons and different cell populations is of massive interest to understand how the nervous system controls tissues, both in homeostatic and pathological conditions. The ability of femtosecond laser ablated, and hot embossed LOCs were assessed by immunocytochemistry for primary hippocampal cell culture. The observations showed that the primary hippocampal neurons are able to grow inside the devices and formed connections with neighboring cells and remained functional after 14 days.

# Introduction

Lab-on-a-chips (LOCs), defined as devices in which multiple laboratory techniques are integrated in a chip of few square centimeters, have tremendous potential for application in various fields of chemistry and life sciences. In the last years, polymeric LOCs have generated a huge interest because of their competitiveness in terms of production costs, production times and easy way to go from an idea to a physical chip. Different techniques are available for the polymeric LOCs production and they can be classified in replication and direct structuration techniques. The formers require the fabrication of a mould, whose geometry depends on the target application, replication and assembling of the entire device. Among all, hot embossing, injection moulding and soft lithography are the most promising replication methods to fabricate polymeric microdevices at low costs and in high quantity. Despite the effort to improve their flexibility due to the presence of the mould, replica technologies are rather inflexible when it comes to rapid prototyping or optimizing the design of novel microfluidic tools. Technologies based on direct micro structuring of the substrate remain much more convenient during the design of a new device. In particular, the flexibility of ultrafast laser technology enables rapid prototyping and high precision micromachining of LOC devices with complex microfluidic channel networks, without the need of expensive masks and facilities, as required by the lithographic process. Furthermore, the ability of femtosecond (fs) laser pulses to produce "cold" ablation of the irradiated volume, thus avoiding debris and recast layers without restriction of the substrate materials, makes this technology particularly suitable for micro- and sub-microfluidic device fabrication, albeit with higher costs compared to other traditional techniques, such as mechanical micro milling which is more convenient for larger features.

In this thesis, two prototypes of polymeric lab-on-a-chip have been designed, fabricated and validated for different biological applications. The rapid prototyping of the LOCs was done by femtosecond laser-based procedures.

The thesis is organized in six chapters:

**Chapter 1** gives a short insight on LOCs concept. The microfluidic phenomena at the microscale and potential for new applications are discussed. Furthermore, LOC

technology for rare cell isolation and LOC for capturing circulating tumour cells and generally used materials in the fabrication of LOCs are outlined.

**Chapter 2** is dealing with the state of the art of the fabrication technologies for rapid prototyping of polymeric lab-on-a-chip devices. Various methods such as soft lithography, hot embossing, mechanical micro milling, femtosecond laser milling and finally various bonding technologies to assemble the micro devices are detailed.

**Chapter 3** is describing the materials, the fabrication setup and the instruments for post process analysis of the machined samples employed during this thesis work. Furthermore, the setups used for the final assembled LOCs validation are described.

**Chapter 4** is detailing an accurate Design of experiment (DoE) procedure to estimate the influence of the laser repetition rate, pulse energy, scanning speed, and hatch distance on the fs-laser micro milling process of polymer specimens in terms of depth of removed material ($D_h$).

In **Chapter 5** the developing and testing of a new smart procedure for the microfabrication of a polymeric LOC for capturing of CTC by exploiting fs-laser technology, mechanical micro milling and solvent assisted thermal bonding is described.

In **Chapter 6** the fabrication of polymeric LOCs by exploiting fs-laser milling and hot embossing for the culturing of primary hippocampal cells is presented.

# Chapter 1
# Lab-On-a-chip

## 1.1 Introduction

A Lab-On-a-Chip (LOC) is a device for controlling and manipulating fluid flows with length scales less than a millimeter. It integrates and automates multiple high-resolution laboratory techniques such as synthesis and analysis of chemicals or fluid testing into a system that fits on a chip.

The core of LOC devices is usually represented by a network of microchannels, as shown in the example in Figure 1.1, that are used to process the sample. These channels are sometimes thinner than a human hair, with a size of about 10 to 100 μm, and allow manipulating small volumes of liquids (generally between $10^{-9}$ and $10^{-18}$ liters).

Over the last 10-20 years, LOC devices have demonstrated their potential and benefits for many applications, including point-of-care diagnostics, genomic and proteomic research, analytical chemistry, environmental monitoring, and the detection of biohazards.

The most significant benefits of miniaturized LOC systems compared to bulkier analytical instruments are associated with the scaling down of the size [1]. Among them, the most important are reduced consumption of reagents and samples, faster reaction times, limited exposure to dangerous chemicals, possibility of parallel and multiplexed analysis, lower power supply, reduced manufacturing costs.

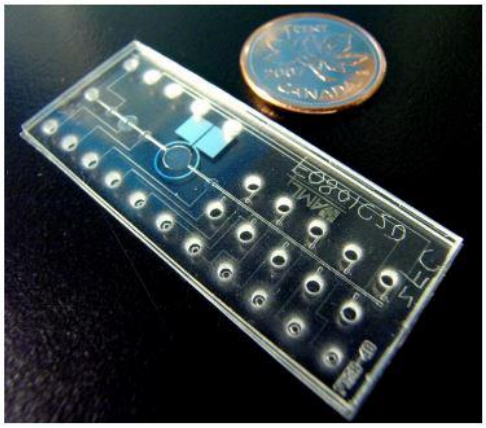

*Figure 1.1: Example of Lab-On-a-Chip device. Image from http://www.elveow.com/microfluidic-tutorials/microfluidic-reviews-and-tutorials/microfluidics/.*

The science that studies liquid properties in such small structures is known as microfluidics. Recently, microfluidics has received enormous attention because of the availability of technologies for fabricating individual and integrated flow configurations with length scales on the order of tens and hundreds of microns [2][3], and the development of new techniques for analysing very small quantities (typically less than 1 microliter) of biological samples and manipulating single cells. Such biotechnological advancements have led to an increasing demand for cheap portable devices able to perform simple analytical tasks. The growing attention of the scientific community towards LOC is remarked by the significant increase of the number of scientific publications in the field in the last 20 years (Figure 1.2).

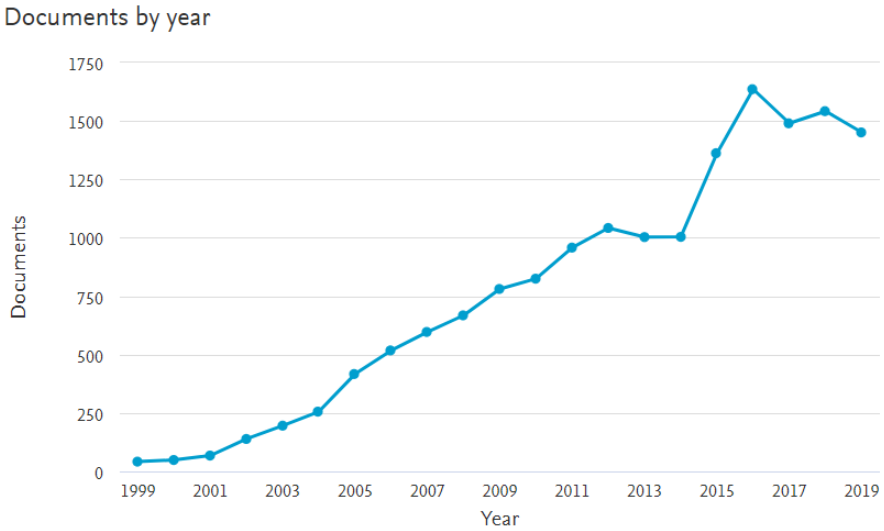


*Figure 1.2: Growth of scientific publications related to Lab-On-a-chip (Analysis result from Scopus).*

A microfluidic system usually includes a series of components with specific functionalities, like i.e. introducing reagents and samples, transporting and mixing these fluids within the microfluidic network by using integrated or external pumps precisely controlled and valves. Furthermore, various other functional elements can be interfaced or directly integrated into the chip, such as optical, electrical or magnetic detectors for microanalysis and components for purification of products for systems used in synthesis. The increasing demand for further miniaturization of devices poses the goal to fully integrate several different functionalities into a unique chip and using only very small fluid volumes.

The fluid phenomena that dominate liquids at the submillimetre length scale are significantly different from those that dominate at the macroscale. For example, the relative effect of the force produced by gravity at microscale dimensions is greatly reduced compared to the macroscale. Conversely, surface tension and capillary forces play a major role at the microscale. These forces can be useful for a variety of tasks, such as passively pumping fluids in microchannels [4]; precisely place cells in a variety of non overlapping patterns in microchannels [5], filtering various analyses [6], and forming monodisperse droplets in multiphase fluid streams [7]. Furthermore, liquid transport inside LOC devices is characterized by a well-defined laminar flow, a controllable diffusion enabling defined concentration gradients on the length scales of single-cells, high-speed serial processing, high degree of parallelization [8]. These examples represent only a fraction of the myriad of scaling effects leading to new phenomena arising at the microscale.

In a near future by the commercialisation, LOC devices with their ability to perform complete diagnosis of a patient during the time of a consultation, will change our way of practicing medicine. Diagnosis will be done by people with lower qualifications, thus enabling doctors to focus only on treatment. Real time diagnosis will increase the chances of survival for patients in emergency services and will allow the appropriate treatment to be given to each patient. A complete diagnosis will greatly reduce antibiotic resistance, which is currently one of the biggest challenges of the decade. The ability to perform diagnosis at low cost will also routinely change the way we see medicine and then enable us to detect illnesses at an earlier stage and treat them as soon as possible. In developing countries, LOC will enable healthcare providers to open diagnostics to a wider population

and to give the appropriate treatment to people who really need it without the use of rare and costly medications.

## 1.2 Lab-on-a-chip for rare cell isolation

Manipulation and analysis of cells and particles suspended in microfluidic platforms raise great interest in biomedical applications, such as oncology [9], stem cell research [10], and genomic mapping [11]. Isolating targeted cells from the surrounding environment, e.g., blood sample, is tremendously beneficial in diagnostic and therapeutic operations. In this regard, capturing the least abundant cells plays a vital role in diagnosis of some lethal diseases, such as malaria [12], cancer [13], and HIV [14]. For example, collecting the circulating tumor cells (CTCs) [15] and fetal cells [16] in peripheral blood is essential for early detection of cancer and parental diagnosis of chromosomal diseases. Moreover, purified cell samples with enhanced concentration of cells of interest provide a rich environment to study the biological and physical properties of those cells. The non-microfluidic techniques developed for cell separation, such as membrane filtration [17], centrifugation method [18], fluorescence activated cell sorting (FACS) [19], and magnetic activated cell sorting (MACS) [20], cover a wide range of applications. However, microfluidic-based devices introduce several advantages, including higher processing rates, lower sample use, enhanced spatial resolution, and increased accessibility due to lower cost [21]. In addition, contrary to the conventional cytometry techniques, which depend on biochemical labels for cell identification and therefore their use is limited to some applications, microfluidic methods are label-free because the trapping of cells and particles is based on their intrinsic physical characteristics, including size, shape, deformability, density, polarizability, and magnetic susceptibility. Exploiting these properties, the separation is achieved by applying the relevant force fields, such as optical [22], electric [23], magnetic [24], acoustic [25] and hydrodynamic forces [26]. The controlling mechanisms in the aforementioned handling techniques can be classified in two categories: passive methods where their functionality is established by harnessing microchannel geometrical effects and nonlinear hydrodynamic forces and active methods based on the application of external force fields.

## Passive separation and sorting techniques

There are several methods that can be implemented to passively separate particles while flowing in the channel. The separation is mainly performed on the basis of particle dimension, and it can be obtained choosing the proper channel geometry.

Filtration is the process of flowing a cell samples through an array of micro-scale filters, constituted by weirs, pillars or pores integrated in the chip orthogonal to the flow propagation direction in order to capture target cells based on a combination of size and deformability (Figure 1.3(a)). This is a simple approach that has the drawback of high risk of clogging, which reduces the separation efficiency and selectivity. A different filtering approach is constituted by hydrodynamic filtration shown in Figure 1.3(b). Side branches, perpendicular to the main flow, are fabricated. A secondary flow injected into the main one pushes the particles asides and allows precise control on the maximum dimension of the particles directed to the lateral channel [27].

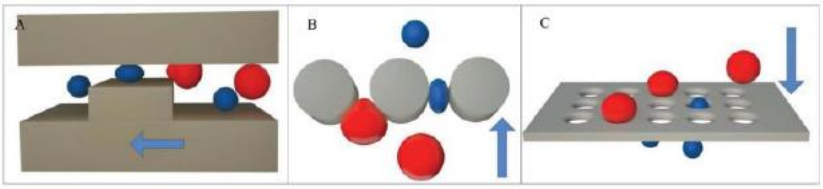


(a)

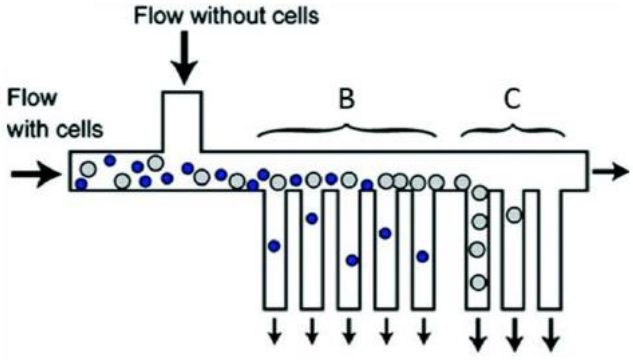


(b)

*Figure 1.3: (a) Filtration mechanisms: (A) weir, (B) pillar, (C) pore [28]. (b) Cell sorting by hydrodynamic filtration. (A) Cells are injected into the microfluidic device and are pushed toward the outlets. (B) Small cells exit out of the proximal branches whereas (C) large cells exit out of the distal branches [29].*

A different method is Deterministic Lateral Displacement (DLD) [30]. Using a matrix of obstacles with optimized dimensions and separations, it is possible to force big particles toward a preferred direction. Figure 1.4 (a) shows the schematic principle of the technique. For example, using micropillars displaced in the channel, it is possible to influence the path of cells larger than a certain threshold diameter. The smaller particles instead are not influenced on average by the presence of the pillars [31].

Pinched flow fractionation (PFF) instead is a passive sorting technique that can be used for continuous sizing of particles in a microchannel by employing the characteristics of laminar flow. The fluid containing the particles to be sorted is focused by a particle-free fluid, as depicted in Figure 1.4 (b). The microchannel includes a 'pinched segment' where particles are aligned to one of the sidewalls by controlling the flow rates of both fluids. In laminar flow, a particle has a tendency to flow along the streamline passing through its center of mass. For smaller particles the streamlines passing through their center of mass are closer to the channel wall, while for larger particles they are closer to the center of the channel. The mixture of fluid and particles coming out of the pinched segment is separated by the spreading of the streamlines according to their sizes [32].

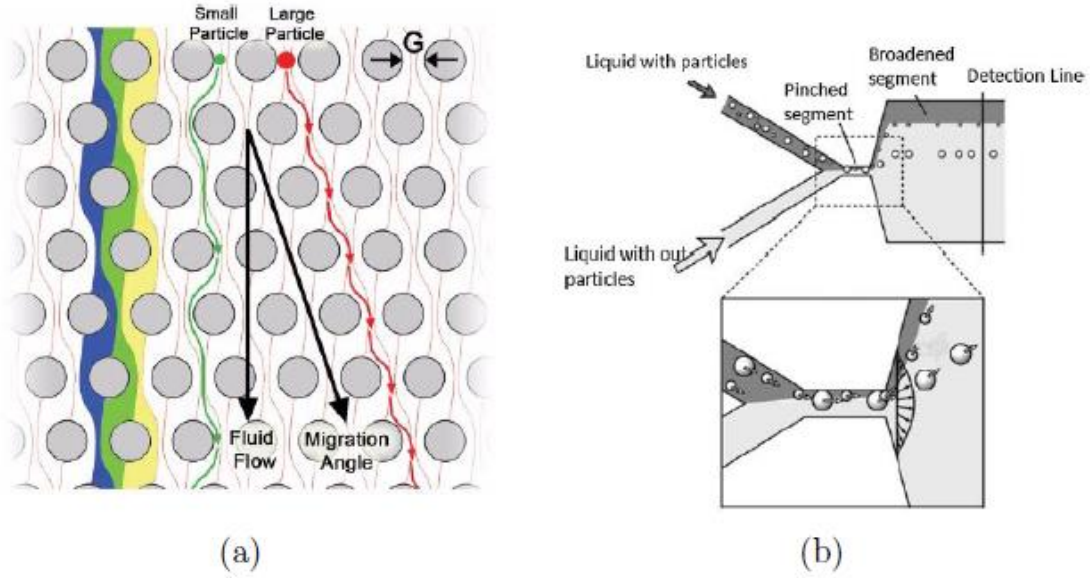


*Figure 1.4: (a) Principle of the deterministic lateral displacement separation method [27]. (b) Schematic illustration of pinched flow fractionation (PFF) [32].*

## Active separation and sorting techniques

Acoustophoresis is the process of deflection of a particle from its fluid path by applying an acoustic standing wave. When a particle is placed in an acoustic field, it undergoes a force proportional to the third power of its radius. Therefore, the larger the particle the higher the force experienced. This effect can be used for size-based sorting of the particles as shown in Figure 1.5 (a) [33].

Dielectrophoresis (DEP) has been widely used for electrically controlled trapping, focusing, translation, fractionation and characterization of particles that are suspended in a fluid [34][35]. In this approach a highly non uniform electric field is applied, which polarizes particles that migrate towards the regions of higher intensity (positive DEP) or in the opposite direction (negative DEP), depending on the electrical permeability of both the particles and the fluid. It is interesting to note that the DEP force is proportional to the cube of the particle's diameter, thus enabling the separation of cells with very small size difference (Figure 1.5 (b)).

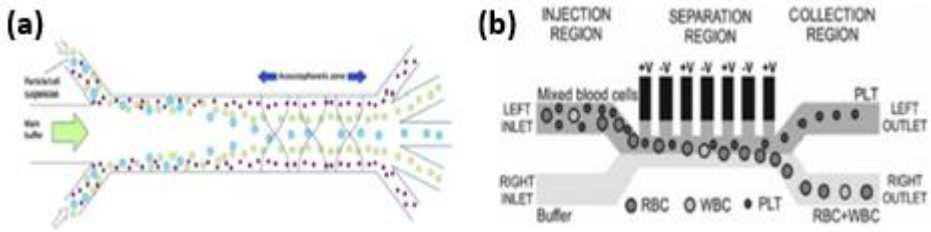


*Figure 1.5: (a) Schematic principle of an acoustic based sorter [33]. (b) Schematic design of a DEP device with liquid microelectrode array on the sidewall, where due to the size dependence of the force it is possible to separate particles [36].*

Magnetophoresis is capable to separate at high throughput magnetically labelled cell populations using magnetic forces [37][38]. The labelling is a necessary step since the only cells that show a sufficient magnetic susceptibility are deoxygenated red blood cells (RBCs) and magnetotactic bacteria. Moreover, using different magnetic targets with different magnetic responses, it is possible to obtain multiple output separations and not only a binary sample separation.

Optical sorting uses the interaction of light with the particles to manipulate the sample positions. Different configurations can be implemented. Particles size, shape and refractive index are just some of the characteristics on which this sorting can be

performed. Moreover, one of the main advantages of this approach is the high spatial selectivity, giving rise to the non ordinary possibility to isolate and to manipulate only one cell per time.

### 1.2.1 LOC techniques for capturing circulating tumour cells (CTC)

Analysis of circulating tumour cells (CTCs) is a promising way to monitor cancer progression and effectiveness of therapy. CTCs are cells that have shed from the primary or metastatic tumour and intravasated into the blood stream. CTC isolation and analysis can give a clear insight into the disease biology and its behaviour. Currently the most common CTC isolation method is relying on immunomagnetic cell capture by targeting the epithelial cell adhesion molecule known as EpCAM. In this method immunomagnetic beads and a cell isolation are incubating with anti-EpCAM or anti-N-cadherin antibodies for conjugation.

From the past few years several techniques have been used for the detection, enrichment and counting of circulating tumour cells (CTCs). All these techniques are targeting distinctive physical (size, density, etc.) or biological (tumour markers, immunoaffinity) characteristics of CTCs and can exploit different working principles such as immunomagnetism or microfluidics.

Size based microfluidic methods have some challenges like membrane clogging when using whole blood samples, due to the high concentration of blood cells. As a solution for this, devices with various pores sizes and shapes have been developed [39]. Moreover, some other techniques are also employed such as fluid assisted separation technology from Clinomics [40], or CTC-iChip (Figure 1.6) which combines three technologies to separate CTCs from whole blood [41].

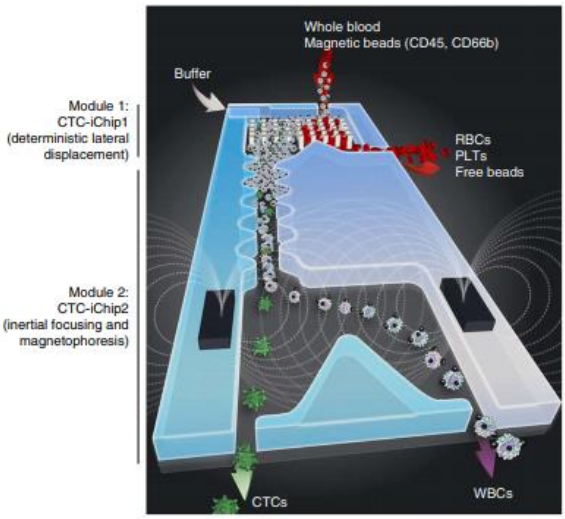


*Figure 1.6: An example of CTC-iChip. This CTC-iChip is composed of two separate microfluidic devices that consists three different microfluidic components engineered for inline operation: DLD to remove nucleated cells from whole blood by size-based deflection by using a specially designed array of posts performed in CTC-iChip1, inertial focusing to line up cells to prepare for precise magnetic separation and magnetophoresis for sensitive separation of bead-labeled WBCs and unlabeled CTCs, which are performed in CTC-iChip2. PLTs, platelets [41].*

In immunoaffinity based (immune magnetic) separation the CTCs are differentiated by targeting surface antigens or removing background cells by targeting antigens that CTCs lack. But the heterogeneity of antigens that are present on the surface of a CTC is a challenge for this type of separation technique [42].

Immunoaffinity based CTC technique is one of the first methods developed for capturing CTCs [43]. This method uses specific antigens that are expressed on the surface of CTCs and are not expressed on other cells. CTCs can be separated from blood cells by targeting surface antigens using specific antibodies. This method is termed as a positive enrichment immunoaffinity based technique. In negative enrichment methods, antigens are expressed on the other blood cell that are marked and are not expressed on CTCs. In positive enrichment methods one type of antigen (EpCAM) is generally used. It is an epithelial surface tumour marker and provide a high purity separation.

## Microfluidic immunocapture positive enrichment

Microfluidic devices, which are created by microfabrication methods contains structures that are comparable to the cell length scale. These devices allow for the precise

control over sample flow, which is important since this affects cell-antibody contact and therefore the cell capture efficiency [42].

An example for microfluidic immunocapture positive enrichment, a microfluidic device as a High Throughput Micro Sampling Unit (HTMSU) (Figure 1.7), that separates CTCs from the blood sample using surface immobilized monoclonal antibodies by targeting unique membrane proteins. The CTCs are captured and fixed on the monoclonal antibody coated walls of the microchannels and, after capturing, they can be released by trypsin. This method results in unlabelled viable cells and, most importantly, it is simple and low cost and can be also automated [44]. A unique attribute of this particular microfluidic device is the ability to detect the CTCs by using an integrated Platinum (Pt) conductivity sensor by detecting the electrical properties of CTCs. Since the detection provides a quantitative measurement of CTCs staining, cytometry is not needed and allows approximately 100% recovery of mostly viable cells [44].

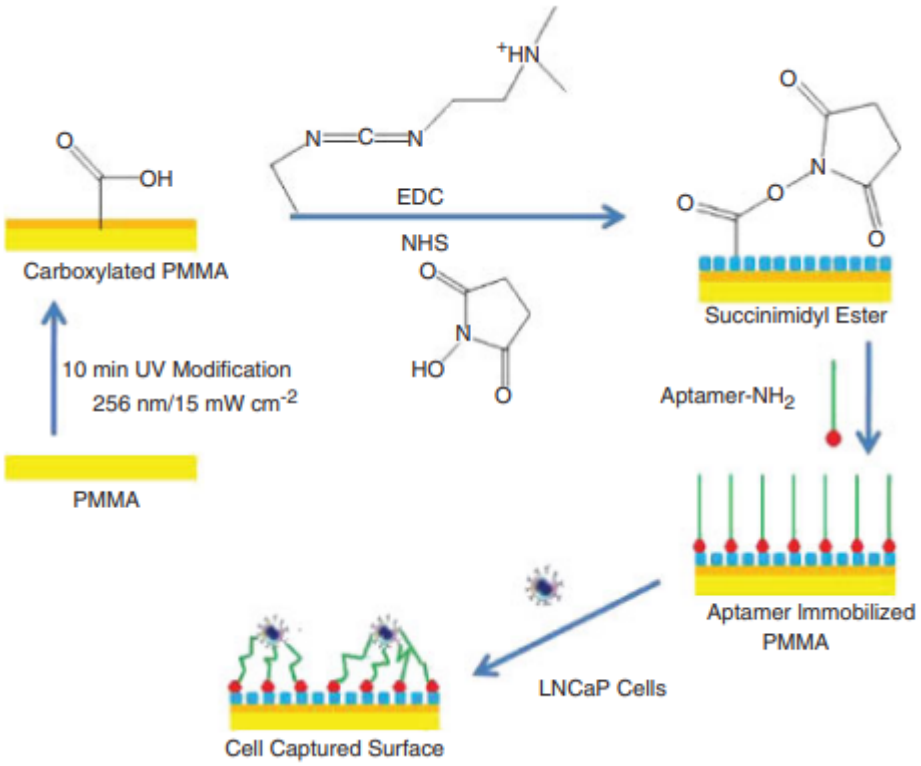


*Figure 1.7: An example for the process operation of the HTMSU used for the positive selection of LNCaP cells. Also shown is the chemistry used for the immobilization of the cell selection elements, aptamers, to the PMMA surface [45].*

Another example for microfluidic immunocapture positive enrichment is a chemically functionalized CTC chip using anti-EpCAM antibody. The microfluidic

device is consisting of an array of micro posts within a surface area which is functionalized with the anti-EpCAM anti body [46]. The geometric arrangement of micro posts and velocity of the fluid flow promote the cell attachment to the antibody. Low throughput and therefore the inability to analyse large sample volume is considered as a drawback of this microfluidic method. It has been reported that approximately 60% recovery rate is achieved with cancer cell line spiked blood samples, and a similar result is obtained with clinical samples from cancerous patients with approximately 98% cell viability [47].

A geometrically enhanced differential immunocapture (GEDI) chip is also a microfluidic method which combines positive enrichment using antibody-coated micro posts with hydrodynamic chromatography to minimize nonspecific leukocyte adhesion. The geometry of the device has been designed to maximize streamline distortion and thus bring CTCs in contact with immune-coated walls for capture [48]. When the impact of the cells with the coated wall does not result in capture, the cells are displaced onto different streamlines depending on their size and collision inclination. This property of the GEDI chip can increase the purity of cell capture by decreasing unwanted interaction opportunities of the nontarget blood cells with immune-coated surfaces.

## 1.3 Lab on a chip for in vitro cell cultures

In vitro studies are performed with microorganisms, cells, or biological molecules outside their normal biological context. Generally called "test-tube experiments", these studies in biology and its subdisciplines are traditionally done in labware such as test tubes, flasks, Petri dishes, and microtiter plates. Studies conducted using components of an organism that have been isolated from their usual biological surroundings permit a more detailed or more convenient analysis than can be done with whole organisms.

Cell culture is the way to study cells behaviour in response to their environment by allowing growing cells in an artificial environment [49]. Several cell culture methods are being used nowadays depending on cells properties and applications. Amongst them, 3D in vitro cell culture has been used very often as it has found to be more convenient features compared to other alternative conventional cell culture methods such as 2D cell culture.

2D cell culture (Figure 1.8) consists of a monolayer system that allows cell growth over a flat surface, typically on polyester or glass [50], in the presence of a medium that

feeds the growing cell population. Due to the simplicity of 2D cell culture, this model cannot accurately depict and simulate the rich environment and complex processes observed in vivo such as cell signalling, chemistry or geometry [51]. Consequently, data gathered with 2D cell culture methods could be misleading and non-predictive for in vivo applications [49].

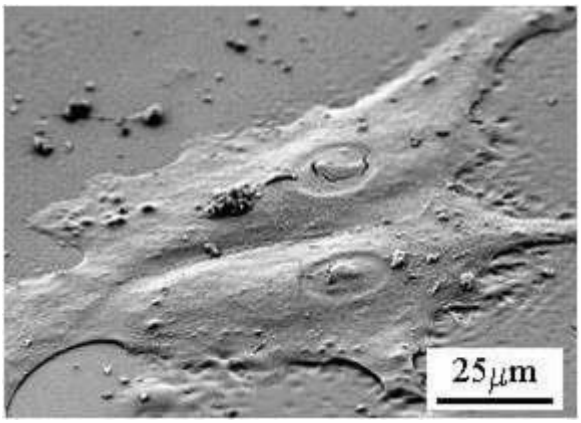


*Figure 1.8: A SEM image of 2D cell culture (from infinitebio.com)*

3D cell culture can be defined as the culture of living cells within micro devices and supports that present a three-dimensional structure mimicking tissue and organ specific microarchitecture [52].

3D cell culture facilitates cell differentiation and tissue organization by using micro-assembled structures and a complex environmental parameters [52]. In the 3D environment the cells tend to be more subjected to morphological and physiological changes. This method possesses easier control and monitoring over growing cells through the adjustment of microenvironment parameters such as temperature, chemical gradients, oxygen rate (gas permeability), pH, etc.

3D cell culture also grants the possibility to grow simultaneously two different cellular populations with co-cultures accurately reproducing cellular functions observed within a tissue. The interactions between the same cells and other cells are obviously a key element in the study of cells functions.

3D cell culture method has some noticeable downsides that would most likely be overcome by technological advances. That is some scaffold matrices incorporate compounds from animal or other unwanted sources (eg: virus) that could interfere with the cell culture [53]. Some other matrices provide good cell adherence and making cell removal more difficult.

Microfluidic technologies bring an accurate, long term and controlled 3D cell culture by using biocompatible microfluidic chips that facilitate tissue manipulation and studies. Particularly, organs-on-chip (OOC), that are considered as a subset of lab-on-a-chips, replicate key functions of living organs [54] by mimicking the microstructures depending on the biochemical functionalities and dynamic mechanical properties of organs. OOCs open a door to mimic human body systems as in vitro for diagnostics, clinical studies etc. Several in vitro models of human body systems are commonly available such as cardiovascular, respiratory, nervous, digestive, endocrine and integumentary systems and pathologies.

## Cardiovascular System

In vitro microfluidic devices are helpful for the diagnostics, clinical studies and drug screening in cardiovascular pathologies by reducing the intervention time and set upping more efficient therapies. A conduit like design of the microfluidic device brings precise control over fluid flow conditions and shear stress. Therefore, microfluidic devices are likely to be used as reductionist models of cardiovascular biology than to study heart related issues as for example, to mimic blood flow and predict injuries to blood vessel.

In vitro models of microfluidic cardiac cell culture would recreate mechanical loading conditions seen in both normal and pathological conditions and allow hemodynamic stimulation of cardiomyocytes by directly coupling cell structure and function with fluid induced loading [55].

Microfluidic in vitro models of cardiovascular system opens a door to study angiogenesis [56], artery structure and network [57], vascular endothelial function [58], vaso occlusive processes [59] (Figure 1.9), thrombosis [60], evaluating hypertensive micro vessels [61], anti hypertensive drug effects [62] and long term vascular contractility [63].

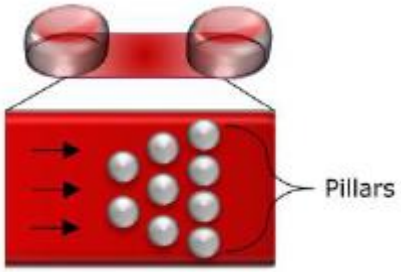


*Figure 1.9: Biochip with subdividing interconnecting microchannels (array of pillars) that decrease in size to mimic cell flow and adhesion in microvasculature to study of vaso-occlusive processes.*

## Respiratory System

The respiratory diseases usually act by affecting the airways, the structure of the lung tissue, blood circulation in the lungs or involve a combination of these three. Microfluidic platform is found to be a tool for studying respiratory system pathophysiology because it allows to successfully model the tissue interface and precisely control the fluidic parameters.

Biomimetic microsystems reproduce the alveolar-capillary interface of the human lung as an alternative to animal and clinical studies, for drug screening and toxicology applications [64] (Figure 1.10). Several biomimetic models, BioMEMs or microfluidic-based devices have been developed with the purpose of highlighting and modelling important issues in lung development, differentiation, homeostasis and disease [65].

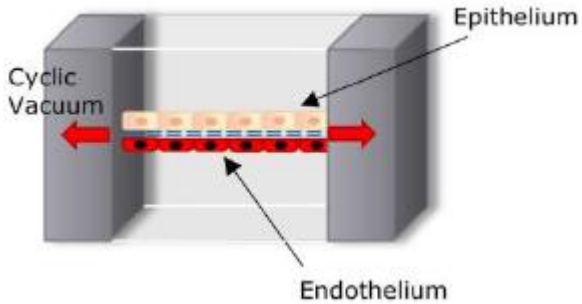


*Figure 1.10: Human breathing lung-on-a-chip microdevice, a biomimetic microsystem that reconstitutes the alveolar-capillary interface of the lungs.*

As far as the onset of lung diseases is concerned, microfluidic devices are necessary for the study and early detection of these diseases. The molecular processes underlying pathologies such as malignant transformation of bronchial epithelial cells due to tobacco

[66], protein-induced lung inflammation [67], chronic obstructive pulmonary disease [68] and idiopathic pulmonary fibrosis [69] are some of them.

## Digestive and Excretory Systems

A variety of diseases negatively affecting the digestive system lead to gastrointestinal organ damage and function deterioration. Stomach and oesophagus cancer, short bowel syndrome, faecal incontinence and trauma are among the pathologies affecting gastrointestinal function and urging for a treatment.

Microfluidic complex systems to create in vitro models of the intestine are valuable tools to study gut function under normal or diseased conditions and also to perform drug screening and toxicity assays. Human gut-on-a-chip is a well-established microfluidic device model for this purpose [70]. It consists of two microfluidic channels with a flexible porous membrane coated with extracellular matrix lined by gut epithelial cells (Caco-2) (Figure 1.11). The device is able to recreate gut structure with its mechanical, absorptive, transport and pathophysiological properties.

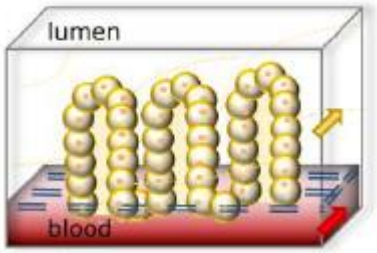


*Figure 1.11: Gut-on-a-chip device. Vertical cross-section representing the on-chip generation of intestinal villi obtained by villus morphogenesis of Caco-2 cells. The up-scale of this system leads to the production of gut-on-a-chip platforms.*

Furthermore, microfluidic-based devices to investigate liver drug metabolism and toxicity [71] are to be considered as fundamental tools to address liver pathologies for the better understanding of molecular toxicity mechanisms and simulate drug-drug and organ-organ interactions.

A perfect example of how microfluidics can be successfully applied to treat pancreatic dysfunctions comes from the “bionic pancreas” developed for type 1 diabetes. This device takes advantage of the continuous glucose monitoring along with subcutaneous delivery of both rapid-acting insulin and glucagon to lower/increase blood glucose levels [72].

## Nervous system

Understanding the central nervous system (CNS) has a relevant role in life science. Development and adapting innovative technologies help to increase our understanding of CNS disorders. To this purpose in vitro techniques are a major tool for investigating cellular changes and dysfunctions associated with CNS disorders.

Different in vitro techniques have already been developed for neuronal cultures to mimic the in vivo settings, where neurons can be probed, controlled and cultured under greater constraints. The compartmentalisation design of the device (Figure 1.12) has made a great breakthrough in neuronal culture and related studies. In such an arrangement, the neurons are cultured in one compartment and extend their axons to a second compartment which allows the control over distinct neuronal regions. Furthermore, the compartmentalised structure opens a door to perform biochemical analysis and precise physicochemical treatments on isolated axonal fractions.

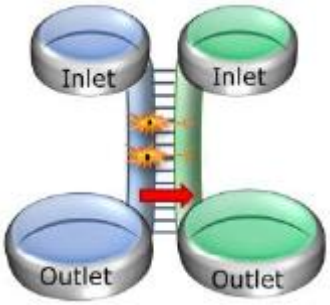


*Figure 1.12: Two-compartment microfluidic culture system bridged by microchannels*

Mixed primary cultures, including both neurons and astrocytes have proven to be a useful method associated with neurobiological research [73]. However, it is difficult to gain control over the parameters that influence the cellular microenvironment and neuronal connectivity. Indeed, creation of patterned neuronal networks that are environmentally isolated or localised transfection of cell population is difficult to achieve using conventional cell culture methods. Microfluidic procedures have been found to be a solution for this problem which enables greater control of cell patterning, manipulation and regulation of extracellular environments.

Compartmentalized microfluidic devices have been shown to be highly advantageous to understand the complex network circuit in the central neural system. Such devices have been used to understand the communication between peripheral

neurons and non-neuron tissues. The communication between neurons and different cell populations helps to understand how the nervous system controls tissues, both in homeostatic and pathological conditions.

The microfluidic devices allow complex but ordered in vitro models for CNS which facilitate the application of localised chemical stimuli, increase the throughput of monitored responses and reduce the amount of drugs required per experiment. This makes microfluidic system a versatile, low cost and useful tool to screen new drugs as well as examine the genetic changes associated with CNS conditions.

Most of the in vitro approaches comprises intra system cocultures such as coculture of neurons and oligodendrocytes [74], neurons and Schwann cells [75]. Some intersystem cocultures are also often used such as neurons and osteoblasts as an example for coculture between the nervous and the skeletal system [76]. Coculture of neurons and myocytes is another example for the combination of nervous and muscular systems [77].

## 1.4 Materials for Lab-On-a-chip

It is possible to identify three main kinds of materials in which LOC devices are usually fabricated.

- Silicon was among the first materials elected in the fabrication of microfluidic devices because of its high surface stability and thermal conductivity, moreover it is compatible with solvents. Today silicon is less employed due to the high costs and the opacity of the surfaces (except for IR) so that it is not adequate for microfluidic devices where optical analyses in the visible wavelength range have to be performed.
- Glass is another material early used in microfluidic chip manufacturing. It has good surface stability, thermal conductivity and solvent compatibility properties. Moreover, glass is biocompatible, chemically inert, hydrophilic and allows efficient coatings. Its surface chemistry, superior optical transparency and high-pressure resistance make it the best choice for many applications. The main drawback of glass in microfluidic chips is its high cost.
- Polymer materials are very common nowadays for the fabrication of LOC devices. Polymers are very cheap as compared to silicon and glass. Thus, they can be used for the mass production of LOC devices for commercial purposes. Apart from the

low cost, polymeric materials meet most of the requirements for a microfluidic device such as chemical stability, biocompatibility, nontoxicity, permeability to oxygen and gas, optical transparency and excellent replication fidelity. Moreover, the hydrophobicity makes polymers suitable/unsuitable for many microfluidic applications. Depending on the fabrication method and microfluidic applications various polymers are being used.

PDMS (polydimethylsiloxane) is a transparent and flexible elastomer that is widely used because it is very easy and cheap to fabricate PDMS LOCs by casting. Moreover, LOCs made of PDMS offer the advantages of easy integration of quake microvalves for fast flow switch and permeability of air for cell culture studies. But PDMS has severe drawbacks from the industrial point of view. It is not suitable for industrial production because the material is subject to aging and it is hard to integrate electrodes into a PDMS chip. Furthermore, it is not compatible with high throughput fabrication methods such as laser micro structuring, mechanical micro milling, injection molding and hot embossing etc.

Thermoplastics such as Polymethylmethacrylate (PMMA), Polycarbonate (PC) and Polystyrene (PS) are also being used for the fabrication of LOCs. Being rigid materials, such polymers compatible with high throughput fabrication processes of chips such as laser micro structuring, mechanical micro milling, hot embossing etc. Since they offer the possibility to integrate microelectrodes, thermoplastic materials are considered as good candidates for the industrialization of LOCs.

Microfluidic elements made of metal or ceramic can also be found, particularly for the micro reaction field, in which high temperatures and very aggressive chemicals are used and which frequently require materials with high thermal conductivity [78].

In conclusion, each material has specific properties that determine advantages and drawbacks, so that the choice has to be done considering the desired features and applications of the resulting microfluidic device [79].

# Chapter 2
# State of the art of various microfabrication techniques

## 2.1 Introduction

This chapter is dealing with the fabrication technologies for rapid prototyping of polymeric Lab-On-a-Chip devices. Various methods such as soft lithography, hot embossing, mechanical micro milling, femtosecond laser ablation and bonding are discussed here. Five different soft lithographic techniques for LOC manufacturing are explained. Three distinct hot embossing methods and mold fabrication for hot embossing are detailed, subsequently fabrication of LOC by hot embossing is described. Mechanical micro milling and its technical aspects are explained. Afterwards, the LOC fabrication by mechanical milling is outlined. Femtosecond laser ablation features of ultra short pulse processing and, eventually, femtosecond laser ablation for LOC fabrication are described. Finally, various indirect, direct bonding methods and surface treatments for thermoplastic microfluidic devices are discussed.

## 2.2 Soft lithography

The transfer of patterns from a mold to another substrate/surface is referred as lithography. The pattern transfer required in microfabrication is usually carried out with photolithography. Photolithography is the basic technology used to fabricate many microelectronic boards or devices. Photolithography is an expensive technique and can only pattern a small area at a time. This technique can be applied to a limited number of materials due to the etching chemistry and is also limited in the geometric designs that can be reproduced. The features size of the pattern is limited by the diffraction of the light. Since photolithography is confined to flat silicon substrates, fabrication of electronic circuits on plastic sheets or curved surfaces is not possible.

To overcome this limitation, a new non-photolithographic micropatterning method for surface modification using flexible molds or stamps has been developed by Whitesides et al. in 1990s [80]. This method allows low cost pattering for laboratory purposes by using a previously patterned stamp instead of using hard radiations (UV/Visible, X-ray or e-beam), therefore this method is named as soft lithography.

Relying on the stamps being used, soft lithography technique is able to produce surface modification in micro and nano scale range. Soft lithography technique can produce three dimensional structures with lateral dimensions of about 30nm-500µm. Soft lithography has a lot of advantages such as the possibility of patterning UV sensitive materials, patterning on nonplanar surfaces as well as large surfaces, does not have any diffraction limits and also it is a clean room free fabrication method. Soft lithography has been used to fabricate micro/nano structures using various polymer materials such as polydimethylsiloxane (PDMS), polystyrene (PS), poly (vinyl alcohol) (PVA), poly(etherimide) (PEI), and polyvinylidene fluoride (PVDF). Many researchers have established various soft lithographic techniques and subsequently developed various microdevices for different applications in life science.

## 2.2.1 Different methods of soft lithography for LOC fabrication

Different methods of soft lithography are available to make precise patterns at the micro- and/or nanoscale on planar and nonplanar surfaces. Some well established soft lithographic methods for different commercial application are (1) replica mold (REM), (2) microcontact printing (µCP), (3) micro molding in capillaries (MIMIC), (4) solvent assisted micro molding (SAMIM) and (5) micro transfer molding (µTM).

### 2.2.1.1 Replica mold (REM) technique

Replica molding is a simple, reliable and very old method by which the micro- or nanopatterns are duplicated on a polymeric material from the surface of a master mold [81]. By this technique patterns with features of less than 100 nm size can be obtained. Usually, replication mold technique is employed for the mass production of commercially available devices such as diffraction gratings [82], microtools [83] compact disks (CDs)

[84] and holograms [85]. The master mold is generally manufactured using standard photo lithography or micromachining techniques on a rigid material such as Silicon, Nickel, glass or SU8. The replica mold or elastomeric stamp is fabricated by cast-molding. Basically, the casting process consists of three steps: a prepolymer of the elastomer is poured onto the master mold, cured and taken off.

PDMS is the most globally accepted and widely used elastomer for casting process compared to other elastomers like polyimides, novolac resins and polyurethanes. PDMS is composed of inorganic siloxane and organic methyl groups. PDMS is commonly available on the market as two parts: one is the prepolymer and the other is its curing agent. They both are usually in liquid form at room temperature and have a very low glass transition temperature. The liquid prepolymer can be easily converted into solid elastomer by cross linking after adding the curing agent.

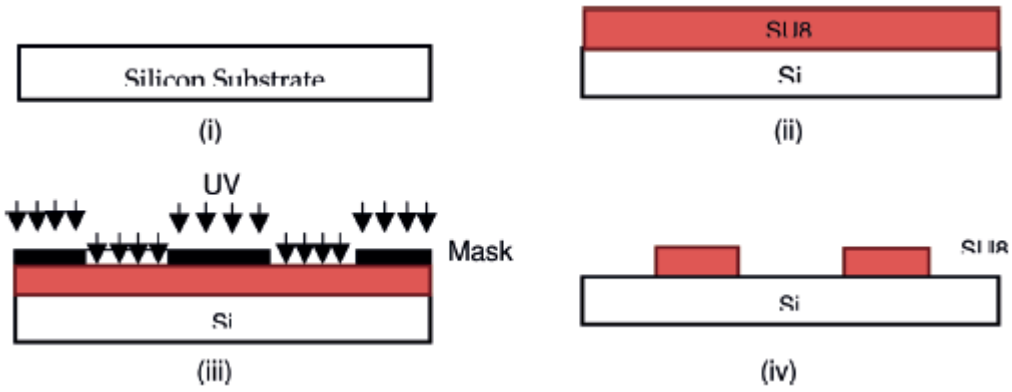


*Figure 2.1: Schematic representation of process flow of master mold fabrication using UV lithography. (i) Silicon substrate, (ii) SU8 is spin coated on silicon wafer, (iii) exposure of UV light and (iv) pattern obtained after developing.*

The Figure (2.1) represents the typical processing steps for the fabrication of a master mold. Since the need of precise structures with minimum feature size ranging from 1µm to tens of micrometers and high aspect ratios ranging from 1 to 20, SU8 negative photoresist is considered as the material for the master. The required thickness of the master can be obtained by spin coating the SU8 on a flat silicon substrate. The required thickness of the photoresist is depending on the spin coating parameters such as spin speed, spin time and acceleration of the spin. The spin coated photoresist is then soft baked two times, usually 5 minutes at $65^0$C and again 12 minutes at $95^0$C. A mask plate, containing the microstructures to be transferred, is kept above the sample which is

exposed to UV light (365nm wavelength) for a few seconds. Then the UV exposed sample undergoes a soft bake for 5 minutes at $65^0$C and again for 1 hour at $95^0$C. The patterns of the mask plate are now transferred to the photoresist and can be repeatedly used as the master for casting process to make polymer replicas.

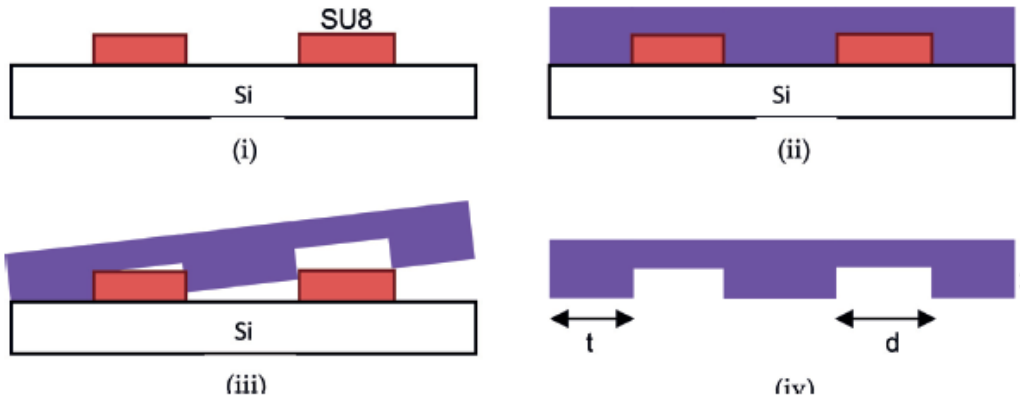


*Figure 2.2: Schematic representation of process flow of PDMS stamps fabrication (i) SU8 master mold on silicon substrate (ii) PDMS prepolymer poured on SU8 (iii) peeling off PDMS replica after curing (iv) fabricated PDMS replica.*

Figure (2.2) shows the cast molding processing steps in the fabrication of PDMS replicas using the prefabricated photoresist master. The silicone base and curing agent of commonly available PDMS elastomer is taken at the ratio of 10:1 in a Petri dish. A manual stirring and vigorous agitation is required for a thorough mixing. During the mixing air bubbles may arise so that the mixture is kept inside a vacuum desiccator for 1 hour to remove the unwanted air bubbles. The mixture is then poured onto the photoresist master mold and put inside a preheated oven at $80^0$C for 2 hours and 30 minutes. The curing of PDMS happens at this time by crosslinking of the prepolymer by the curing agent. The casted PDMS can be peeled off from photoresist master mold after allowing it to cool down at the room temperature. The obtained PDMS replica will have a reverse pattern of the photoresist master mold. Figure (2.3) shows the SEM images of three different photoresist master molds and Figure (2.4) shows the corresponding PDMS replica patterns.

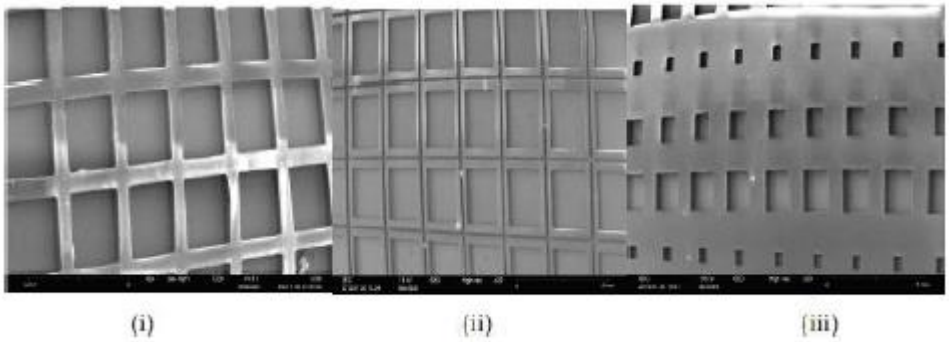


*Figure 2.3: SEM images of three different SU8 master mold patterns*

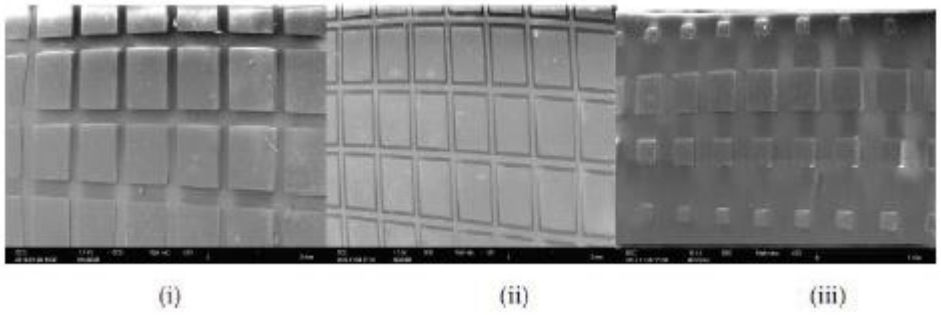


*Figure 2.4: SEM images of three different PDMS mold patterns corresponding to SU8 master mold patterns shown in Figure 2.3*

Replica molding is generally used for the rapid prototyping of the microfluidic devices [86] in which the microchannels are imprinted to PDMS stamp from the photoresist master mold. The microchannels are covered with a plane glass plate and bonding of both surfaces is carried out by oxygen plasma treatment. Since PDMS is flexible, the inlet and outlet holes to the microchannels are made simply by punching at the desired dimensions.

Replica molding has several disadvantages for fabricating complex features with enough precision and it is necessary to use photo lithography each time in case of experimenting various features and feature size for the master mold. In the particular case of PDMS, it has approximately 1% of shrinking tendency upon curing [87]. Also, treating with organic solvents such as toluene and hexane causes swelling of the cured PDMS. PDMS has low thermal expansion and Young's Modulus so that dimensional variations arise especially for multilayered structures. Furthermore, very high or very low aspect ratios (h/l) of the microstructures would cause defects in patterns (Figure 2.5) due to the elastomeric character of PDMS. Due to gravity, adhesion or capillary forces, a stress may be induced on PDMS which eventually leads to the failure of microchannel formation.

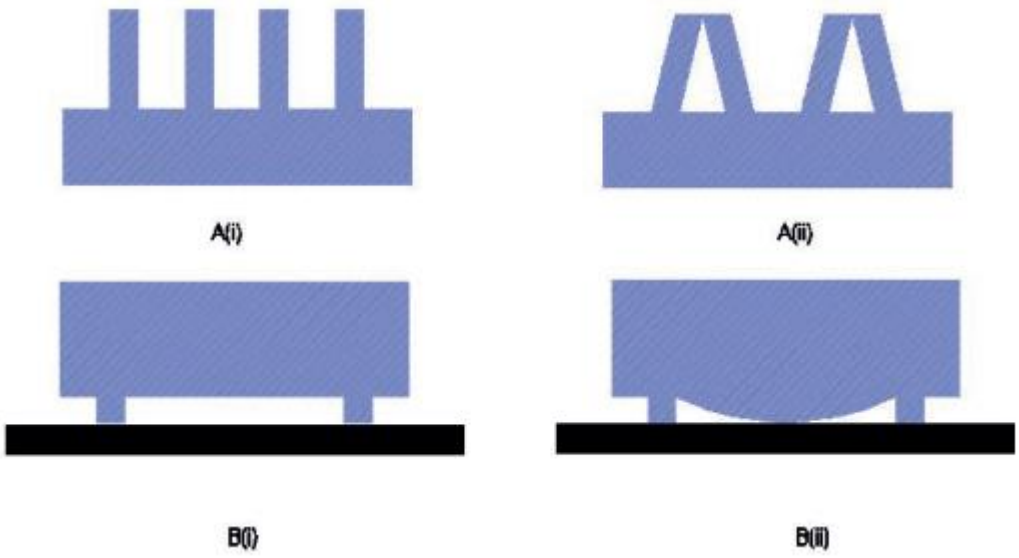


*Figure 2.5: Schematic representation of defects in patterns due to high or low aspect ratio structures: A(i) expected structure with high aspect ratio A(ii) resultant collapsed structure; B(i) expected structure with low aspect ratio B(ii) resultant sagged structure.*

The main technical problems are:

(1) The PDMS microstructures fall under their own weight at very higher aspect ratio. Figure 5 A(i) shows the structure with high aspect ratio to be obtained and A(ii) shows the resultant collapsed structure. At the best, aspect ratios ranging from 0.2 to 2 can be achieved to get defect-free replicas.

(2) The PDMS microstructures with very low aspect ratio usually sag down at because the structures are not able to withstand the compression force and adhesion between the stamp and substrate. Figure 5 B(i) shows a typical expected structure with low aspect ratio features while B(ii) shows the resultant sagged structure. The sagging of microstructures can be avoided by adding non-functional posts or rigid supports in the design.

Several researchers have successfully developed replica mold techniques for fabricating microfluidic devices for various biomedical purposes. Ian D. Block et al., demonstrated a replica-molding method for submicron patterning (550nm periodic) of a low-index sol–gel nano porous glass for the purpose of fabricating large-area ($80cm^2$) label-free photonic crystal optical biosensors [88]. Jeffrey T. Borenstein et al., have used this method to construct microfabricated scaffolds in order to develop microvasculature enabling the development of bulk organ scaffolds. The development of the PDMS

template was made by using a micromachined silicon mold. Moreover, the scaffold was successfully seeded with endothelial cells in channels with dimensions as small as the capillaries to promote vascularization [89]. Christopher J. Bettinger et al., have fabricated a topographical patterning by poly (glycerol sebacate) on sucrose coated silicon to control cell orientation and morphology. The fabricated microstructures were biocompatible, flexible and biodegradable with features in the range of 500 nm. The micro-curvatures residing in the fabricated structures represented a stronger topographic cue in order to align and elongate aortic endothelial cells [90].

### 2.2.1.2 Microcontact print (μCP) technique

Microcontact printing (μCP) is a simple and effective method for transferring of precise microscale patterns for the applications in biotechnology domain. Microcontact printing allows modify the properties of a surface by self assembled monolayers (SAMs) at molecular level. The SAMs are usually prepared by immersing the stamp in a solution containing a ligand (Y($(CH_2)_n$X) which is reactive towards the surface or by the exposure of a reactive species vapour to the stamp [91]. The thickness of a SAM is depending on the number (n) of methylene groups in the alkyl chain. The surface of a monolayer can be changed by changing the head group (X) of the chain. The binding of anchoring group Y is selective to the substrate material. Some of the well established SAMs methods are alkylsiloxanes on hydroxyl-terminated surfaces such as Si/SiO2 [92], Al/Al2O3 [93], glass [94], mica [95], and plasma-treated polymers and alkanethiolates on Au and Ag.

Figure (2.6) indicating the processing step in microcontact printing technique. A thin film of metals such as copper (Cu), gold (Au), silver (Ag), platinum (Pt) or palladium (Pd) is deposit on the substrate by using physical vapour deposition methods like e-beam evaporation and thermal evaporation. A PDMS stamp (Figure 2.6 a) is immerse in hexadecanethiol in ethanol (Figure 2.6 b) and bring it into contact with an Au surface for few seconds. Due to the contact hexadecanethiol could transfer from PDMS stamp to gold and produces hexadecanethiolate. Subsequently it will make SAMs patterns on the gold surface (Figure 2.6 c).

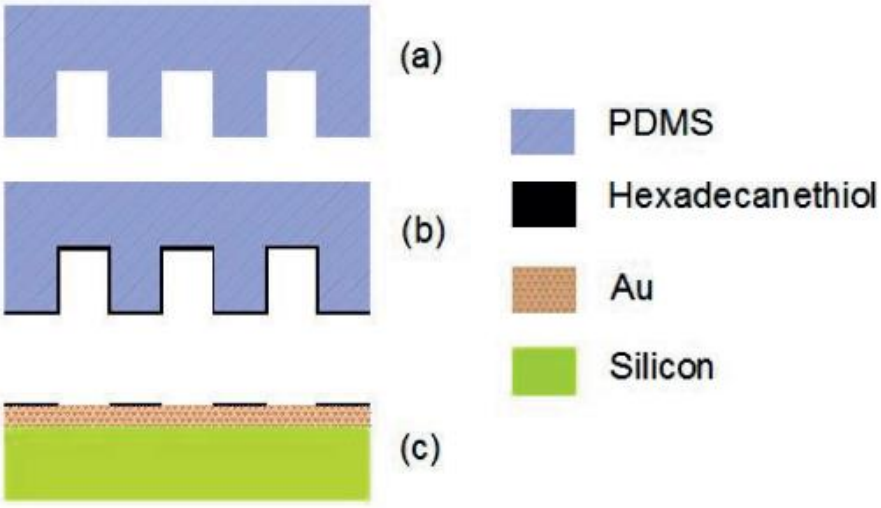


*Figure 2.6: Schematic representation of process steps for microcontact printing (a) PDMS stamp (b) PDMS stamp immersed in hexadecanethiol solution and (c) SAM pattern transferred to the substrate with gold (Au) coating by bringing the stamp in contact upon the substrate.*

Several studies were reported about the use of micro contact printing technique. R. N. Orth et al., presented a method for creating patches of fluid lipid bilayers with conjugated biotin and other compounds down to 1µm resolution using a photolithographically patterned polymer lift-off technique. The method has been functionalized fluid lipid bilayers as micron-scale platforms to immobilize biomaterials, capture antibodies and biotinylated reagents from solution, and form antigenic stimuli for cell stimulation [96]. Milan Mrksich et al., have used µCP to pattern the formation of SAMs at the micrometer scale in order to promote the attachment of mammalian cells in a PDMS stamp. SAMs were coated with fibronectin and the preferential adhesion of the cells was observed [97]. Tamal Das et al., analyzed the interaction of the mammalian cells using µCP patterns on PDMS which resulted in the modification of the morphology of the fibroblast cells and subsequently used to control cell shape-functionality on-chip [98].

### 2.2.1.3 Micromolding in capillaries (MIMIC)

Micro molding in capillaries is another method to produce micropatterns using PDMS stamps (Figure 2.7). In this technique a mold consisting of microchannels is made with PDMS and is placed on another substrate in a manner that channels are facing down to the substrate (Figure 2.7a). The void microchannels create a chance for capillary action inside the channels. Polymer materials such as polyurethane or epoxy are generally used

to fill the channels (Figure 2.7b). At the time the polymeric material is placed at one end of the void microchannels, it starts flowing into the channels due to the capillary forces (Figure 2.7c). The void microchannels or capillaries are filled with the polymeric materials within a few minutes. Then the polymeric material is cured by heat, UV or using a curing agent. The PDMS mold can be removed once the polymer is cured and it produces a counter part of the microchannels (Figure 2.7d). The filling rate of the polymer inside the capillary depends on surface tension, viscosity of the fluid, contact angle radius of the channel, length of the capillary and pressure difference at the end of the capillaries.

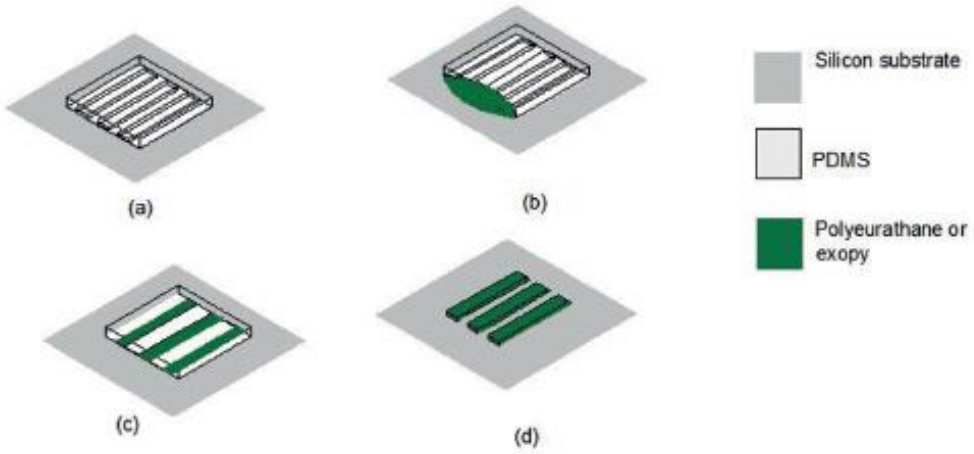


*Figure 2.7: Schematic representation of the process flow for micro molding in capillaries (a) PDMS mold with microchannels on silicon substrate (b) Polyeurathane or epoxy in the form of fluid at the end of the microchannels (c) fluid flows inside the microchannels by capillary force and (d) cured epoxy and removal of the PDMS mold.*

Some researchers have utilized the MIMIC technique to fabricate lab-on-chip devices. Giovanni Vozzi et al., demonstrated 3D scaffolds of poly (lactic-co-glycolic acid) (PLGA) with feature resolution of 10–30 μm on PDMS for tissue engineering applications [99]. Albert Folch et al., developed 3D microfluidic molding structures as models for scaffold production on PDMS. Polyurethane (PU) precursor was injected into the network mold of PDMS and the obtained 3-dimensional scaffolds were used for tissue growth and regeneration [100].

### 2.2.1.4 Solvent-assisted micromolding (SAMIM)

In solvent assisted micro molding (SAMIM) method (Figure 2.8) a PDMS mold (Figure 2.8a) is used to fabricate microstructures with the assistance of a solvent. A fluid

or gel is made by mixing a polymer material and a solvent (Figure 2.8b). The solvent is chosen based on the solubility of the polymer material, but it must not affect PDMS when in contact. Solvents having high surface tension are generally used such as ethanol, isopropanol, methanol, acetone and toluene. Since PDMS is hydrophobic in nature, an oxygen plasma treatment is required to improve its wettability. The polymer material mixed fluid is poured over a substrate and oxygen plasma treated PDMS is placed upon it (Figure 2.8c). The microchannels in the PDMS get filled with the mixture. As the solvent is nonreactive with PDMS, it starts to evaporate (Figure 2.8d) and the resulting fluid or gel gets solidified inside the PDMS mold. The counter section of the microchannels of the PDMS mold is finally obtained on the substrate by removing the PDMS mold (Figure 2.8e). The formation of a thin film at the bottom of the structure is considered as the main drawback of the solvent assisted micro molding technique. This film can be removed by a suitable etchant before using it for the defined application, but this adds an extra step for the realisation of microdevices.

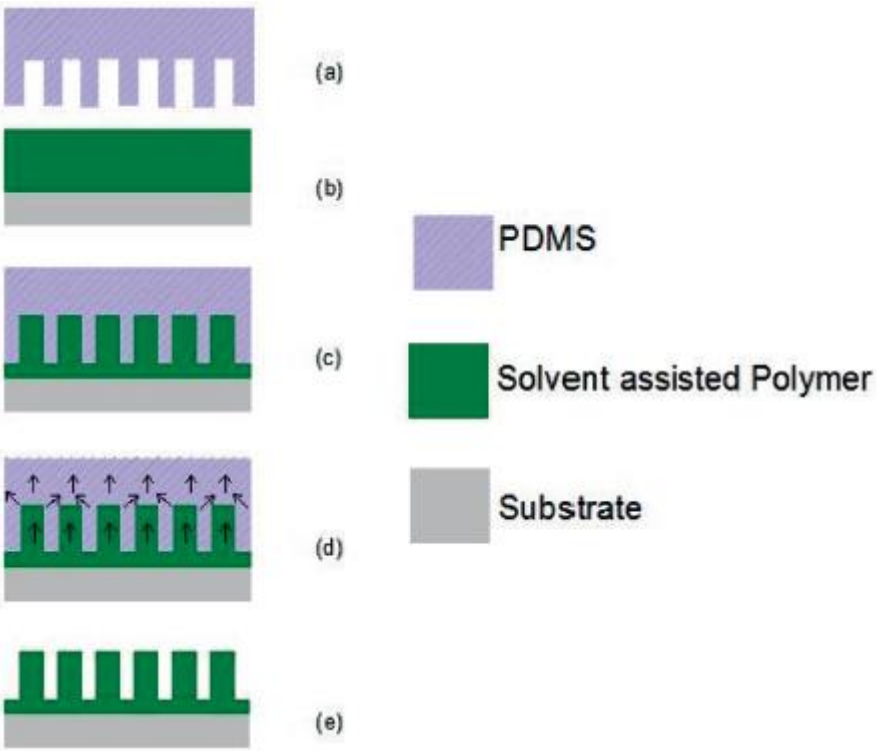


*Figure 2.8: Schematic representation of the process steps for SAMIM (a) PDMS mold (b) solvent assisted polymer on a substrate (c) polymer mold placed on the solvent (d) solvent evaporates and (e) microstructures of solidified polymer after solvent evaporation.*

Some researchers have successfully applied SAMIM technique for LOC fabrication. Shoutarou Terane at el., have proposed a process for integrating elastomeric micro elements into plastic substrates by the micro molding of a dispensed liquid prepolymer with the aid of the capillary force. A self standing elastomer membrane was fabricated by dispensing PDMS prepolymer into a coaxial cylindrical tube microstructure pre-engraved on a plastic substrate with subsequent curing agent. Furthermore, the molding process was applied for the fabrication of pneumatic microvalves on a plastic based microfluidic device and its successful operation was demonstrated [101].

#### 2.2.1.5 Micro transfer molding (μTM)

Micro transfer molding (μTM) (Figure 2.9) is also a kind of simple soft lithography method to produce micropatterns on a large area. Polymers such as organic polymer or polyeurathane are typically employed for this technique. Polymers doped with fluorescent material like rhodamine may also be used with this method. A pre-polymer is filled in a pre-patterned surface of a PDMS mold (Figure 2.9a). The removal of excess fluid can be done by another flat PDMS sheet to get a flat surface (Figure 2.9b). The prepolymer filled PDMS mold is then placed on a substrate in upside down position (Figure 2.9c). The pre-polymer is cured by heating or by UV light. Once the pre-polymer is solidified by curing, the patterns of the PDMS mold are then transferred to the polymer. Now the PDMS mold can be peeled off to leave the patterned polymer on the surface of the substrate (figure 2.9d). A very thin layer (100nm) of polymer may be formed in between the fabricated microstructure, which is interpreted as the drawback of this method. The forming thin layer can be etched by reactive ion etching (RIE). Micro transfer molding is generally used for the fabrication of couplers, interferometers and waveguides.

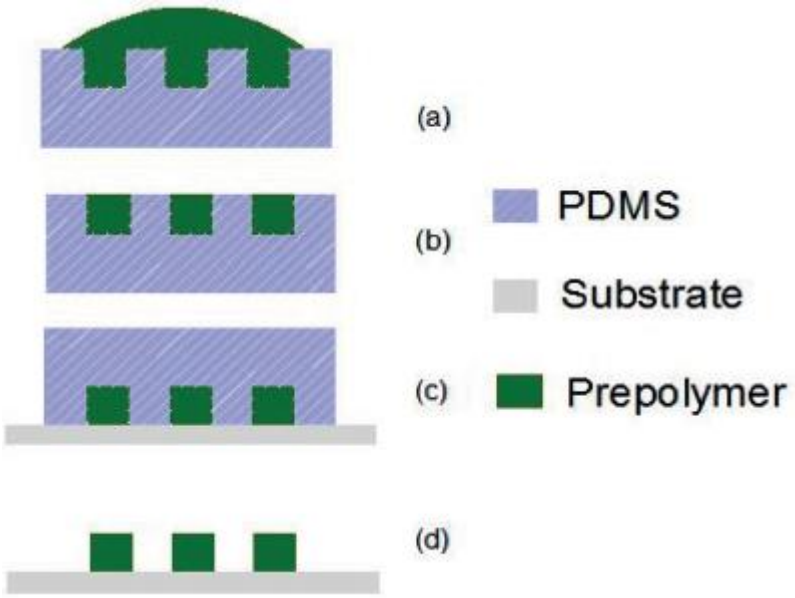


*Figure 2.9: Schematic representation of the process flow for the fabrication of polymer microstructures using micro transfer molding technique (a) PDMS mold filled with pre-polymer (b) excess fluid is removed and the surface is flattened (c) the mold with pre-polymer is kept on the substrate in upside down position (d) Pre-polymer is cured and the PDMS mold is peeled off.*

Few researchers have used the micro transfer molding technique for various microfluidic applications. Jae-Hwang Lee et al., presented a two-polymer micro transfer molding (2P-μTM) method for the 3D microfabrication of polymeric devices. Using 2P-μTM, they have achieved highly layered polymeric microstructures on PDMS by stacking planar structures layer by layer and fabricated 3D optical waveguides [102].

Soft lithography seems to be a simple and promising inexpensive method to fabricate micro and nanostructures. However, there are several challenges to promote this method into the market. The foremost disadvantage is the distortion of elastomeric materials, which limits the achievable spatial resolution of micropatterns in soft lithography. This problem can be almost surpassed by using rigid supporting structures and thick samples. Another drawback is the distortion of micropatterns or nanopatterns in the mold due to the shrinking of elastomer, swelling, sagging and pairing. The method may also form defects as a result of poor release from stamp or mold, bubbles in the pre-polymer, poor adhesion to substrate and dust particles. The presence of polymer thin films after the fabrication by soft lithography is commonly removed by reactive ion etching but this may lead to the damage of the small features.

# 2.3 Hot embossing

Hot embossing is a replication technology that consists in transferring micro patterns from a master mold onto another substrate at particular temperature and applied pressure. Micro hot embossing is considered as one of the methods to fabricate micro/nano features with high precision and quality [103]. Hot embossing technique was first implemented in 1970 by RCA Laboratories, Princeton, USA to replicate hologram motion pictures for television playback [104]. They have successfully imprinted a sequence of holograms onto a vinyl tap. Later this method has been used for fabricating numerous features for various applications [105].

A typical hot embossing process consists of four main steps (Figure 2.10) [106]: (1) heating the substrate and mold to the temperature needed for imprinting patterns (molding temperature), (2) embossing micro structures patterns at embossing temperature, (3) cooling down both the substrate and mold to demolding temperature and (4) demolding the sample by opening the tools. Thermoplastic materials, particularly polymers, undergo two deformation stages in the whole hot embossing process: one is a stress concentration and strain hardening stage that arises during heating and embossing, and the other is a stress relaxation and deformation recovery stage that takes place during cooling and demolding [107]. The most important parameters to take into account for hot embossing process are the applied pressure, the glass transition temperature of the substrate and the mold and holding time.

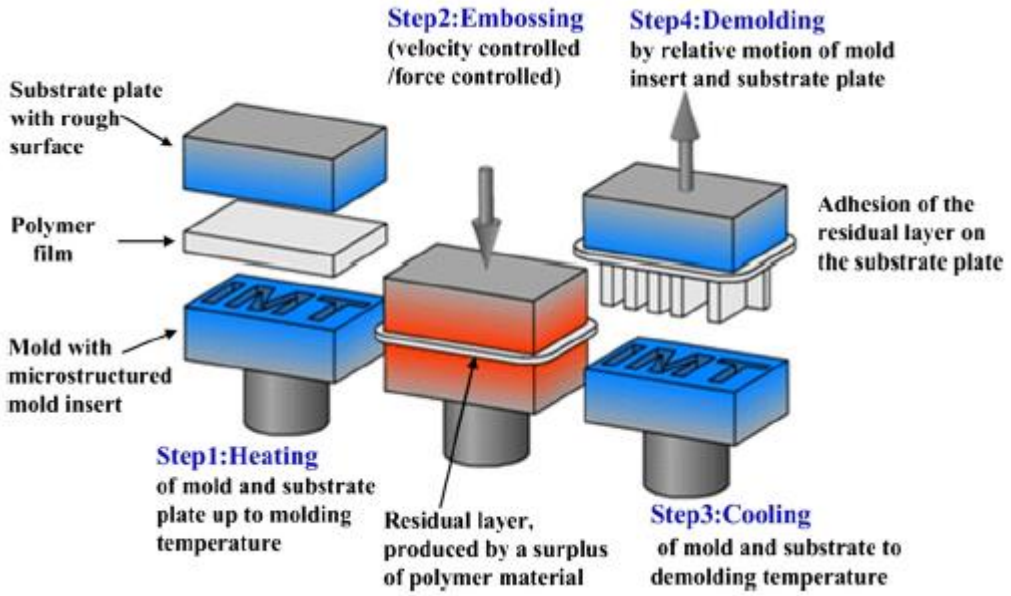


*Figure 2.10: Schematic representation of a typical hot embossing process with four major steps: heating, molding, cooling and demolding*

Thermoplastic polymers are often preferred for hot embossing due to their low molding temperature and wide range of optical, chemical and thermal properties. Thermoplastic polymers can be converted from solid or glassy state to rubbery and flow state by increasing the temperature [108]. Indeed, the low glass transition temperature of polymers (Eg: $T_g\ of\ PMMA = 120^0C - 160^0C$) makes them a very suitable material for hot embossing. The material remains as glassy state when the operating temperature is below its glass transition temperature (Tg). In glassy state the deformation on the material is ideally elastic and it comes only from elongation of the atomic distance [109]. As the temperature increases the material tend to convert into rubbery state and at that state the material will behave like approximately incompressible rubber.

Micro hot embossing can be differentiated in three types by the configuration of the molding tools being used: plate-to-plate (P2P), roll-to-plate (R2P) and roll-to-roll (R2R).

## 2.3.1 Different types of hot embossing

### 2.3.1.1 Plate-to-plate (P2P) hot embossing

P2P hot embossing is a very common and relatively mature technology. It consists of a mold plate with microstructures and a substrate plate (Figure 2.11).

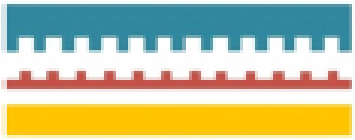

*Figure 2.11: Schematic representation of a plate-to-plate hot embossing technique, consist of mold, substrate and supporting platform*

During P2P micro hot embossing the depth of replicated patterns increases with the operational temperature, pressure load and holding time [110], owing to the deformation and filling behaviour of thermoplastic polymers. It has to be noticed that the patterns get collapsed with further increase in temperature and pressure load above an experimentally optimized threshold value. Finite element analysis (FEA) models are generally accepted as a valuable tool for studying filling process in micro hot embossing [111].

P2P hot embossing cannot be suitable for all micro fabrication applications. Especially for the fabrication of patterns with high aspect ratio, defects may occur such as breakage and distortion of features while demolding. The demolding related defects are mainly attributed to the significant difference in thermal contraction behaviour between polymer substrate and molds (mostly silicon or metal). This mismatch generates a large thermal stress during cooling, thus making it difficult to separate micro patterned surface from molds. Adhesion and sidewall friction have an important role in demolding. Adhesion is degraded by thermal stress and friction is exacerbated while the substrate is cooling down. The demolding efficiency can be increased by using coatings of amorphous silicon carbide and Teflon like fluoropolymer [112]. Self assembled n-octadecyltrichlorosilane can also be used to coat Si molds to reduce the adhesion between mold and micro patterned polymers [113]. Furthermore, material recovery may happen after hot embossing process. That is the stored imprint energy get released, once the mold and substrate are separated. This is strongly depending on the imprint and demolding temperatures.

Long cycle time for heating as well as cooling, and low uniformity of the structure, especially when the working area is large, are some other drawbacks of P2P hot embossing. However, these problems can be avoided by introducing rubber pads, ultrasonic vibrations and gas pressure.

**(1) Rubber-assisted embossing**

A rubber pad is applied to the metal sheet to enhance flexibility of operation and protect the sheet surface. Further advantages are the low tooling cost and the capability to obtain complex parts [114]. In the case of hot embossing of thermoplastic polymers, a thin thermoplastic film is pressurized between the mold surface and the rubber pad. As a soft counter-tool, the rubber pad gets deformed onto the hard mold surface, resulting in the transfer of features from hard surface and formation of the shell type structures on the film [115].

**(2) Ultrasonic-assisted embossing**

Ultra sonic energy is used as an auxiliary heating source for hot embossing. The asperities at the interface of master mold and plastic plate create intermolecular friction and thus ultrasonic sonic energy is converted into heat energy (Figure 2.12 b). This generated heat is able to melt the thermoplastic polymers and results in material flow to fill the interface [116]. Ultra sonic heating is much more effective and usually takes 1-2 seconds as compared to convective heat transfer (Figure 2.12 a). In addition, it is also beneficial during the demolding step for the release of mold from the imprinted substrate.

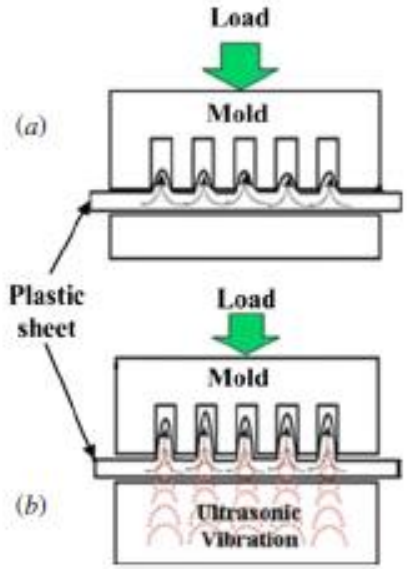


*Figure 2.12: (a) schematic representation of conventional P2P hot embossing, (b) schematic representation of ultrasonic-assisted P2P hot embossing*

**(3) Gas-assisted embossing**

The pressure load for P2P hot embossing is usually applied by hydraulic pressure units or spindle drives. When the molding area is large, it is difficult to get a homogeneous pressure at each embossing area. Using a gas pressure load instead of conventional pressure load drives guarantees the homogeneous contact between mold and polymer film [117]. An example of this technique is shown in Figures (2.13 (a)-(e)). A PC film is placed on a heating plate with the mold and a seal film is placed upon it. After closing the chamber, the stacked materials are heated by a coil to soften the PC film. In the meantime, nitrogen gas is applied into the chamber to attain uniform embossing pressure all over the film. The chamber is degassed, once the mold and PC substrate are cooled. Finally, the chamber is opened, and stacker of mold and PC substrate are removed from the chamber [118].

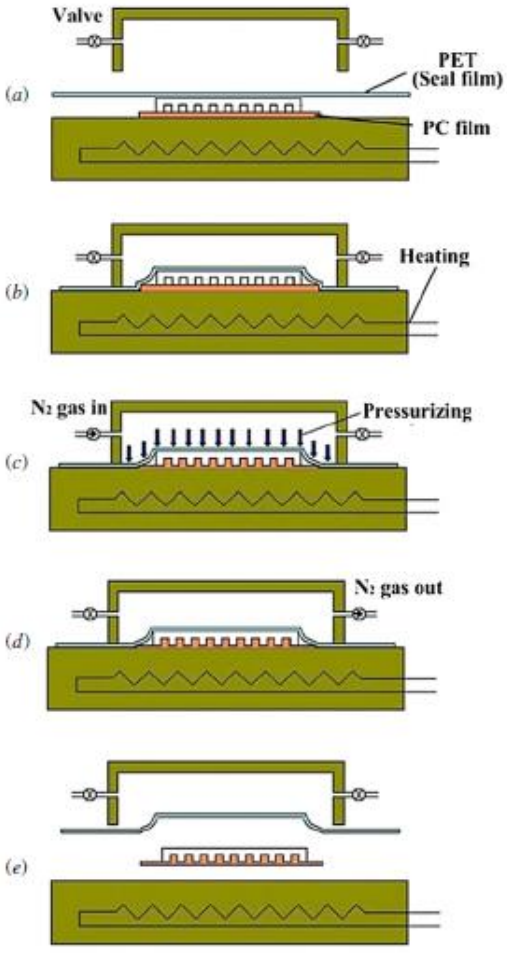


*Figure 2.13: Schematic representation of the gas-assisted hot embossing process: (a) material preparation, (b) heating, (c) $N_2$ gas pressurizing, (d) cooling and degassing, (e) opening the chamber*

P2P hot embossing is the most conventional type of hot embossing method and is still largely used for some industrial applications such as the production of compact disc (CD), digital versatile disc (DVD) and fabrication of micropatterns for laboratory applications with high accuracy. P2P also has some drawbacks like less efficiency, limited replication area, high deformation due to the discontinuous batch wise mode [119]. The machine systems for this method are widely available in the market, being P2P frequently used in industry. There are several companies capable to offer different categories of P2P micro hot embossing machines [120]. Jenoptik Mikrotechnik GmbH is one of the pioneers providing complete hot embossing machine systems for the fabrication of microstructured patterns with high aspect ratios.

### 2.3.1.2 Roll-to-plate hot embossing

Roll-to-plate (R2P) hot embossing (Figures 2.14 (a) and (b)) concept was introduced in 1998 [121]. R2P is characterized by a flat plate and a rotation cylinder. This type of hot embossing is used in applications where large area patterning of polymeric films is needed such as e-paper, flexible solar cells and flexible displays [122]. Two types of R2P can be distinguished depending on the mode of operation. One is rolling a cylinder mold on a flat substrate (Figure 3a) and the other is rolling a smooth roller on a flat mold which is placed over a substrate (Figure 2.5b). R2P hot embossing enables to increase the replication area from tens of square centimeters to several square meters.

*(a)* *(b)*

*Figure 2.14: schematic representation of roll-to-plate hot embossing technique. (a) rolling a cylinder mold on the substrate. (b) rolling a smooth roller on a flat mold placed over the substrate*

In both methods the temperature of the roller should be above the glass transition temperature (Tg) of the substrate while the temperature of the supporting platform is below the Tg of the substrate. Consequently, only the substrate-roller contact area will have higher temperature than Tg, which helps to melt the polymer and get it imprinted

with patterns only in that area. Whereas in P2P hot embossing the entire polymer is imprinted simultaneously after heating above Tg and it is required to keep pressure load until the polymer cools down.

A modified R2P hot embossing system has been developed, which has an automatic stamp release mechanism that allows reducing pattern distortions due to the shrinkage difference between substrate and stamp. This system (Figure 2.15) consists of an air cylinder to operate roller press, a one axis moving stage, and an automatic stamp release mechanism.

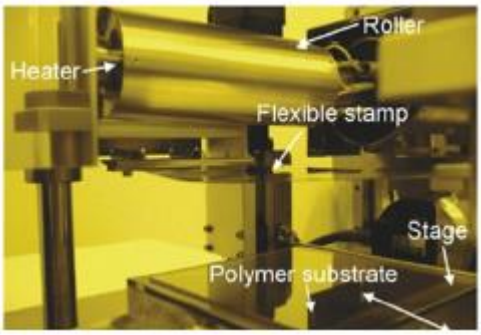


*Figure 2.15: A hot embossing system (R2P) with automatic stamp release mechanism*

Another modified R2P system (Figure 2.16 a & b) that does not require roll stamp is also available. It can easily transfer the micro patterns from a hard stamp to flexible substrates. As the press roller moves in vertical and horizontal directions, the substrate and stamp are stacked line-by-line. The flexible substrate is fed from the supply roller to the pickup roller. When the press roller comes into contact with the stamp, the heat transfer occurs first to the stamp and then to the substrate. The substrate gets cooled by compressed air after embossing with micro patterns.

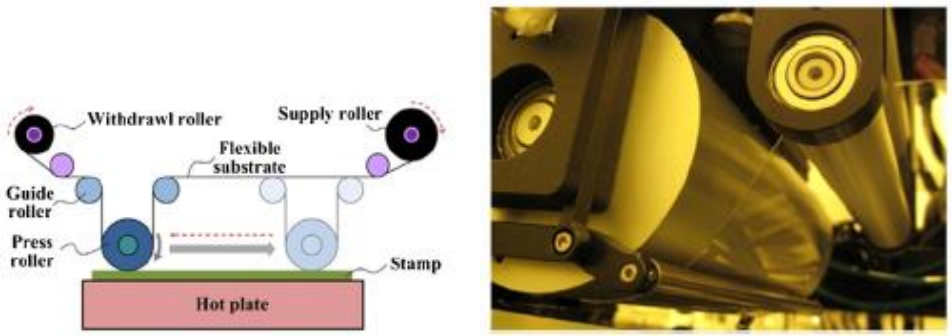


*(a)* *(b)*

*Figure 2.16: (a) schematic representation of R2P system which does not require roll stamp. (b) industrial set up of this system*

In R2P hot embossing higher replication ratio can be achieved thanks to the significant amount of polymer that can flow at high temperature and relatively high imprinting speed and loading pressure.

### 2.3.1.3 Roll-to-roll hot embossing

A typical R2R hot embossing system (Figure 2.17) consists of two rollers and a polymer film in between them. One roller is micro patterned and embeds a heater, while the other is a smooth roller for supporting the substrate.

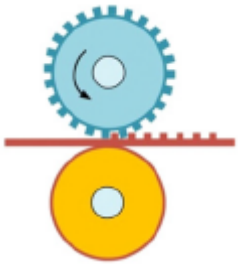

*Figure 2.17: schematic representation of roll-to-roll hot embossing, consist of cylinder mold, smooth roll and a substrate between them*

The heat can be embedded in different ways employing either an infrared heater, or a ceramic heater or an induction heating coil etc. [123]. R2R hot embossing offers high throughput and continuous fabrication of patterns [124]. The R2R method has been used in many industrial applications such as flex printing and gravure printing which is being used in printing of magazines, newspapers and packages. This method is also used for fabrication of micro/nano structures on polymer substrates [125].

R2R hot embossing machines with induction heating coils inside (Figure 2.18) provide a more even distribution of temperature on the surface of the heating roll. The microstructures on the mold can be transferred to the substrate by heating the substrate to its Tg with the induction roll. The molding process by this method is very sensitive to the feeding speed. At high feeding speeds one cannot achieve Tg and poor embossing results are obtained. On the other hand, at low feeding speeds the polymer film melts resulting in tearing. These problems can be overcome by preheating the substrate prior to bonding. The embossed channel depth can be conceivably improved at high embossing pressure and by preheating the polymer substrate [123].

*Figure 2.18: A setup of R2R system with an induction heating coil inside the heating roller*

In most of the R2R hot embossing processes the mold and embossing temperatures are the same. Since there is no cooling phase to freeze the features imprinted by the mold, the demolding of the polymer substrate occurs at the same mold temperature. Consequently, the polymer tends to reflow immediately after separation from the mold. This phenomenon is more frequent at high temperatures. This problem can be circumvented by employing a conveyor belt and local inductive heating to the R2R hot embossing system in order to heat only a local area of the ribbon mold to transfer the features to the substrate [126].

R2R is a continuous batch mode hot embossing process, that is microstructures are continuously imprinted from a roller mold onto a substrate. The imprinting of micro features is mainly depending on process parameters such as roller temperature, feeding speed and applied pressure. Molds with less pattern density offer better replication quality at lower roller temperatures and higher pressure loads, coupled with a preliminary heating at high-temperature [127]. Rolling direction has also an influence on the quality of the micro features obtained. Pile-up of material is higher at the trailing edge than the leading edge [128].

### 2.3.2 Mold fabrication

Mold fabrication is one of the most crucial factors to achieve high quality patterns on the replicas with the hot embossing technology. Mold fabrication methods can be divided into two categories. One is direct structuring methods and the other is lithographic

(LIGA) based methods. Each structuring method has peculiar characteristics and is chosen depending on of the final application. These techniques are capable of producing molds with micro-scaled and nano-scaled patterns.

Direct structuring microfabrication technologies of molds include mechanical milling, laser micro machining, micro discharge machining (µEDM) and electroplating. Direct structuring methods offer the following advantages: ease of operation, shorter processing time, high accuracy, large area fabrication and possibility to fabricate of metallic molds.

LIGA technology is a multi-step micro structuring process. It was developed in 1990s and is seeking industrial scale commercialization. LIGA technology includes X-ray LIGA [129], UV-LIGA [130], E-beam LIGA [131] and laser LIGA [132]. Basic processing steps of this technology are: coating of seed layers with a conductive material onto the substrate surface for the following electroplating step. Deposition of X-ray or UV sensitive polymers onto the seed layers. A mask possessing desired micro patterns is stacked on the thick resist layer. the following step is irradiation with a light source whose wavelength depends on the sensitivity of the material that is used. A replica of the masked patterns can be obtained by disintegration of unmasked materials or dissolution of chemically modified materials.

Electroplating usually takes place in an electrolytic cell in which a cathode and an anode are plunged into an electrolytic bath. A LIGA method for mold fabrication is generally chosen by considering the transmissivity of the mask and sensitivity of the polymer layers to the irradiating beam. LIGA technique enables to create micro patterned molds with features of high aspect ratio. Furthermore, for some applications, a hybrid mold fabrication approach is also possible by combining LIGA and µEDM [133].

### 2.3.3 Hot embossing for LOC fabrication

A wide range of microfluidic lab-on-a-chip devices have been manufactured by hot embossing using polymers as substrate material.

Several researchers have fabricated microfluidic devices by hot embossing. Larry J. Kricka et al., have developed PMMA LOC devices with microchannels (100µm wide, 40µm deep) of variable size using hot embossing with an electroform tool and a silicon master mold. The devices have been tested with semen samples and used for analytical

applications [134]. Vasiliy N Goral et al., presented a poly(dimethylsiloxane) (PDMS)-based hot embossing process for low-cost rapid prototyping of plastic microfluidic devices. They successfully replicated devices for C3A cell culture in 1.5 mm thick polystyrene substrates using a PDMS mold [135]. Ralph Liedert et al., have demonstrated the use of continuous roll-to-roll hot embossing in high-throughput manufacturing of disposable thermoplastic foil-based chips in PMMA. The microfluidic chips served as a platform in a sensitive CE assay to detect an antibiotic resistance indicator mecA gene in S. epidermidis [124]. Asger Laurberg Vig et al., proposed a high-volume fabrication scheme using a roll-to-roll method. They have fabricated microfluidic devices on 95µm thick and 50mm wide cellulose acetate (CA) films. The function of the devices was to separate microspheres of different size (ranging from 0.5 to 5 µm in diameter) through the pinched flow fractionation [136]. Yiqiang Fan et al., demonstrated several Polycaprolactone (PCL) based microfluidic devices using a SU-8 master mold. A single T-junction droplet generator was fabricated and utilized with mineral oil as the continuous phase, and DI water with cresol red as the discrete phase. A diffusion mixer was also fabricated and validated with parallel laminar flow streams of DI water with dyes [137].

# 2.4 Mechanical micro milling

Mechanical milling is a subtractive fabrication method that consists in removing material from a stock piece, generally called as the workpiece, by moving the cutting tool in different directions. The concept of milling was originated in the year 1818 [138]. Micro milling was derived from conventional macro milling. The major difference between micro and macro milling is the size of the cutting tool that is used. Micro milling brings typical tools size less than 1 mm in contrast to the 1 cm tool size of conventional macro milling. In addition, the fragile nature of the micro tool [139], the ratio of undeformed chip thickness to cutting edge radius [140] and the microstructure of workpiece material [141] all bring about the size effect which differentiates micro milling from conventional or macro scale milling. In spite of the cutting tool size, almost all monitoring methods of micro milling are owed from conventional macro milling.

The basic milling system or mill contains (1) a worktable for positioning the workpiece, (2) a cutting tool (commonly using an endmill) and (3) an overhead spindle to attain the motion of the cutting tool (Figure 2.19). In a milling system the worktable

has degrees of freedom in X and Y axes as well spindle has in Z axis and the motions in each direction are adjusted traditionally by hand with cranks and mechanical levers. But modern mills are now able to automate the process by employing computer numerical control (CNC). After the introduction of CNC, milling technology has achieved several advantages such as improving precision and repeatability, adding advanced capabilities (e.g. the direct conversion of computer aided designs (CADs) to final product) and reducing human errors.

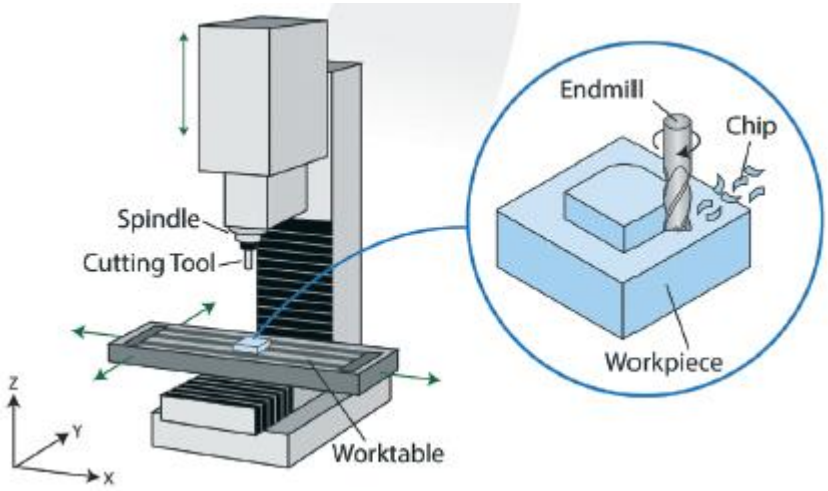


*Figure 2.19: Schematic representation of a basic milling machine consisting of worktable, cutting tool and spindle. Insert represents the milling action on a work piece by an end mill tool apparently producing the chips.*

The CNC capable milling machines have wide range of technical specifications encompassing varying level of stage precision, automation and spindle speed. Advanced CNC mills are versatile and capable to fabricate devices having features size ranging from tens of microns to several meters [142]. Since the wide range availability of cutting tool materials, shapes and sizes [143] mills are manageable to fabricate numerous features in many different materials. The ability of CNC mill to fabricate a part directly from a three-dimensional (3D) CAD model gives a faster and easier conversion of design concepts to working prototypes. The improved technical specifications enable to size down the resolution of features to the micro-scale and leads to the fabrication of more complex parts on the microscale.

Micro milling is generally useful in microfluidics applications mainly for two functions: (1) machining of molds needed for other microfabrication technologies (lithography, embossing, injection molds) [144] and (2) direct machining of final parts

having microchannels and other features. In the latter case micro milling offers a significant reduction of working time to realise the final product from design. For example, a plastic workpiece can be milled into a micro device in less than 30 minutes (the milling time is variable depending upon the complexity of designs).

Large features in common machining materials such as steel and aluminium can be well produced by milling. The technical information regarding the manufacturing is available from online resources, machining books and shop technicians [145]. Furthermore, comprehensive databases are also available for cutting of metals by using multifunctional machines [146]. In contrast, micro milling of non-traditional milling materials like plastics for microfluidic devices is not fully characterized or explored, yet.

Nevertheless, micro milling technique remains unexplored in many ways as compared with other micro fabrication methods. The foremost reason for this is the high start up cost, the need for large lab space and machine size and the need for a special technical expert to operate the system. However, the recent developments in this technique have overcome most of these drawbacks and micro milling is getting more importance in the micro fabrication area.

### 2.4.1 Technical aspects of micro milling

Micro milling has gathered increased interest in microdevice manufacturing due to the wide range of materials that can be machined, versatility, and rapid prototyping capabilities. Micro milling is compatible with metals, wood, and polymers. In particular, it can be used with inexpensive and biocompatible polymers such as polystyrene, polycarbonate, and poly (methyl methacrylate) (PMMA). The major advantage of micro milling is that it can fabricate the final product from a design of microdevice in a single step process. Whereas other techniques such as hot embossing and soft lithography require initial creation of a master mold. As a result, micro milling can produce precise prototypes of test designs. The fabrication time will vary according to the complexity of the design. Apart from the direct milling of final product it can also be used to fabricate the molds for soft lithography, hot embossing and other techniques.

Though micro milling is a promising method for the fabrication of microdevices in various materials, it has also some limitations. In particular, due to the ductile property of polymers, micro milling leads to poor surface finish and burr formation.

Burrs are generated often when cutting soft materials like polymers and it is undesirable for microfluidic devices because they can cause leakage of the fluidic sample, blockage of microchannel and/or undesired flow turbulences.

Micro milling is a major method for machining metals [147] and also commonly used for plastics. Machining of elastomers can also be possible by milling but large elastic deformation of elastomers prevents effective material removal [148]. The brittleness of glass and ceramics makes it difficult to machine these materials since it often leads to cracking, chipping and other defects. While micro milling offers a wide range of feature accessibility with less process steps (complexity).

Micro milling can achieve complex features such as sharp internal corners, rounded surfaces and undercuts by using proper tooling and longer process times. The surface roughness in micro milling is depending on the profile, tool features, wear of the cutting tool and operational parameters chosen for the tool. Reduced surface roughness can be obtained with optimized values of these parameters.

Apart from surface roughness, another important metric of quality is fidelity of feature transfer. When mechanical milling is used for the fabrication of molds for replica technologies, to ensure that the final part has same dimensions as the original design, one must take into account the mold shrinkage. Mold shrinkage is a well-known effect where the parts shrink thermally as a result of cooling. Also, in case of direct fabrication by milling, friction from the cutting tool can cause an increase in temperature which may affect surface quality and feature tolerance. However, in plastic materials these temperature variations are normally localized around the cutting tool and can be mitigated by choosing appropriate cutting parameters (speed and feed rate) and with sufficient use of coolant. The bulk molecular orientation of polymer chains within the plastic materials do not change by milling. The molecular orientation changes only at high temperatures. Therefore, thermal effects do not have a significant role in feature fidelity and tolerance compared to work holding and tool alignment.

Choosing of appropriate micro milling equipment has a significant role in ensuring the desired quality of the end product. Milling equipment can be divided into two major categories: (1) the CNC vertical machining center (the central unit that operates the milling process), and (2) the tooling, which includes the accessories and interchangeable parts that are connected to the central unit.

CNC vertical machining centers well known as mills are available in a wide range of configurations that differ depending on their market price and technical specifications [149]. Several systemas are available on the market: from affordable entry level ones to advanced high precision systems. Despite the availability, choosing a right mill for a particular application is complicated. Most CNC machines are characterized by the following features: (1) work envelope (the area defined by the allowable motion in X,Y and Z directions), (2) spindle speed (the rotational speed of the spindle which holds the cutting tool), (3) feed rate (the translational speed of the stage), (4) power supplied by the motor, which often depends on the speed and used to determine proper feed rates and spindle speeds for machining processes, (5) precision and accuracy, and (6) the automatic tool changer (ATC), (a mechanism which automatically changes the cutting tools during milling, thus preventing the user interventions during the milling process). Several factors like geometrical errors and wear, stiffness errors, kinematic errors and thermal errors are influencing the accuracy of the mill [150]. Amongst these characteristics, cost of the CNC mill machine is mostly depending on accuracy and speed. For example, a basic CNC milling machine with comparatively less accuracy (accuracy of <25µm) can be available around at $15000, while milling machine with high accuracy (accuracy of <3µm) and automated tool alignment may cost more than $200000. In general, CNC mill system can be customized with more feature to improve the accuracy and throughput, but at a higher cost. Most CNC mills that costs more than $100000 usually have integrated systems to align and position the workpiece and cutting tool [149].

End mills are the most commonly used tools. End mills can remove a portion of material from bulk substrate in any axis (i.e., X, Y and Z). They are commercially available in various materials, sizes and profiles (shapes) (Figure 2.20) [151]. The end mills have flutes or sharp helical grooves which wind from the tip of the end mill, thus removal of material takes place. The selection of appropriate number of flutes and helical angle of flutes are depending on the target application and the material to be cut. The size of the end mill is chosen largely depending on the desired feature dimension and its resolution. Because of the vast array of available options, the selection of appropriate material and profile is more challenging. The dynamics and potential errors at the cutting edges is significantly depending on the combination of size, shape and profile of end mills [152]. The ball end mills and square (cylindrical) end mills are called workhorse profiles

and can be use for almost all applications. Simple flat features can be milled by square end mills while milling of additional 3D features such as tapered edges, contoured features and filleted corners are done by ball end mills [144]. The tapered edges and filleted corners can also be created by using tapered and bull nose end mills, which allow to reduce the required cutting time compared to ball end mill. Custom manufacturing of the profile for a particular application is also possible. Drill bits are preferred to machining holes with a depth-to-diameter ratio greater than 3:1. Unlike end mills, drill bit cut only in the vertical Z-direction. The holes can also be easily machined by square end mills. Woodruff cutters are used to produce undercut features in a secondary machining process where an edge or slot is first made using any of the previous tools. The availability of a wide variety of end mill profiles allows to produce direct 3D surface contours, thus enabling the fabrication of complex microfluidic features in a cost and time effective manner. Nonetheless, some geometries such as threads and undercuts remain challenging tasks with micro milling.

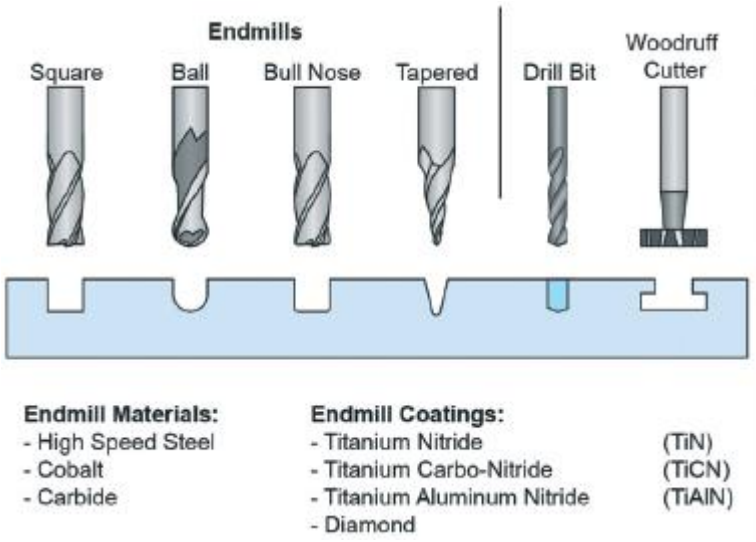


*Figure 2.20: Various type of end mill tool styles for CNC milling*

The most common end mills are made of carbide, cobalt and high-speed steel. In particular, carbide is typically used for micro end mills. Several end mill coatings are available to increase the lubricity and strength, endorse the chip (small pieces of material removed from the workpiece) removal and for boosting the resistance to both heat and wear in order to extend the tool life. Thus, coatings have a significant role in machining tough materials such as stainless steel [153] and should be considered and selected

carefully. But they are not so much critical for machining of soft materials like plastics where heat and wear are much less.

End mills have several physical and dimensional characteristics further than material and profile (Figure 2.21). The maximum cutting depth and minimum channel width are determined by the length of the flute and the cutting diameter, respectively. Generally, it is not possible to mill deeper beyond the flute length. However, special extended- reach end mills are also available, but they are more expensive and less flexible as a result of the length, thus the tool can easily brake while using. Shank is the top part of the end mill and is the part that is inserted into the milling machine. Therefore, the diameter of shank and tool holder or collector in the milling machine must be matched. The helix angle facilitates the removal of chips from the workpiece. Insufficient removal of chips can lead to clogging of the flutes, which generates heat and sequentially causes damage of the device or the end mill or both. Lower helix angle ($30^0$ is the industry standard) [149] is preferred for milling of plastics and other soft materials to avoid the heat accumulation. Lower helix angle improves the chip removal by providing more space between flutes. In addition, the number of flutes is also influencing the chip removal. In case of plastics, end mills having two flutes achieve better chip removal and can be operated at faster cutting speed than four flute end mills. On the other hand, end mills with four flutes provide lower surface roughness than two flute end mills. The cutting center characteristic indicates whether the end mill is able to cut in Z-direction. Non center cutting end mills manage to cut in Z direction and simultaneously have a movement in X, Y direction. This ability can be achieved by cutting with a spiral or ramp like motion. In brief, careful selection of end mill characteristics such as material, size and profile yield high quality parts.

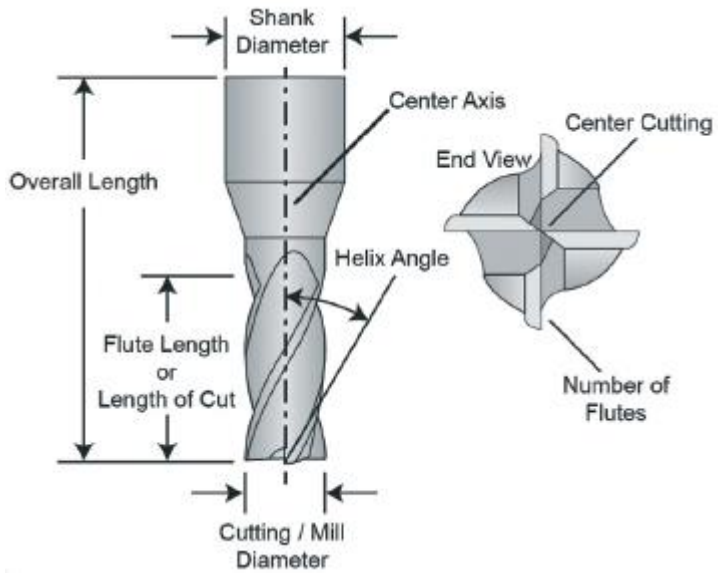


*Figure 2.21: Characteristics of an end mill*

The quality of milled parts can be significantly improved by proper setting the milling process. In particular, tool alignment and workpiece fastening are considered as the most influential factors on quality [154]. Surface roughness is mainly depending on spindle speed and feed rate. Minimum surface roughness can be achieved at optimal spindle speed. The optimized value of spindle speed may vary for each CNC mills depending on the chances of vibration in the machine. In general, surface roughness is inversely proportional to the feed rate [155]. However, there are some studies in which surface roughness is directly proportional to the feed rate [149]. This may also be because of system specific vibrations [156]. Apart from spindle speed and feed rate, depth of the cut has minimal effect on surface roughness. David J. Guckenberger and coworkers have measured surface roughness and resolution of milled microchannels in Polystyrene (PS), PMMA and Cyclic olefin copolymer (COC) by using three different end mill sizes (127, 254, 508 µm diameter). They have obtained surface roughness ranging from 0.420 to 1.52µm as a function of spindle speed and feed rate. Furthermore, the resolution was assessed by comparing actual size of a fabricated feature to its targeted nominal size represents a precision of resolution in pixels (p) =0.79 [149].

Another important aspect about surface roughness is the presence of burrs, that is small burrs that remain sticked to the workpiece after machining [157]. Most commonly burrs appear in ductile plastics (polypropylene or COC) and are prevalent at the edges and side faces of microstructures. Sometimes burrs can occur in brittle plastics (PMMA

or PS), too, but are limited to edges. The burrs can be reduced by some simple tricks [158]. The first trick is the proper choice of one of the two cutting directions, that is referred to as conventional (up) milling and climb (down) milling [159]. In conventional milling the work piece moves directly against the cutting teeth of end mill at the point of contact. So that end mill creates a resistance to the work piece motion and thus milling occur. In contrast, climb milling represents the workpiece moving in the same direction as the rotating cutting teeth at the point of contact, as if the endmill is reducing resistance to the workpiece motion, and "climbing" occurs along the workpiece surface in the direction of travel. To minimize burrs, conventional milling is recommended for non-brittle plastic. Climb milling is preferred for brittle plastics such as PMMA and PS and it can also produce high quality finishes in metals [160]. The second trick is to choose the sharpest tool available. Heat can be generated when using dull tool at high spindle speeds or low feed rates as a result of the high-level of friction. Successively, heat increases the ductility of material resulting in the formation of burrs or it may also lead to melting of plastic and breakage of the tool. The third approach is to adjust the toolpath in order to avoid tool exits, especially for the burrs present on vertical corners [161]. Many of these factors can be adjusted with computer aided modelling (CAM).

Milling resolution depends on setup, operational parameters and mill tolerance specified by the manufacturer. Therefore, resolution can be assessed in terms of accuracy (ability to attain the target dimension) and precision (consistency of the features). Resolution in XY-plane depends only on the technical capabilities of the mill, despite the misalignment.

Like all fabrication methods, micro milling has also its own advantages and limitations. Tool bending induced by increased cutting depth, misdirection of cut, and higher chip loads leads to lower accuracy. However, accuracy can be increased by employing a final finishing cut with low chip load. It further reduces surface roughness but significantly increases the processing time.

For microfluidic applications in which optical transparency is needed such as cell imaging, micro milled devices may not be applicable because of the high surface roughness created by the milling process. However, roughness can be reduced by some surface treatments, but this implies a secondary process. Apart from imaging, a high

surface roughness may also lead to the formation of undesired bubbles at the micro milled surface of microchannels.

The operator is free to perform other tasks once the machine has been initiated for run. But it is recommended to monitor the progress of run frequently to ensure that the run completes without any failure. Fabrication runs do fail rarely, most of the failures occur as a result of avoidable operational issues. End mills with sub millimeter diameter may break during run if there is excessive chip loads or inadequate removal of chips. The end mill breakage can be reduced by using end mills with fewer flutes or by using flood coolant for efficient removal of chips. The breaking of endmills due to excessive chip loads can simply be avoided by reducing feed rate or increasing spindle speed. Finally, other possible issues such as machine vibrations, workpiece vibrations and offsets in workpiece setup perhaps trouble shoot with careful examinations.

### 2.4.2 Mechanical micro milling for LOC fabrication

Micro milling is an alternative method for rapid prototyping microdevices for microfluidic applications. This technique creates microstructures via cutting tools that remove bulk material. Compared to other rapid prototyping techniques, micro milling has some advantages like its fast fabrication time, independence from cleanroom facilities.

The direct conversion of design to a prototype of microfluidic device in a wide range of materials makes micro milling a promising fabrication technology. The use of advanced CNC motor systems along with high spindle speeds and rotational speeds brings micro metric precision in fabrication of microfluidic devices by micro milling. Depending upon the application of microfluidic device CNC micro milling is capable of providing various dimensions of microstructures as well as reduced surface roughness and high resolution. For the past few years many researchers have productively applied micro milling for the fabrication of lab on chip in various materials with different experimental conditions and parameters.

Daniel P. Yen at el., assessed the capabilities of a low cost 3-D mill in polycarbonate material for the production of a microfluidic device. They have fabricated a herringbone micromixer on polycarbonate substrate by micro milling. The device was composed of a 100µm tall, 1mm wide and 30mm long mixing microchannel as well as 100µm tall, 100µm wide herringbone ridges with 500µm lateral period along the channel. A

combination of sanding and vapor polishing yielded a smooth surface with a roughness of 1.8µm [162].

Ampara Aramcharoen et al., have fabricated a microfluidic chip using two materials: PC and PMMA. This LOC prototype was composed of microchannels (straight, spiral and zigzag) and micro pillars. The microchannels on the PC LOC prototype had width and height of 300µm. For PMMA LOC prototype the microchannels had width and height of 50µm and 100µm, respectively. In both cases pillars were characterized by a diameter of 200µm and height of 100µm. For both LOC prototypes a surface roughness of approximately 0.29µm was achieved with minimised burrs [163].

Raquel Lopes et al., have developed a microfluidic device on acrylic glass capable of performing separation of red blood cells (RBCs) from plasma. In this device they have manufactured microchannels with width down to 30µm using micro milling technology [164].

Ali Lashkaripour et al., have designed, fabricated using desktop micro mill, assembled and tested a microfluidic flow focusing droplet generator on polycarbonate with an orifice having a width of 75µm. In this work they were able to achieve a surface roughness of Ra = 0.205µm for the microchannels. This droplet generator was able to produce 0.2nL droplets at a rate of 80Hz [165].

Xiaoyong Ku et al., have proposed a method for rapid prototyping of glass microfluidic devices utilizing a commercial micro milling machine. They have fabricated and tested several types of microfluidic devices such as a Y-shape diffusive mixer with serpentine channel of a rectangular cross-section (300µm x 50µm) and a T-junction droplet generator with stepped channels. The T-junction droplet generator consisted of two small inlet branches that combined to connect with a wider and deeper main channel downstream. The inlet branches were 300µm wide, 50µm deep and 10mm long, while the main channel was 800µm wide, 250µm deep and 43mm long [166].

# 2.5 Femtosecond laser milling

Ultrashort laser is nowadays one of the most important contact-free tools for micro structuring on a wide variety of materials [167], such as metals [168][169], dielectrics [170][171], semiconductors [172][173] etc. [174].

In fact, thanks to the time duration shorter than 10 ps and the very high peak power, ultrashort laser pulses enable new mechanisms of material modification and removal, due to a peculiar timescale characterizing the laser-matter interaction [175]. This allows reaching high quality and precision. Several applications were developed, which have been prevented by traditional micro-machining techniques. Among them, there is the cutting process of ultrathin hardened glass used for displays [176]. Successful manufacturing of tools for medical and biological applications have been reported as well [174][175][176]. Ultrashort laser pulses have been also used in electronics and solar cells industry [177].

The ultrashort laser fabrication of LOC devices represents a niche market, in response to the need to find alternative processes to manufacture these components with high accuracy and high-quality surface finishing. In fact, the fs-laser direct-write techniques appear as an alternative to photolithography in the production of microfluidics devices, especially when customization or rapid design modifications are required.

### 2.5.1 Fs-laser micro-milling: an outstanding ablation procedure

Laser milling is a relatively new machining process that removes material in a layer-by-layer fashion. Femtosecond laser micro milling is emerged as an important technology for applications in material manufacturing, rapid prototyping and component miniaturization. It is an ablation procedure that causes the vaporization of material as a result of interaction between a laser beam and the work piece being machined [178].

Several studies have been focused on the understanding of this phenomenon. An exhaustive theoretical analysis is peculiarly demanding since non-equilibrium physics characterizes particularly in ultrashort laser pulses ablation. Many differences can be noticed between material processing with short and ultrashort laser pulses. Nevertheless, common features can be found. Laser ablation is ignited by the absorption of the laser energy from a focused beam impinging on a solid target. It is necessary for the laser fluence (energy density on the surface) to be above a characteristic threshold value. The ablation threshold depends on several factors: pulse duration, number of laser pulses, repetition rate and target.

In the following, the main absorption mechanisms are shortly described, in order to understand how laser ablation can be ignited. Furthermore, the differences between short and ultrashort laser pulses-matter interaction is explained and the ultrashort laser milling is discussed in deeper. The focus of this brief description is placed on metals and dielectric materials, in particular polymer material was used for the experimental studies of this thesis (Chapter 4).

#### 2.5.1.1 Linear absorption

If a dielectric target is irradiated, linear absorption is possible when the laser photon energy exceeds the energy gap. In this case, photons are absorbed by electrons in the last occupied level in the valence band to reach the conduction band. Furthermore, linear absorption occurs also in case of photons with energy less than the energy gap, as a result of impurities. In metals, the conduction band is partially fulfilled, and unoccupied energy levels are available for electron absorbing laser photons.

#### 2.5.1.2 Nonlinear absorption

In dielectrics, if the laser photons energy is smaller than the energy gap, nonlinear absorption processes can be possible. In particular, multiphoton absorption consists in the simultaneous absorption of multiple photons by an electron. At the end of the process, the acquired electron energy (i.e. the sum of all absorbed photons energy) should be higher than the energy gap. The probability of such a process is proportional to the $m$ power of the beam intensity $I$; in fact, it is necessary to have the simultaneous interaction of $m$ photons with a single electron for having multiphoton absorption. Therefore, the higher the intensity of the laser, the more likely multiphoton absorption is. If free carriers are promoted in the conduction band (e.g through multiphoton absorption), they may act as seed electrons for avalanche ionization which is based on free carriers absorption and further impact ionization. This means that seed electrons can acquire energy higher than the last available level in conduction band by sequentially absorbing laser photons; consequently, they ionize the atoms of the lattice, thus generating other electrons in the lowest conduction band level.

The so produced free electrons are responsible for strong absorption of laser radiation and for subsequent material removal. In the Figure 2.22, the three presented absorption process are sketched.

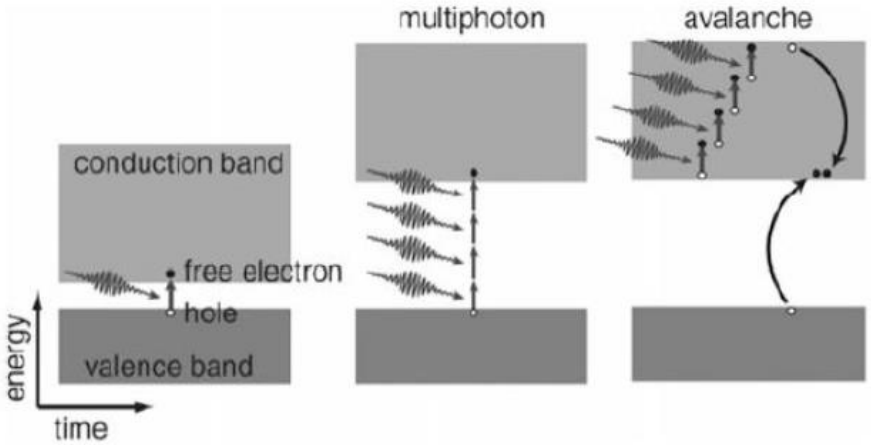


*Figure 2.22: Achievable absorption mechanisms in femtosecond laser ablation. For metals and material with energy gap smaller than the photon energy, linear absorption (left side) dominates. If the energy gap is higher than the photon energy, multiphoton absorption (central figure) and avalanche ionization (right panel) can be possible [179].*

### 2.5.1.3 Short and ultrashort laser pulses ablation process and timescales

When a laser beam impinges on materials surface, it interacts firstly with electrons, which absorb the laser energy. Then, the electron sub-system is subjected to a rapid increase of temperature. Through scattering phenomena, the absorbed energy is transferred to the lattice [175][180]. The pulse duration $t_p$ can determine the time to deposit the absorbed laser energy in the irradiated material. In order to understand the main difference between short and ultrashort laser pulses ablation it is necessary to introduce two temporal scales: $t_e$, the electron cooling time and $t_{e-ph}$, the electron-phonon coupling time. Depending on the pulse duration, it is possible to distinguish between short ( $t_p > t_{e-ph}$) and ultrashort regime ($t_p < t_{e-ph}$).

In order to remove an atom from a solid by the means of a laser pulse one should deliver energy in excess of the binding energy of that atom. Thus, to ablate the same amount of material with a short pulse respect to an ultrashort pulse, one should apply a larger laser intensity approximately in inverse proportion to the pulse duration. Following

ionization, the laser energy is absorbed by free electrons due to *inverse Brehmstrahlung* and resonance absorption mechanisms and does not depend on the initial state of the target. Consequently, the interaction with both metals and dielectrics proceeds in a similar way which contrasts to the situation for a long pulse, where ablation of metals occurs at relatively low intensity compared with that for a transparent dielectric whose absorption is negligibly small [181].

When an ultrashort laser pulse ($t_p$ is of the order of femtoseconds to ten picoseconds) impinges on a material, the electron system reaches the thermal equilibrium only after a few hundred femtoseconds, when the electrons thermalize. Then, the electron sub-system can be described by a temperature $T_e$. A time interval ranging from 1 ps to 100 ps (i.e. $t_{e-ph}$, the electron phonon coupling time) is necessary for the electron system and the lattice to reach thermal equilibrium. In the meantime, the temperature of the lattice $T_l$ remains almost thermally unaffected. Each sub-system of the irradiated material (i.e. electrons and lattice) stays in thermal equilibrium, though having two different temperatures. Therefore, the evolution of the temperature of the electron system and the lattice needs to be studied separately, by means of the Two-Temperature Model (TTM) based on the model proposed by Anisimov in 1974 [182].

In Figure 2.23, the temporal evolution of the electron and lattice temperature is presented, for ultrashort laser pulses irradiation of copper. The electrons are more energetic than lattice for a time interval of about several picoseconds and reaches thermal equilibrium with lattice only after a time interval comparable with the electron-phonon coupling time. So, in case of ultrashort laser pulses, a melting free ablation process is possible if the applied fluence is high enough. Therefore, the process is referred to as cold ablation and the removal process is due to direct vaporization of material from solid state.

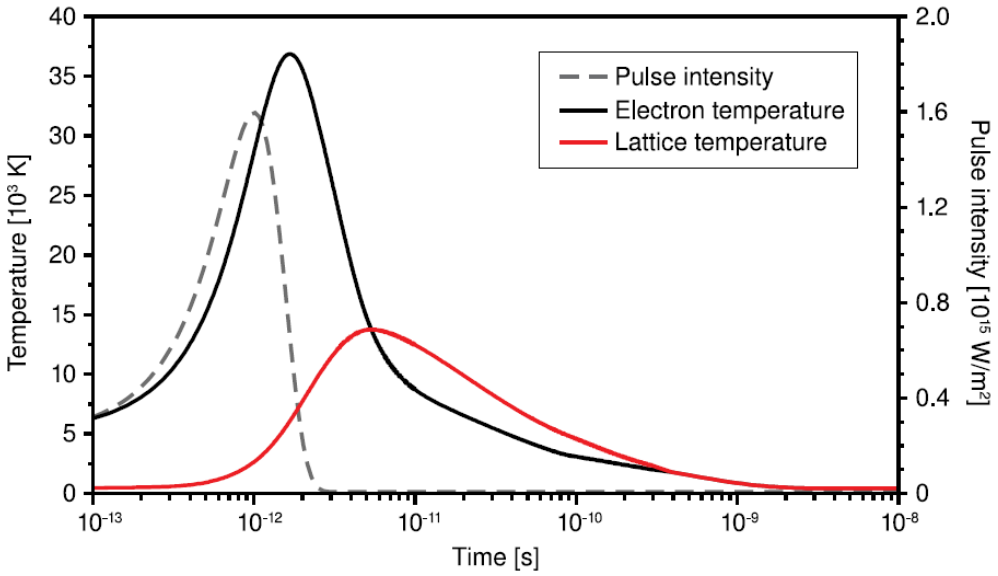


*Figure 2.23: Simulated trend of electron system and lattice temperature in copper. In the figure, the dashed profile indicates the laser pulse. The duration of the pulse is equal to 1 ps [183].*

If the pulse duration is longer than the electron-phonon coupling time ($t_p$ > 10 ps), the heating process of electrons is comparably slower, while the relaxation process is faster. The energy is almost instantaneously transferred to the lattice. In fact, in case of short laser pulse irradiation, heat diffusion already occurs during irradiation. Consequently, the whole system will reach the thermal equilibrium already during the laser pulse.

In this case, the main energy loss process is due to the heat conduction in the target and then the material is first melted. If the fluence of the beam is high enough, it is vaporized beginning from the melted state.

Furthermore, two distinct ablation regimes can be observed according to the incident laser fluence [184]. At lower laser fluences, the density of hot electrons is too low, and the energy transfer out of the optical penetration zone, typically on the order of a few nanometres depth, is negligible. A so-called gentle ablation regime is established with lower ablation threshold and reduced material removal rate. For higher-pulse energies a second ablation regime appears. In this regime, the influence of electronic heat conduction becomes important. The absorbed laser energy cannot be stored in the interaction volume defined by the optical penetration depth δ, but diffuses deeper into the metal target. The effective heat penetration depth $l$ is in the range of several tens to hundreds of nanometres. A strong ablation regime takes place, characterized by an

increased material removal rate and higher ablation threshold. The first ablation regime, dominated by the optical penetration depth, is only accessible if femtosecond pulses are used and is not observed for longer pulse durations. During gentle ablation with fs-pulses at relatively low laser fluences, the role of thermal diffusion is significantly reduced, which is important for precise micro structuring of metals. So, it may be stated that, in comparison to short pulsed lasers, ultrashort laser ablation has many advantages.

In Fig. 2.24 nanosecond and femtosecond pulsed laser are compared [185]. Avoiding thermal effect, fs-laser yields precision materials processing resulting from efficient energy deposition, while simultaneously minimizing heat conduction and thermal damage to the surrounding material [186]. The absence of melting and recast layers makes the micromachining clean and accurate with smooth edges, moreover the absence of debris makes post-processing surface cleaning unnecessary. These benefits product development by reducing risk and time to market, thereby increasing product competitiveness, improving performance and reliability [178][187].

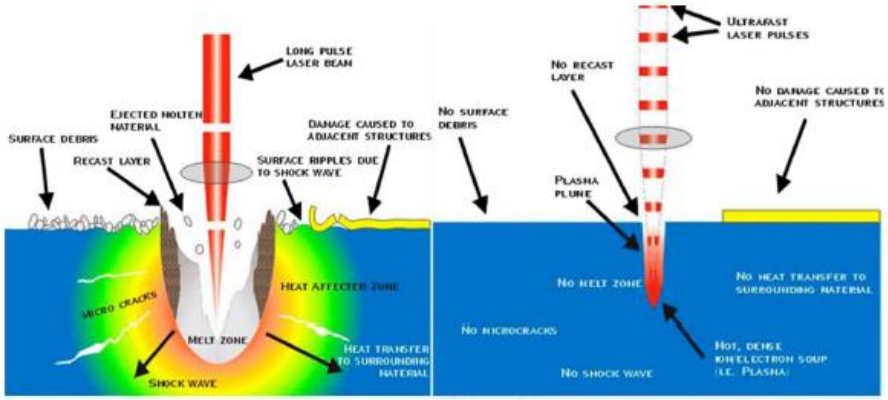


*Figure 2.24: The effects of a nanosecond pulsed laser compared to a femtosecond laser [185].*

Several research groups have investigated femtosecond laser micromachining of basic geometric features on a variety of materials such as borosilicate glass, silicon [186], fused silica [188][189], aluminum [189], copper [169], lithium niobite [190], nitinol [30], stell [191], PMMA [192], confirming the high quality of the microstructure obtained.

### 2.5.1.4 Ultrashort laser milling

Laser milling or engraving allows fabricating micro-components of complex 3D shapes. Starting from the bulk workpiece, the micro structuring process is realized by

precisely removing the material via laser ablation in a layer-by-layer fashion. The 3D structure to be fabricated is divided into several slices by a suitable CAD-CAM software. Each slice is removed with a path of parallel or crossed lines, whose geometry and spacing defines the hatching strategy. This can be achieved by keeping the focused laser beam fixed and moving the work-piece underneath though a Computer Numeric Control (CNC) system or rather by scanning the laser beam over the surface of the work-piece which is positioned in the beam focal plane by one of the machine axes. In the first case, positioning of the laser beam is very accurate and its energy is delivered quite uniformly over the whole working area, but the moving speed is limited by the machine dynamics. The second approach is more flexible and ensures high scanning speeds for increased productivity. Here, the laser beam is directed onto the sample by two folding galvanometric mirrors. The main disadvantage of this method is that the energy delivered by the laser beam onto the sample surface may change according to its angular deviation from the optical axis. The effective working area is limited by the optics. Hence, in order to machine larger pieces, repositioning of the workpiece is required which may introduce precision errors.

The laser pulse duration and the repetition rate regime have a direct impact on the accuracy of the laser milling process and on the quality of the micro structured surfaces. In case of metals, it has been found using nanosecond or longer laser pulses that the removal rate is high but the excessive thermal load delivered onto the working area causes burrs, micro-cracks, uncontrolled surface roughness and a considerable layer of molten material which, once re-solidified, leads to rounded edges [175] detrimental to the process accuracy. Furthermore, for laser pulses longer than the plasma plume extinguishing time (typically of a few tens of nanoseconds [193], the trailing part of the incoming pulse is absorbed, leading to a decrease of the ablation efficiency. Laser milling with femtosecond pulses provides high precision and reduced thermal damages and/or structural modifications of the irradiated surface. Moreover, it has been demonstrated that the threshold fluence decreases as the pulse duration is reduced [194]. It has been further observed that the ablation rate per pulse is higher for femtosecond pulses compared to picosecond ones [195], probably because the energy penetration depth increases for shorter pulses. Indeed, a reduction of the pulse duration from 10 ps down to 500 fs has improved by 75% the ablation efficiency of copper and steel samples during laser milling

experiments performed under similar conditions [196]. Even in the ultrashort pulse regime it is always advisable to work with near threshold fluences because for higher fluences the ablation mechanism is once again dominated by melting [175]. However, a trade-off between high removal rates and the processed surface quality has to be found. A possible solution would be to work with large spot areas as well as multi-spots. Another way to overcome this limitation is to employ laser sources with repetition rates higher than several hundred kHz up to the MHz regime [197]. Experimental results reveal that the process efficiency (ablated volume per Watt of incident laser power) increases with the repetition rate, probably due to heat accumulation which facilitates the ablation mechanism [198]. Employing an appropriate laser milling strategy may help to minimize the thermal load and prevent melting due to heat accumulation even when working at repetition rates in the MHz regime. Several studies have clearly shown that the process strategy significantly affects the resulting surface quality and edge sharpness [199][200]. In particular, the surface roughness and its homogeneity are highly influenced by the line pattern scanned by the laser beam. If the lateral distance between the lines is too wide, a wavy structure is obtained characterized by deep grooves resulting in a high surface roughness. Conversely, if the line spacing is considerably smaller than the spot size, the formation of irregular conical microstructures may affect the surface roughness of the processed surface. This phenomenon is more evident at low scan speeds and high laser powers and is attributed to local melting of the surface induced by heat accumulation due to the high spatial overlap between consecutive pulses at high repetition rates [201]. Experimental studies on stainless steel and copper have shown that to obtain a homogeneous surface with sub-micrometer roughness, the line distance should be about half the spot radius and the pulse-to-pulse overlap should be typically in the range of 30% [200][202]. This implies moving the beam at several tens or even hundreds of meters per second when working with laser sources operating in the MHz regime. This would allow distributing the incident laser power over an adequate surface to prevent heat accumulation. For this reason, novel techniques to deflect the beam at high speed, as well as a new generation of scan heads like polygon scanners are being developed. Enlarging the focused spot size improves the surface homogeneity but reduces the achievable precision. Splitting the energy of intense femtosecond laser pulses into groups of pulses with close temporal distance (so called bursts or pulse trains) so that each pulse is well

above the ablation threshold, but still in the range of low-fluence ablation regime, is another technique which may be employed to improve the ablation rate preventing heat accumulation at relatively high laser average powers [202]. The so-called burst mode exploits the incubation effect to increase the material removal rate. An undesired side-effect of 3D laser milling is the inclination of the micro-structure sidewalls. Such wall angle increases with both higher laser power and deeper ablation depths. This defect can be mitigated working with linearly polarized light oriented parallel to the sidewalls or implementing suitable acceleration and deceleration sections at the edges of the machined structures [201]. The accuracy of the laser milling process at the sidewalls can be enhanced also by synchronizing the pulse train repetition rate to the beam guiding system in order to start each line of the pattern with the laser spot always in the same point. In conclusion, high precision laser milling of complex 3D micro-structures can be realized exploiting the advantages of the femtosecond laser technology by choosing the appropriate set of laser parameters and a suitable machining strategy.

### 2.5.2 Femtosecond laser ablation for the fabrication of lab-on-a-chips

Femtosecond laser micromachining by direct ablation process has long been considered as a powerful tool for the fabrication of microstructures on various materials. Ultrafast laser micromachining with the programmable processing capability is being used for the rapid prototyping of lab on a chip (LOC) devices. The designed patterns to be machined can be prepared on the program software despite of the complexity of design. The LOC fabrication by direct femtosecond laser ablation is realized by irradiating the substrate with the pattern either by translating the laser beam using Galvanometer-controlled scanning mirrors and flat field lenses or by translating the substrate through a three-dimensional XYZ translational stage. Automation of the movement of laser beam via a galvo scan head or XYZ translation stage can be done by integrating a CAD-CAM software.

Several parameters are involved in a direct femtosecond laser micromachining process. They can be categorized major into four: (1) laser beam parameters, (2) sample parameters, (3) scanning parameters, (4) processing parameters. Laser beam parameters

include the average power, the pulse energy, pulse duration, beam profile, wavelength, pulse repetition rate, beam diameter and polarization of the light. The physical-chemical characteristics of the substrate material and its surface roughness are considered as sample parameters. The scan velocity, scanner/stage distance from the focusing lens, number of scans, overlap and angle of incidence are summarized as scanning parameters. Processing parameters include micromachining environment, gas pressure, mobility of the sample relative to the laser and temperature of sample. All the parameters may vary according to the layout of the microfluidic device. In particular, the laser parameters (wavelength, pulse duration, pulse energy, repetition rate) and material parameters (bandgap, thermal properties) have significant influence on the structure morphology in the fabrication of microfluidic chips. Irradiation with ultra short pulses at low fluence close to the ablation threshold yield high quality material processing and surface roughness in the range of few tens of nanometers without any visible mechanical and thermal damages.

Several researchers have established femtosecond laser technology as a viable tool for the fabrication of lab-on-a-chip devices in various materials such as glass, fused silica and thermoplastic polymers etc.,

Ya Cheng et al., developed a micro mixer consisting of Y branched microchannels in glass for LOC applications [203]. Yang Liao et al., demonstrated a passive microfluidic mixer consisting of geometrically complex 3D microchannels in glass, which showed superior mixing efficiency as compared to 1D microfluidic channels [204].

F. Bragheri et al., presented a microfluidic device in fused silica acting as an integrated micro fluorescence activated cell sorter (microFACS) for analysis and sorting at the single cell level, allowing the isolation of subpopulations with high selectivity from a heterogenous cell sample. The cell sample constituted of human transformed fibroblasts transfected with a plasmid encoding the enhanced green fluorescent protein [205]. Allison Schaap et al., fabricated a optofluidic device comprises a straight microchannel with a curved waveguide in fused silica, that can detect, monitor and qualitatively distinguish algae species free flowing in a water stream [206].

Annalisa Volpe et al., reported femtosecond laser microfabrication of a PMMA inertial microfluidic sorter that enabled to separate particles based on their size and provided an enhanced throughput capability of capture efficiency (> 80%) of large beads. The LOC device consisted of a microchannel with expansion chambers provided with

siphoning outlets [207]. The same research group fabricated and assembled a PMMA microfluidic optical stretcher for the manipulation of single cells. They combined femtosecond laser micromachining and micro-injection moulding [208] technologies for the fabrication of the device. R. Martínez Vázquez et al., have demonstrated a plastic optofluidic chip with integrated microfluidic and optical excitation/detection functionalities fabricated by femtosecond laser micromachining. The integrated chip consisted of a microfluidic channel probed by fibers inserted in fiber groove channels with binary Fresnel zones formed on the opposite surface for capturing fluorescence [209]. They have also fabricated a lab on chip with the combination of femtosecond laser micromachining and micro injection moulding for counting fluorescent micrometric particles. The complete platform was coupled with a mobile phone and allows performing point of care fluorescence analysis [210].

# 2.6 Bonding of thermoplastic microfluidic devices

Bonding techniques for the assembly of microfluidic devices can be classified into indirect and direct bonding methods. In the former case, adhesive layers are used to bond two substrates having microstructures in one or both substrates fabricated by different micromachining procedures. In contrast, direct bonding methods do not use any additional material at the interface between the two substrates. In direct bonding technique, the bulk polymer substrates itself comprises the adhesive.

## 2.6.1 Indirect bonding

### 2.6.1.1 Adhesive bonding

Sealing of thermoplastic microfluidic chips using adhesive bonding techniques have been used widely due to its simplicity. One of the simplest adhesive bonding techniques is the use of glues, i.e. liquid adhesives that set through the evaporation of solvent, or epoxies and acrylates that cure (polymerize and crosslink) after mixing with a catalyzing agent. A very common approach is to apply a thin layer of a high viscosity adhesive liquid at the interface between the thermoplastic substrates to bond. After exposure to UV light the adhesive gets cross linked to become a bond between the

substrates. Synthetic resins containing photo initiators at specific wavelengths of light are generally used.

In all adhesive boding techniques, there is the risk of microchannel clogging. Channel clogging may happen in many ways for example adhesive materials used for bonding may remain in the channel and make a constrain or block the fluid flow and, especially when using heating and pressure for adhesive bonding, the channel may get damaged. Several approaches were found in past years to overcome clogging of microchannel when using adhesive bonding.

A contact printing process in which adhesive layer can be precisely controlled by the stainless-steel plate having a hole inside (hollow) and use sacrificial channel network design to remove air bubbles and excessive adhesive, ensuring that the adhesive cannot enter the channels (Figure 2.25) [211].

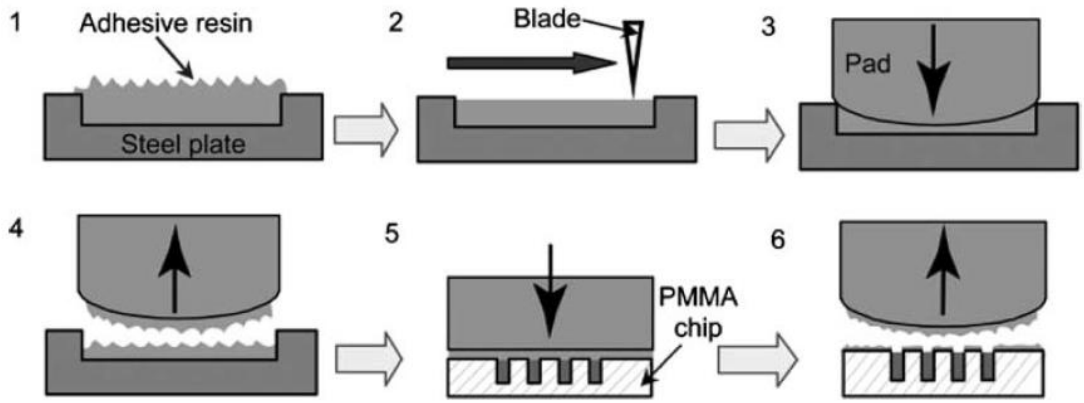


*Figure 2.25: Adhesive application using a contact printing process. Adhesive was poured on steel plate with a having hole inside and spread over the plate using a blade (step 1, 2). Adhesive was applied on the rubber pad (step 3, 4). The adhesive on the rubber pad was deposited on the PMMA chip, the adhesive thickness on PMMA chip was nearly one fourth of the hollow depth and excessive adhesive was removed by sacrificial channels (step 5, 6). [211].*

A further benefit of this approach is, with the exception of the exposed thickness of the adhesive layer, the resulting microchannels possess homogeneous surface properties. Screen printing of cover plate for applying adhesive to the surface before bonding have also produced same results [212]. In this approach, a precise alignment is required between microchannels and adhesive patterns, which is a considerable challenge.

Bonding by means of lamination films have been considered as another common method for adhesive bonding [213]. Lamination films are available in both solvated liquid as well as dry film. The dry lamination films are less expensive and easy to use. Commercially available lamination films have thickness as low as 40µm. This method of bonding does not need any experimental procedures or any other instrument. The process has the advantage of high throughput and scalability, thus it is suitable for mass production. Another approach of thermoplastic microfluidic bonding is also a kind of lamination but by thermally activated adhesives. A polymer layer coated with an adhesive resin is used as the thermal lamination film. At elevated temperatures from the range of $100^0$C to $150^0$C the lamination film gets activated and gives rise to bonding.

Some other variants of lamination bonding methods being used are, adhesive lamination film of COC sheet plasticized by a solvent mixture [214]. A 7.5% v/v mixture of hexadecane in isopropanol has been used as the solvent mixture [214]. An uncrosslinked photo patternable resin (SU-8) has been spun onto a PET dry lamination film using as laminating layer on a cross linked SU-8 having microchannels [215]. In a related lamination process, standard laser printer toner was used as a binding agent, allowing printed transparency films to be bonded by thermal lamination with the toner acting as both adhesive and microchannel sidewalls [216].

## 2.6.2 Direct bonding

### 2.6.2.1 Thermal fusion bonding

Direct thermal bonding takes place by elevating the temperature of one or both substrates being joined to near or above their glass transition temperature $T_g$ and parallelly applying a pressure to get enough contacting force between the mating surfaces. A sufficient polymer flow happens at the interface and achieve intimate contact due to the applied temperature and pressure. The polymer chains of both substrates at the interface inter-diffuse leading to a strong bond. Under ideal conditions, the bonding strength can achieve values comparable to the cohesive strength of the bulk material. Direct thermal bonding offers the advantage of homogeneous surface properties for microchannels due to the usage of identical materials for the patterning microchannel and the capping layer. The simplicity of the bonding approach and higher bonding strength have made direct

thermal bonding as one of the most common methods for sealing of microfluidic devices in many applications.

Thermal fusion bonding is already used for various thermoplastic materials such as polycarbonate (PC) [217], PMMA [218] and COC [219] depending on the application and requirements of the microfluidic device. Furthermore, thermal fusion bonding has also been successfully applied to polymers including polystyrene, nylon, polysulfone [220], copolyester [221] and several fluoropolymers [222]. Thermal fusion bonding can also be used to bond dissimilar materials mostly in a low temperature condition [223]. Thermal bonding of dissimilar materials is achieved preferably on thermoplastics with similar glass transition temperatures. The bonding takes place by setting the bonding temperature near or above the $T_g$ of the material having lower $T_g$ to prevent channel distortions.

Channel deformation caused by unoptimized temperature and pressure is a major challenge in thermal fusion bonding. To achieve high bonding strength and limit the deformation of microchannels it is necessary to control temperature, pressure and time duration. Thus, the use of a programmable commercial hot press [224] and roller laminator [225] are recommended. In a commercial hot press, the critical step is selecting the process parameters (to be configured for each different application) to limit the channel deformation during the bonding. Due to variations in $T_g$ of different material grades of specific thermoplastic types, a significant adjustment of the parameters is needed for bonding. Moreover, to get optimal bonding one should keep the substrate as much flat, clean and dry as possible. A cleanroom environment can prevent the chances of trapping tiny particles inside the sealed microchannel.

In order to reduce the prospect of channel collapse during thermal bonding, several practices have also been developed. For thermoplastic substrates it has been found that elevating the temperature above $T_g$ while applying a lower pressure [226] or applying high pressure at temperature well below $T_g$ [219] allows reducing the channel deformation and attaining a stable bond.

#### 2.6.2.2 Solvent bonding

Solvent bonding is one of the several methods of adhesive bonding. The mating surfaces of bonding substrates are solvated and softens the polymers at the interface. The

polymer chains become mobile and readily diffuse across the solvated layer leading to intertwining of the polymer chains and resulting in a strong bond. Solvent bonding can be a high throughput process, which can be easily scaled from prototyping to mass production depending on the specific approach employed. The solvent can be applied in liquid or in vapor phase to the polymer substrates. A chemical acts as a solvent for another substance when there is no propensity for the molecules of the materials to set apart from one another, that is if the total molecular attraction force between dissimilar materials exceeds the attraction force of the material itself [227]. Solvent bonding of thermoplastics takes advantage of polymer solubility in order to secure the entanglement between polymer chains at the interface. Solubility of polymers in organic solvents can be appropriately described by the Hildebrandt Parameter (d), which is defined as the square root of cohesive energy density for each molecular system [228].

The cohesive energy is defined as the attractive molecular forces and can be calculated starting from the material's vaporizing energy ($U_{vap}$), that is the difference between the latent heat of vaporization (.$H^0$) and the mechanical work resulting from the evaporation. The product of the gas constant (R) and the absolute temperature (T) is approximately equal to the mechanical work resulting from the evaporation (latter term). Therefore,

$$U_{vap} = .H^{0} - RT$$

The vaporizing energy divided by the molar volume of the solvent (m) gives the cohesive energy density. The square root of cohesive energy density provides the Hildebrandt solubility parameter. That is,

$$\delta = [(.H^0 - RT)/v]^{1/2}$$

The unit of Hildebrandt solubility parameter is $(J/cm^3)^{1/2}$ or $MPa^{1/2}$ and gives the measurement of cohesive molecular forces for both solute and solvent. The molecules of each material can easily coexist if the materials have similar cohesive forces which leads to dissolution of the solutes in solvents[228].

For amorphous non-polar polymers, the cohesive forces between the materials can be approximated as the geometric mean of the individual cohesive forces. Therefore, when the Hildebrandt solubility parameters are similar or equal to another material, one of the given materials will act as a solvent for another [227]. The solubility parameters of common thermoplastic polymers and organic solvents are summarized in Table 2.1. [227].

**Table 2.1. Solubility parameters for few thermoplastic polymers and organic solvents**

| **Thermoplastic** | **Solubility parameter ($\delta$) [$(J/cm^3)^{1/2}$]** |
|---|---|
| **PTFE** | 12.6 |
| **PE** | 16.3 |
| **PP** | 16.3 |
| **COC** | 17.7 |
| **PMMA** | 20.1 |
| **PS** | 18.7 |
| **PVC** | 19.4 |
| **PC** | 19.4 |
| **PET** | 21.8 |
| **Solvents** | **Solubility parameter ($\delta$) [$(J/cm^3)^{1/2}$]** |
| **Cyclohexane** | 16.7 |
| **Methylene dichloride** | 19.8 |
| **Ethylene dichloride** | 20.0 |
| **Acetone** | 20.4 |
| **n-Hexanol** | 21.8 |
| **Isopropanol** | 23.4 |
| **Acetonitrile** | 25.1 |
| **Ethanol** | 26.0 |
| **Dimethyl sulfoxide** | 26.7 |
| **Methanol** | 29.6 |
| **Water** | 47.7 |

From the Table 2.1, it is understood that there are several solvents available for various thermoplastics. PMMA is a typical material suitable for solvent bonding. Majority of the solvents in the Table 2.1 have been already demonstrated suitable for bonding PMMA, like e.g. ethanol [229], methanol, isopropanol [230], acetonitrile [231], dimethyl sulfoxide [232], ethylene dichloride [233]. By controlling the solvent composition, exposure time and temperature, it is possible to increase the bonding strength. On the other hand, an excessive quantity of solvent affects the bonding strength and increases the chances of solvent residue in the microchannels, which is a challenging setback of solvent bonding.

#### 2.6.2.3 Localized welding

The use of ultrasonic energy for inducing heat and softening at the interface between the 2 substrates is a popular non-adhesive and non-mechanical method for bonding at the macroscale thermoplastic components. A benefit of this approach is that the energy can be applied locally to specific regions to be bonded or globally to all mating surfaces to get a uniform bonding [234]. By using a commercially available welding system operating at 35KHz, ultrasonic welding has been efficiently demonstrated on PMMA and Polyether ether ketone (PEEK) microfluidic devices [235]. The precise bonding of the substrates by ultrasonic bonding is achieved by optimizing the welding parameters comprising force, power and time.

The use of microwave energy to heat embedded metal films between the desired surfaces to be bonded is an alternative way to achieve localized welding on thermoplastics. Few researchers have achieved localized bonding by microwave energy [236] with an embossed PMMA having a 100nm layer of chromium/gold covered by a 100nm metal film and placed in a microwave chamber operating at 2.4GHz. The incident RF energy was absorbed by the metal film and guided to melting of gold layer, thus achieving localized bonding of the polymer substrate.

Localized bonding of thermoplastic microfluidic chips has also been attained via infrared (IR) welding [237]. An IR transparent thermoplastic microfluidic chip was sealed with an opaque thermoplastic substrate by focusing a 1100nm laser beam at the interface

of the substrates. The heat produced by the laser beam lead to the localized bonding in between them.

Even though localized bonding of thermoplastics can be obtained with different techniques, there are several reasons for not adopting this method for assembling microfluidic devices. In spite of the advantages offered by the ultrasonic bonding, like e.g. compatibility with any thermoplastics, ability to bond dissimilar plastics as well as plastics to other materials like metals, unfortunately, this method requires special chip designs to productively direct and focus the energy at desired bonding surfaces. This limits the use of ultrasonic bonding for prototyping of microfluidic chips. In the case of microwave RF energy bonding the requirement of an additional step for metal deposition introduces restrictions in the fabrication process and the metal itself could contaminate the microfluidic device or behave as an electrical shunt, which is not suitable for many applications. Different absorption behaviour of the substrates to the laser wavelength may also impose unwanted constraints in laser bonding technique [212].

#### 2.6.2.4 Wax bonding

The oldest thermoplastic material known to human being is wax (beeswax). Hot melted waxes can be used to coat the substrates and bond them together after cooling. In comparison to other homogenous chemical compounds, beeswax does not melt instantly upon heating but undergoes several intermediate states (solid-plastic−semi plastic−semiliquid-liquid), starting from a temperature of 40°C and fully melt at about 64°C [238]. Wax is well suitable for low temperature bonding because of this unique melting behaviour. Ironically, beeswax is a renewable natural material. But the chemical composition of beeswax differs depending on the species of bee and its geographical origin [238].

In wax bonding both the microstructures and adhesive are with wax. The microchannels are defined by the space between the two glass substrates. A specially developed decal-transfer microlithography can be used for producing wax pattern on a glass substrate at dimension down to 25µm. The wax patterned layer covered with a plane glass substrate can represent a complete microfluidic device. Effective glass-wax bonding has been achieved at $40^0$C temperature with a soft pressure without needing any pre surface treatment for glass [238] relying on the special melting behaviour of waxes.

Moreover, wax bonding offers an effective sealing for microfluidic devices even if the microfluidic network is on a non flat glass substrate.

### 2.6.3 Surface treatments and modifications

Increased surface energy provides a number of advantages in thermoplastic bonding technology. Enhanced wettability of mating surfaces enables more intimate contact and eventually improve the mechanical interlocking and interdiffusion of the polymer chains at the bonding interface. Higher surface energy can also offer a higher bonding strength through the generation of electrostatic interactions. Surfaces with high-specific energy can create hydrogen or covalent interface bonds when they are in the form of polar functional groups and are able to provide the bonding strength to surpass the cohesive strength of the bulk polymer. In macro scale polymer engineering, surface treatments are widely used to increase the surface energy before bonding. Different surface treatment approaches include solvent or acid treatment [239], surface grafting [240], and both vacuum [241] and atmospheric [242] plasmas.

Plasma activation is typically used in microfluidic applications to modify PDMS surfaces with silanol groups [243], which result in covalent bonding between the elastomer matting layers. It has also been widely applied to thermoplastic microfluidics. Energetic ions, electrons and UV photons can have enough energy to break down chemical bonds on the target surface and create highly reactive free radicals, which help to form desired charging surface groups and increase the total energy density of the surface. Plasma modification has been used to fabricate thermoplastic microfluidic chips at reduced processing temperature but with improved bonding strength. Various thermoplastics has been already successfully joined by plasma surface modification, including PMMA [232], COC [219], PC [244], PS [224] and PET [245] and using both oxygen and atmospheric air plasma.

The application of ultraviolet light is a simpler alternative to plasma activation for the enhancement of thermoplastic surface energy. UV energy exposure to the thermoplastic surface results in photodegradation due to photo-oxidation and polymer chain scission at the surface [246]. Generally, an exposure of light in the range of 300-400 nm is sufficient to break the chemical bonds in thermoplastics [247]. The chain scission of polymers leads to the formation of lower molecular weight radicals in addition

to the reduction of glass transition temperature at the UV exposed polymer surface. The optical absorption range of the polymer determines the thickness of the modified polymer layer, while the thermomechanical properties of the bulk polymer remain unchanged. By UV exposure the Tg of the PMMA can be reduced below to its original Tg value [212]. This allows to successfully bond microfluidic chips at temperatures well below the Tg of the bulk polymer with less channel deformation and without reducing the bond strength. The same method has been successfully practiced attaining low temperature bonding of various PMMA [248], PC [249] and cellulose acetate [250] microfluidic chips.

A combination of UV light exposure and photogenerated oxygen radicals has also been demonstrated as a suitable surface treatment that improves bonding. By this method a thermoplastic microfluidic device has been bonded at low process temperature with an exceptionally high bond strength [251]. This approach is based on a UV / ozone exposure technique and was originally developed as an alternative to oxygen plasma ashing [252] for the removal of organic contaminants from semiconductors. The UV/ozone exposure can increase the surface energy of the polymer by breaking polymer chains and insert oxygen containing functional group [253]. UV/ozone treated polymer surface offer a bond strength comparable to the one achieved on the untreated surfaces heated at the glass transition temperature. Sometimes UV/ozone treated surfaces can achieve 10-100 times higher bond strength than their mother counterparts [212].

Comprehensively, the bond strength of thermoplastic microfluidic devices can be increased by surface treatments either by plasma, UV, or UV/ozone exposure. UV or UV/ozone treatments can be used to activate the surfaces prior to thermal bonding in practical prototyping, considering the high throughput and minimal equipment required. Commercial UV/ozone instruments are much cheaper than the plasma systems.

Another important consideration is the effect of surface modifications on the microchannel wall chemistry. The enhanced hydrophilicity may allow simple channel formation through surface tension driven wetting, whereas unwanted electrostatic interactions with analyte molecules and excessive or poorly controlled electro-osmotic flows can be produced with charged surface groups resulting from plasma, UV or UV/ozone exposure [212].

# Chapter 3
# Materials and methods

## 3.1 Introduction

In this thesis, two different polymeric LOCs were developed:

1. a chip for circulating tumour cell capturing;
2. a chip for neuronal cell culturing

The development of the devices included the following steps:

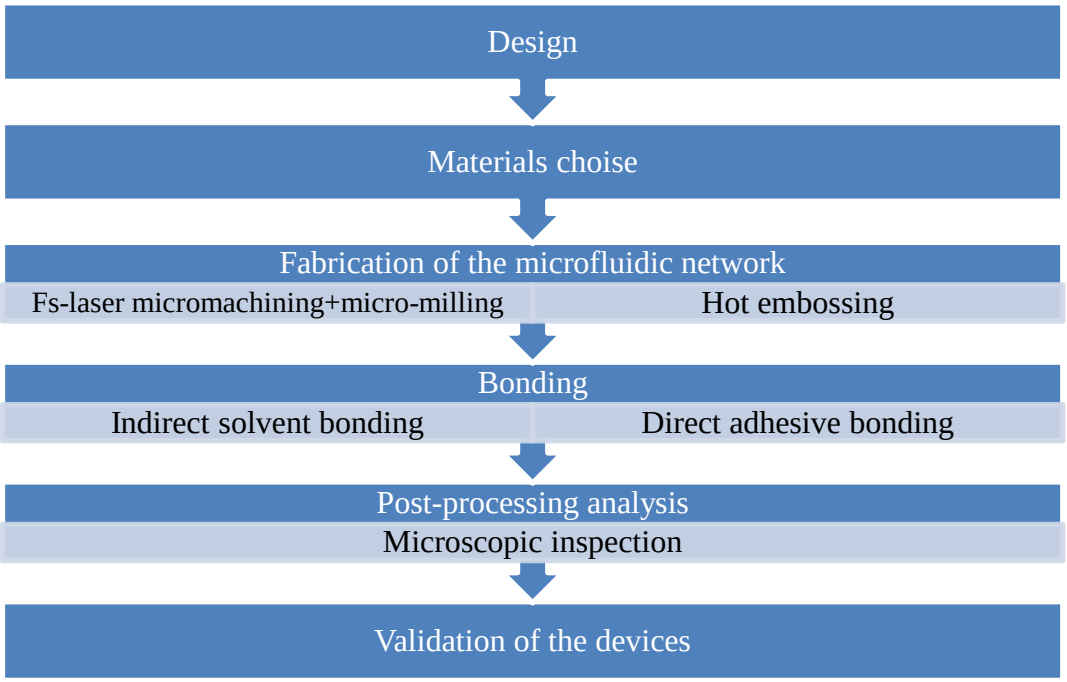


In this chapter the main steps of this procedure, namely the choice of the materials, the fabrication setup for machining the samples, and the instruments for post process characterization and analysis are presented. Furthermore, the setups used for the final validation of the assembled LOCs are described. It is worth noting that the fs-laser parameters used were found following the statistical approach described in chapter 4.

## 3.2 Materials

The device 1 was fabricated using PMMA samples (Vistacryl CQ, Vista Optics Ltd) with optical quality (measured surface roughness Ra<5nm). The milling tests were carried out on PMMA square plates (3cmx3cm) of thickness <5 mm, without any pre-treatment.

Among all the polymeric materials, PMMA has been selected for its specific characteristics such as rigidity, transparency in the visible light spectral range, biocompatibility and good environmental stability, which make it a valid and cheaper alternative to glass for the fabrication of microfluidic devices.

For microchannel functionalization we used Aptes (Sigma Aldrich) 5% in Ethanol, Glutaraldehyde (Sigma Aldrich) 0.05% in water and antibodies Anti-Epithelial Cell Adhesion Molecule (EpCAM) Mouse monoclonal (Sigma Aldrich). Anti-EpCAM antibody, specifically recognizes human EpCAM expressed at the surface of epithelial cells and is not reactive with normal or neoplastic non-epithelial cells.

OECM-1 Human Oral Squamous Carcinoma cell line (purchased by SCC/Sigma-Aldrich) is suitable for studies of cancer cell signaling, epithelial-mesenchymal transition (EMT), metastasis, invasion, and cancer cell stemness. Jurkat cell lines (purchased by ATCC) are human blood (leukemic T-cell lymphoblast)-derived cells.

The device 2 was also fabricated using a transparent PMMA plate of thickness 5mm without any pre-treatment. The master mould for device 2 was fabricated by EpoxyAcast 690 from Smooth-On. The two parts A and B has been taken at a ratio 100 parts (A): 30 parts (B) by weight.

Part A contains: Oxirane,2,2'-((1-methylethylidene) bis (4,1-phenyleneoxymethylene)) bis-, homopolymer (CAS No. 25085-99-8).

Part B contains: Polyoxypropylenediamine (CAS No. 9046-10-0).

The EpoxyAcast 690 master has been chosen because it is reusable, and it can withstand without cracks up to a pressure load more than that of offered by the silicon and the SU8 Photoresist.

The fabricated PMMA devices were exposed to oxygen plasma (Pico A, Diener Electric, Germany) to render the surfaces hydrophilic and ethanol was introduced via wells to prevent bubble formation in the channels. Ethanol was removed and poly-L-ornithine (PLO, Sigma) added to the top of the two wells and left for 3 hours to improve cell attachment. PLO was removed and channels were rinsed with medium, before filling all wells. Devices were stored in a humidified incubator (37°C/5% CO2) prior to cell seeding.

Two different bonding technologies have been derived for PMMA microfluidic devices. One was Isopropanol assisted indirect thermal bonding and the other technique relied on using ThermalSeal RTS pressure sensitive adhesive film.

# 3.3 Device fabrication setup

## 3.3.1 Femtosecond laser micromachining

Two laser sources were used for milling experiments.

### 3.3.1.1 Trumpf Laser

An ultrafast solid-state laser system (mod. *TruMicro Femto Ed*. From *Trumpf GmbH)* (Figure 3.1) based on the chirped pulse amplification technique (CPA) and emitting laser pulses at the wavelength of 1030 nm was used. The laser source provides an almost diffraction limited beam ($M^2$<1.3) linearly polarized with pulse duration of 900 fs, maximum average power of 40 W, maximum pulse energy of 400 μJ, and repetition rate ranging from 100 kHz to 800 kHz. An external modulator allows reducing the repetition rate below 100 kHz and down to 1 kHz.

A quarter-wave-plate circularly polarizes the beam, and then a galvo-scan head (*IntelliSCANNse 14, SCAN-LAB, Puchheim, Germany*), equipped with a telecentric lens of 100 mm focal length, focuses and moves the beam onto the polymeric surface.

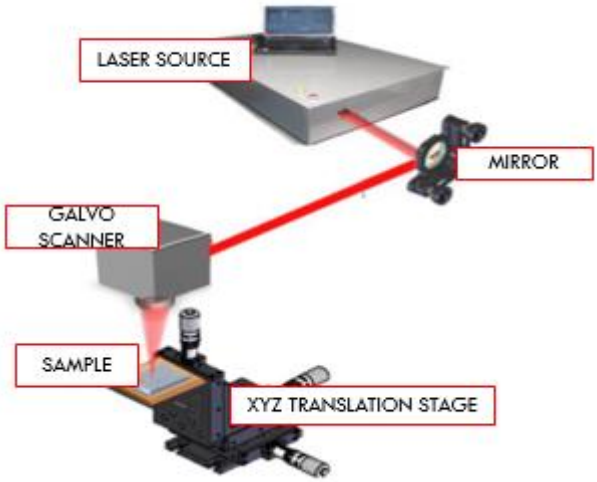


*Figure 3.1: Schematic of Trumpf laser system set up*

Several process parameters contribute to the final surface quality and *depth* of a laser milled parts. In particular, the laser pulse energy ($E_p$), the repetition rate (*R.R.*), the scanning speed (*s*) and the hatch distance (*d*), are relevant parameters that have been investigated in this work:

- pulse energy is the whole optical energy contained in a pulse. The output average power of the laser can be calculated by multiplying the pulse energy by the pulse frequency;

- repetition rate or pulsing frequency is the number of pulses per second emitted by the laser;

- scanning speed is the velocity with which the laser beam travels on the material surface;

- hatch distance is the distance between two consecutive scanning lines.

Each laser milling test was performed superimposing two perpendicular scanning patterns, illustrated in Figure 3.2, in order to obtain uniform ablation all over the milled area.

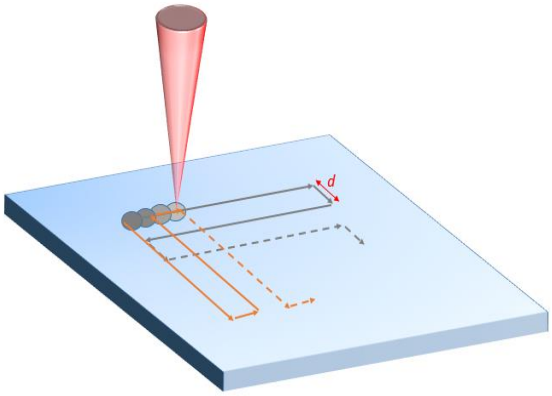


*Figure 3.2: A schematic of the laser scanning pattern employed during milling of PMMA specimens; d is the distance between two consecutive scanning lines.*

Each test has been carried out on a target area of 1-mm x 5-mm. After fs-laser milling, the samples were washed with ultrapure water in an ultrasound bath for 15 min, in order to remove the processing residues.

Complex designs, i.e. the serpentine (chapter 5) and the compartmentalized structure (chapter 6) were designed with Rhinoceros 5 CAD software and then transferred to the galvo-scanner software.

### 3.3.1.2 Pharos laser

The second laser source employed was the Pharos SP 1.5 from Light Conversion, providing 200 fs pulses with variable repetition rate from a single pulse to 1 MHz. The almost diffraction limited laser beam ($M^2$<1.3) was characterized by a central wavelength of 1030 nm and had a maximum average power of 6 W and maximum pulse energy $E_p$ of 1.5 mJ.

The linearly polarized exit beam passed through a half-wave plate and a polarizer, which allowed to tune the average power by rotating the half waveplate. Then, the laser beam was passed to a short focal length objective with a focal length of 2.5 cm (the estimated focused spot diameter d in air was 10 µm) mounted on a PC controlled motorized axis (Aerotech, ANT130 LZS, Pittsburgh, PA, USA) (Figure 3.3). This enabled the beam focus to be finely positioned in the polymeric samples that were moved on a XY plane, perpendicular to the beam axis by two Aerotech ABL1500 motorized stages with sub micrometer resolution.

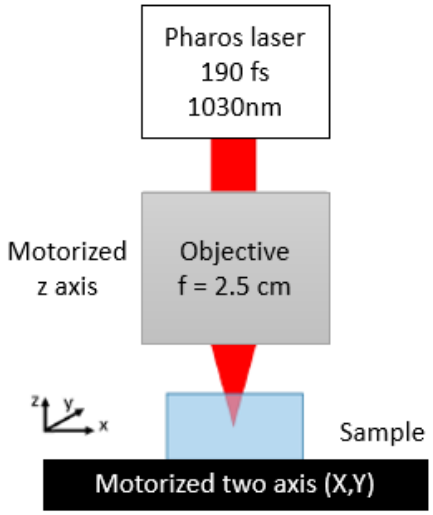


*Figure 3.3: Schematic of Pharos laser system set up*

The Pharos laser system was used to mill the array of microchannels in compartmentalized design (chapter 6).

## 3.3.2 Mechanical micro-milling

The micro milling machine used was the Mini Mill GX by Minitech Machinery, USA. A 400µm-sized tool was used to mill the PMMA layer with 20000 RPM and air

cooling. The geometries were designed using computer-aided design software (Rhinoceros 5) and CAD-CAM software transferred CAD information in machine-code file for the micro milling control.

### 3.3.3 Hot embossing

Hot embossing was conducted on 5mm thickened PMMA sheet using an epoxy resin master as stamp. The hot embossing machine used was Specac Atlas Manual Hydraulic Press 15T customized with a capacity of 0.9 tonnes load (Figure 3.4). It was fitted with two metal platens (top and bottom) and these were connected to a temperature controller. Cooling was achieved by a chiller circulated cold water connected to the machine. The micropatterned epoxy resin master stamp and pre-cut PMMA substrate were hitched up into a set (Figure 3.5). The unpatterned open surfaces of this master-sample set were covered by Polytetrafluoroethylene (PTFE) sheets to avoid the direct contact between master/sample with the metal platens. Prior to start hot embossing, the pressure release valve on the machine was firmly tightened and water cooling supplied to the machine. The master-sample set was placed in between the two metal platens with the covering of PTFE sheets. The top plate was screwed down until it made compressed contact with the master-sample set (Figure 3.6).

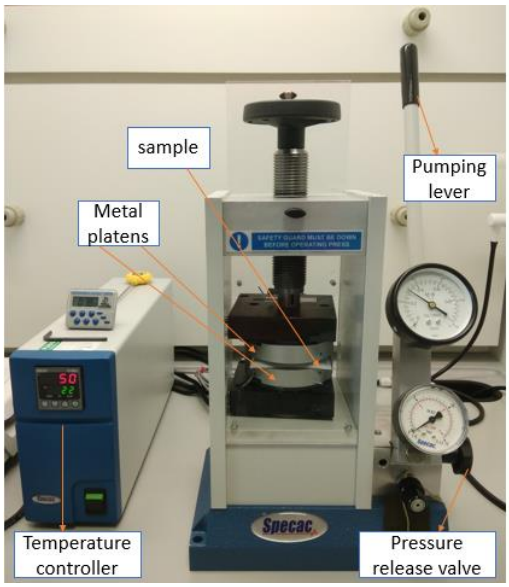


*Figure 3.4: Hydraulic press machine for hot embossing*

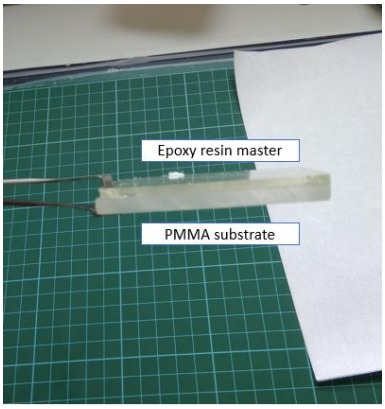


*Figure 3.5: Hitched up epoxy resin master and PMMA substrate*

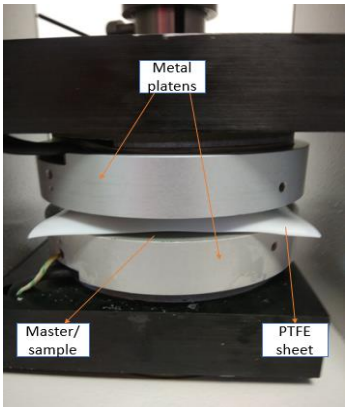


*Figure 3.6: Compressed set of master-sample in between metal platens*

The master-sample set was heated to different temperatures (loading temperature $L_T$) above glass transition temperature ($T_g$=120$^0$C) of PMMA (from 130$^0$C to 150$^0$C) by using temperature controller under different pressure loads (loading pressure$L_P$, 0.2 ton to 0.3 ton) for 15 minutes. After 15 minutes the loading temperature was decreased to room temperature (22$^0$C), maintaining the pressure load at the same level and left the system for 1 hour to reach room temperature. Once the master-sample set was cooled, pressure release valve was released, and the sample was taken out from the machine. The imprinted PMMA substrate was demoulded from the epoxy resin master by hand. A 4-mm-diameter inlet and outlet holes for the device were drilled by a mechanical drilling machine.

## 3.3.4 Bonding

### 3.3.4.1 Isopropanol assisted indirect thermal bonding

A cheap, simple, fast and deformation free method for bonding the two PMMA substrates was introduced here. This method is based on depositing isopropyl alcohol (IPA) {$((CH_3)_2$CHOH)} using spin coater at the coating speed of 2000 RPM on the flat bottom substrate and capping it with the micropatterned PMMA substrate. The excess solvent was eliminated through blotting paper. The two PMMA slices were hold by two plastic clamps which provided a low-pressure condition and a temperature was applied

below the glass transition temperature 120˚C of PMMA, which led to the bonding of PMMA substrates.

Since PMMA has less solubility parameter ($20(Jcm^{-2})^{1/2}$ ) than that of IPA (23.4 $(Jcm^{-2})^{1/2}$), PMMA cannot be dissolved in IPA at room temperature (see chapter 2 section 2.6.2.2). The micro patterned PMMA plate and another plane PMMA plate were cleaned with IPA by shaking them inside a petri dish and dried by using nitrogen ($N_2$) gas prior to bonding. Few drops of hot IPA (70°C) were spin coated onto the plane PMMA plate which was capped with the micropatterned PMMA plate. Both PMMA plates were stacked together with a plastic clamp (Figure 3.7). The Plastic clamp provided a low pressure onto the stacked PMMA plates, which avoided deformations of the chip after bonding. An oven was preheated to a temperature of 60˚C below the glass transition temperature of PMMA. The pre-treated sample was put into the preheated oven for 20 minutes. At this temperature and pressure the PMMA monomers at the interface got cross linked by the solvent assistance of isopropyl acid. The bonded chip was allowed to cool down to room temperature for 5 minutes.

*Figure 3.7: Stacked PMMA slabs with plastic clamp*

# 3.4 Post-processing analysis equipments

The morphological characterization of the laser machined samples was done by using optical, confocal microscopes as well as an optical profilometer, which are described in this section.

### 3.4.1 Optical microscope

After the micromachining of device 1 the samples were firstly checked with an optical microscope Nikon Eclipse ME600. It is equipped with five objectives for 5X, 10X, 20X, 50X and 100X magnification and a PC-interfaced digital camera which allows measurements of samples features. A motorized z-axis sample holder allows to precisely focus on the sample surface and to make evaluations of the depth of the ablated structures. Two light sources are provided, thus allowing measurements in both reflection and transmission configuration.

For device 2, an inverted microscope (AxioObserver Z1, Zeiss) was used and images were taken with a CMOS camera (ORCA-Flash 4, Hamamatsu) and 5x, 10x, 20x and 40x lenses (all from Zeiss). Processing of images were undertaken using Zen Pro (Blue edition, Zeiss) or Fiji/ImageJ.

### 3.4.2 Confocal microscope

A 3D non-contact ZEISS Axio CSM 700 confocal microscope was used to accurately measure the surface topography and roughness of the sample. The confocal microscope specifications are reported in Table 3.1 [254].

*Table 3.1: Confocal microscope AXIO CSM700 Zeiss specifications*

| | |
|---|---|
| **Lateral resolution** | 0,16 µm |
| **Repeatability on the lateral measurements (3 σ)** | 0,01 µm |
| **Repeatability on height measurements (1 σ)** | 0,02 µm |
| **Objective lens** | 10× EC Epiplan-Neofluar |
| **Numerical Aperture** | 0.25 |
| **Lateral digital resolution (line-space-pattern)** | 160 nm |
| **Repeatability on the lateral measurements (3 σ (1 σ))** | 20 (30) nm |
| **Vertical resolution** | 0.5 µm |

# 3.5 Validation setup of the final devices

## 3.5.1 Lab-on-a-chip for circulating tumour cells capturing

For the functionalization and testing of the LoC for tumor cells capturing the assembled device was connected to capillary tubes perfectly fitting with micro milled shaped inlet/outlet and connected to the microfluidic setup using miniaturized piezoelectric pumps (Bartels' mp6 series) controlled by STM32 Nucleo32 board and National Instruments Labview user interface. Real-time acquisition of the capture test was performed using an Olympus inverted microscope integrated into an Okolab setup equipped with a temperature-controlled box and a camera. Cell cultures were grown in an incubator at 37 °C with 5% $CO_2$ and cultured in suspension in RPMI 1640 complete growth medium (Jurkat cells) or in adhesion (OECM-1 cells) in complete Dulbecco's Modified Eagle's Medium (DMEM), and the medium was renewed every two days. Few minutes before the capture experiments cancer cells were suspended and harvested using 0.05% trypsin. After detachment, cells were washed and resuspended in DMEM medium at the right dilution. Jurkat cells were collected from the flask, centrifuged, counted and resuspended at the right dilution, too. Solutions were then loaded into capillary tubes using piezoelectric micropumps set at a flow velocity value of 8µl/min.

## 3.5.2 Lab-on-a-chip for neuronal cell culturing

### 3.5.2.1 Primary hippocampal cell culture

One to two days old Sprague Dawley rat pups were killed via cervical dislocation and the hippocampus dissected out. The tissue was chopped up and incubated in papain solution (1.5 mg/ml) followed by trituration in bovine serum albumin solution (10 mg/ml). The isolated cells were then spun down, and the pellet resuspended in culture medium at a density of 3-4 x $10^6$ cells/ml. This medium consisted of Neurobasal-A supplemented with L-glutamine (2 mM) and B27 (2% v/v). Cells were loaded into the culture chambers of devices by pipetting close to the entrance of the channel through the emptied wells and incubated for ~1 hour. Wells were filled with medium in a staggered process and media was refreshed every 2-3 days by removing half the well volume and

replacing with fresh media. Devices were incubated at 37°C/5% $CO_2$ and analysed after 12-14 days *in vitro* (DIV).

### 3.5.2.2 Immunocytochemistry

Immunocytochemical staining was performed on cultures as previously described [255]. Cells in devices were washed with phosphate buffered saline (PBS) and fixed by applying paraformaldehyde (4%) for 10 minutes. Cells were washed with PBS and permeabilised by applying 0.01-0.1% Triton-X 100 for 10 minutes. Cultures were then incubated with a blocking solution containing foetal bovine serum (5% v/v) and BSA (1% w/v) in PBS for 1 hour at room temperature. Primary antibodies were diluted in blocking solution (1:500) and incubated with the cultures at 4°C overnight. Antibodies used were for ßIII-tubulin (neuronal marker), synaptophysin (synaptic vesicle marker) and glial fibrillary acidic protein (GFAP, marker for astrocytes). Cells were then rinsed with PBS and incubated with complimentary fluorescently labelled secondary antibodies (diluted 1:200 in blocking solution) for 1 hour at room temperature. Finally, cells were rinsed with PBS and wells were filled with PBS prior to imaging.

# Chapter 4
# Prediction model of the depth of the femtosecond laser micro-milling of PMMA

## 4.1 Introduction

The femtosecond laser technology is emerging as a powerful and flexible tool for the fabrication of miniaturized polymeric devices, thanks to the micrometric precision and the minimum thermal damage on the work piece obtainable through ultrafast laser ablation. However, parametrization of femtosecond laser processes is often based on a trial and error approach, which requires a lot of expensive experimental efforts. The design of experiment (DoE) approach can offer a methodical way to quickly determine the laser process settings limiting the use of resources. Here, an accurate DoE procedure has been defined to estimate the influence of the laser repetition rate, pulse energy, scanning speed, and hatch distance on the fs-laser micro milling process of PMMA specimens in terms of depth of removed material ($D_h$). It has been shown that the laser pulse energy is the parameter that mainly affects the milling depth. A predictive model describing the relationship between the response variable *depth* and the main laser parameters is defined and then validated.

## 4.2 Statistical approach for laser micromachining

Laser micro milling consists of removing layer by layer the material from a workpiece by laser ablation until the designed shape is achieved. Unlike conventional mechanical milling, where the single removed layer depth is an input process parameter set at the beginning and the surface quality depends on the employed tools, in fs-laser milling these features depend on several laser parameters such as laser pulse energy and repetition rate, pulse duration, scanning speed and hatching pattern. When collateral thermal damages (i.e. recast layers, burrs, spatters and microcracks) to the material

substrate are not an issue, cheaper and more affordable laser sources with “short” pulse durations in the nanosecond, microsecond or millisecond range are used.

Extensive literature has been produced on the study of short-pulsed laser processes using trial and error as well as statistical approaches. Campanelli et al. [256] planned a full factorial design aiming to study the influence of the main laser parameters on the depth and surface roughness of the area milled by laser ablation with nanosecond pulses of aluminium–magnesium alloy specimens. In particular, the effect of the pulse repetition rate and overlap on the milling depth was studied, finding that the highest ablation depth per single layer is obtained when the pulse overlap, and the repetition rate are lower. In their review, Dubey and Yadava [257] have cited several studies which employed the Design of Experiments (DoE) to increase the quality of drilling, cutting, and micro milling of several materials, i.e. metals and ceramics, using a Nd:YAG nanosecond laser source. Teixidor et al. [ref 302][258] presented a multi objective optimization of the nanosecond laser micro-milling of cavities on 316L Stainless Steel for the development of drug eluting stents (DES). They used a DoE approach to improve the reproducibility of laser milled cavities of different geometries by optimizing the pulse energy, pulse frequency, and scan speed. Leone et al. [259] also used the DoE to study the milling of aluminium oxide (Al2O3) plates with a nanosecond fiber laser, aiming to find the relationship between the working parameters, the surface quality and the material removal rate. They found a linear dependence of the milled-area depth on the released energy; moreover, the maximum achievable depth was found to be also affected by the scan speed and the hatch distance.

Recently, laser ablation with “ultrashort” laser pulses in the femtosecond (fs) and picosecond (ps) range, is gaining momentum in the field of micromachining. Thanks to its peculiar laser-matter interaction timescale, such technology allows minimizing the thermal load to the material thus providing ablated features with sharp edges and free from burrs, recast layers and microcracks [175]. In addition, fine control of the removal rate is possible, which improves the achievable precision and the reproducibility of the micromachining processes [260]. With femtosecond laser sources it is also possible to structure dielectric materials that are usually transparent to the irradiation wavelength. Indeed, when intense ultrashort pulses are tightly focused into the bulk material, non-linear absorption phenomena are promoted, which cause absorption of the laser energy [261]. Therefore, the precise structuring [262], milling [263] and joining [174] of

polymers and glass, which are materials widely used for the fabrication of biomedical micro-device, is possible with femtosecond laser ablation.

However, the fs-laser processes require an accurate study and optimization of the laser parameters in order to guarantee the reliability necessary to promote the use of this technology on an industrial scale. Often such studies are performed using a trial and error approach. In particular, a few studies are available in literature on the ultrafast laser machining of transparent polymeric materials for microfluidic applications. Cheng et al. [264] used a trial and error approach for the rapid prototyping of polymethylmethacrylate (PMMA) LOC by direct laser writing. Suriano et al. [192] performed an extensive investigation of the properties of microfluidic channels ablated by femtosecond laser. They studied the thermoplastic polymers more used for microfluidics, i.e. PMMA, polystyrene (PS), and cyclic olefin polymer (COP), concluding that, due to its stable molecular structure, PMMA is the most suitable thermoplastic material for fs-laser milling of microfluidic channels. De Marco et al. [265] studied the effect of the laser fluence on the chemical and physical properties of ablated PMMA surface. They observed a change in wettability when a porous microscale morphology was induced by the laser irradiation.

Very few studies have extensively investigated the fs-laser machining of transparent polymers using a statistical approach based on DoE and ANOVA analysis. Gomez et al. [266] have investigated the femtosecond laser ablation of polymers and glass using a Ti:sapphire laser source aiming to fabricate microfluidic networks comprising channels, reservoirs, and through-holes. A very simplified DoE was performed on PMMA and 12 channels were microstructured corresponding to three different laser fluence values and four scanning speeds. After this study, micro-channels with desired width and depth with an error below 5 μm and good-quality finishing were fabricated.

Understanding more deeply the relationship between the fs-laser parameters and the ablation depth and/or surface quality for the micro-milling of transparent polymers would reduce the number of expensive and time-consuming empirical tests necessary for the assessment of this technology for the fabrication of microfluidic disposable devices for biomedical applications.

Here, an in-depth study of the fs-laser micro milling of PMMA has been carried out. The DoE was used to study the influence of the main laser parameters involved in

the micro-milling process on the depth of removed material (Dh), trying to find and evaluate a statistical prediction model describing this relationship.

# 4.3 Experimental procedure

A 2-level full factorial Design of Experiments has been carried out in order to analyse the effect of each main factor involved in the PMMA fs-laser milling on the response variable depth.

In Table 4.1, the laser process parameters taken into account in the experimentation are listed, with their central point, higher and lower values.

*Table 4.1: Fs-laser main process parameters and process window to be investigated*

| **Factors** | **Abbreviation** | **Description** | **Fs-laser parameters range** | | |
|---|---|---|---|---|---|
| | | | Low level (-1) | Central point | High level (+1) |
| ***Rep. rate*** | A | Repetition rate [kHz] | 10 | 25 | 40 |
| ***Pulse energy*** | B | Energy for impulse [µJ] | 6.5 | 7.8 | 9.1 |
| ***Scan. speed*** | C | Scanning speed [mm/s] | 5 | 15 | 25 |
| ***Hatch dist.*** | D | Hatch distance [µm] | 1 | 3 | 5 |

The experimentation has been divided into three phases: i) a preliminary phase to define the minimum number of replicas through the Power analysis; ii) an experimental plan that was including the main factors for identifying a predictive model; iii) a validation phase to test the prediction capability of the model. The software used for the statistical analysis was Minitab®18.

The Power is defined as the probability to identify the smallest difference between the factor levels with highest and lowest means. The right number of replicas for the

design plan give the chance to identify smaller differences. The goal is the detection of the smallest difference with practical consequences on the application we are interested in. Defining a power value of 0.9 can be considered a good target to detect such difference, because it means that there is a 90% chance of identifying a difference between the factor settings [267].

In order to assess the variability of the fs-laser machine, the laser micro milling process of PMMA has been repeated three times using the central point parameters (see Table 4.1). The machine was turned off after each operation and waited an hour before the subsequent trial. The measured *depth*s, and the mean value with its standard deviation, are reported in Table 4.2.

*Table 4.2: Plan of experiment to define the standard deviation of the fs-laser machine*

| Values | Description | Depth [µm] |
|---|---|---|
| ***T1*** | First trial | 67 |
| ***T2*** | Second trial | 68 |
| ***T3*** | Third trial | 65 |
| ***mean*** | Mean value | 66.8 |
| ***StDev*** | Standard deviation | 1.5 |

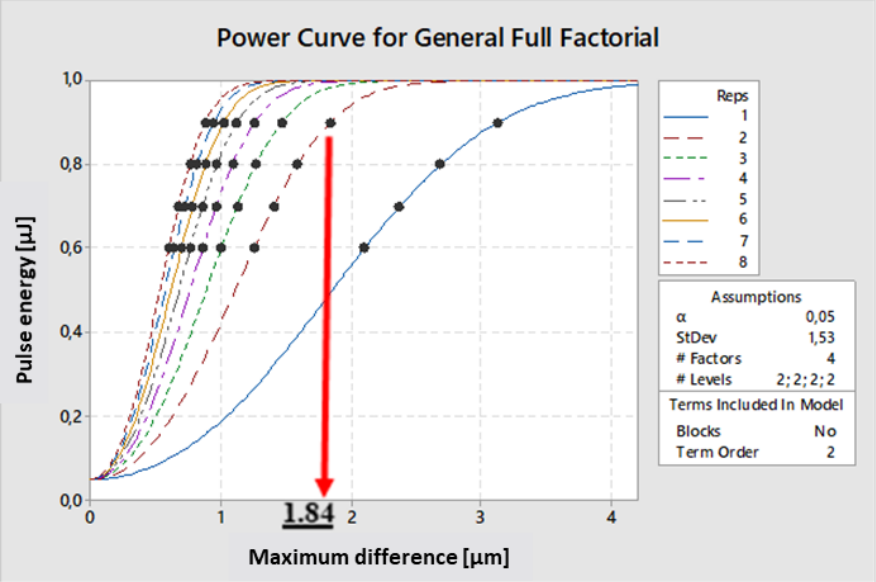


*Figure 4.1: Power curves for general full factorial design: the maximum difference value highlighted is the smallest variation of depth that we can appreciate using 2 replicas with a power of 90%.*

In Figure 4.1, the synthesis of the Power analysis using Minitab®2018 for a two-level full factorial design is reported. Here, the power curves from 1 up to 8 replicas, obtained after setting the number of factors and the standard deviation of the process, are plotted. The value of the standard deviation was obtained from the machine variability test reported in Table 4.2. From Figure 4.1, it can be noticed that a number of replicas equal to two is already sufficient to get an acceptable difference of 1.84 μm with a power of 90%.

Therefore, a two-level, four-factors full factorial design with two replications, as defined with Power analysis (Figure 4.2) has been implemented, for a total amount of 32 fs-laser micromachined pockets.

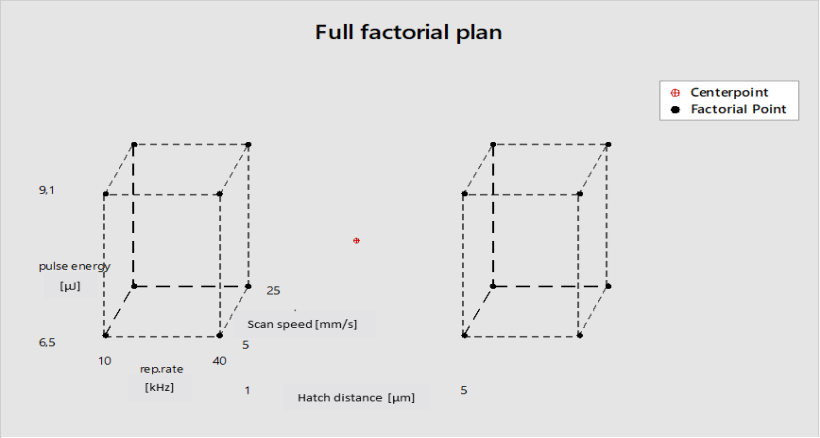


*Figure 4.2: Cube plot of the full factorial plan*

The randomized plan has been divided into two blocks, as many as the replicas. A block is a categorical variable introduced in a factorial plan to help explaining the variations in the response variable that are not directly related to the factors. Each block of experiments has been performed on consecutive days in order to evaluate if the day was a source of variability (nuisance factor). Finally, 3 replications of the central point (ct pt) have been executed for each block, for a total of 6 replicated central points, to evaluate the curvature effect (lack of fit of linear regression model) and to allow an independent estimate of error [267].

In Figure 4.3, the PMMA samples with the micromachined regions are shown. The 38 pockets have been micromachined following the procedure described in Chapter 3, section 3.3.1.1 and exploiting the laser parameters provided by the full factorial plan. A microscopic magnification of two pockets has been also provided in the inset.

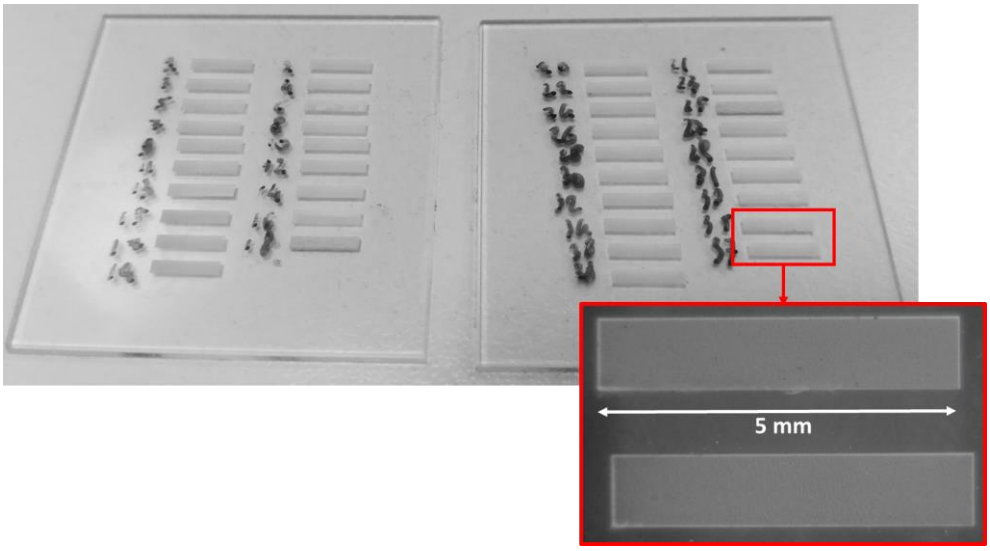


*Figure 4.3: Image of the PMMA plates with the 38 pocket micromachined for different processing conditions. In the inset the optical image of 2 micromachined areas*

# 4.4 Results and discussions

## 4.4.1 Full Factorial plan

In Figure 4.4, the depth measurements for both the replications are reported (the values of the second replication are overlapped to the equivalent ones of the first replication so that a comparison is possible). The repetition capability for the response variable depth is high since the standard deviation between the two replications for each of the depth measurements is minimal and even negligible in most cases. This means that the response of the process is reliable in the range observed.

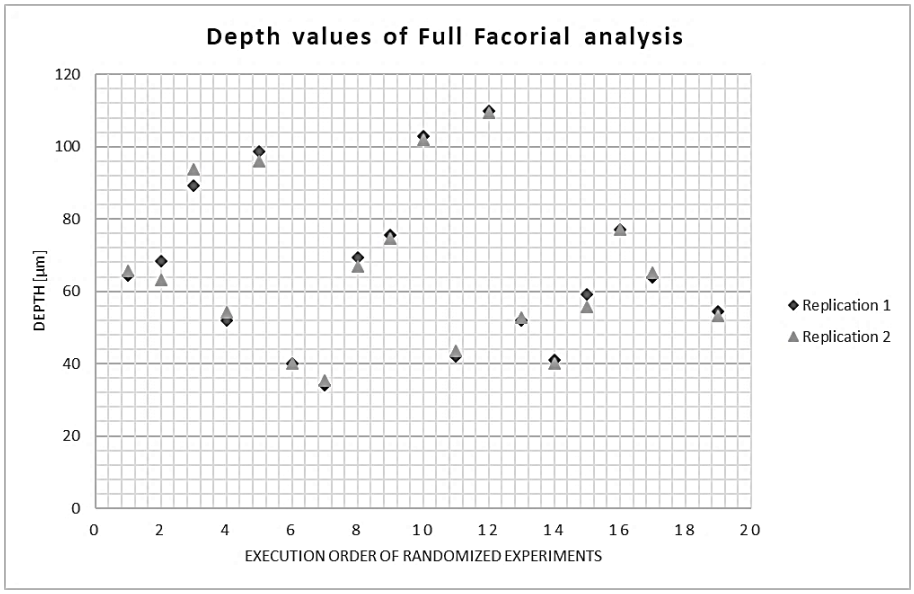


*Figure 4.4: Comparison of depth measurements for the two replications of Full Factorial Design*

The analysis of the central point replicated in the two blocks is reported in Figure 4.5. The within variability for the two blocking days is comparable and acceptable (Figure 4.5(a)). The variability between the blocking days, with a standard deviation of 1.8 µm, is in line with the variability of the machine measured and reported in the previous section, which is 1.5 µm.

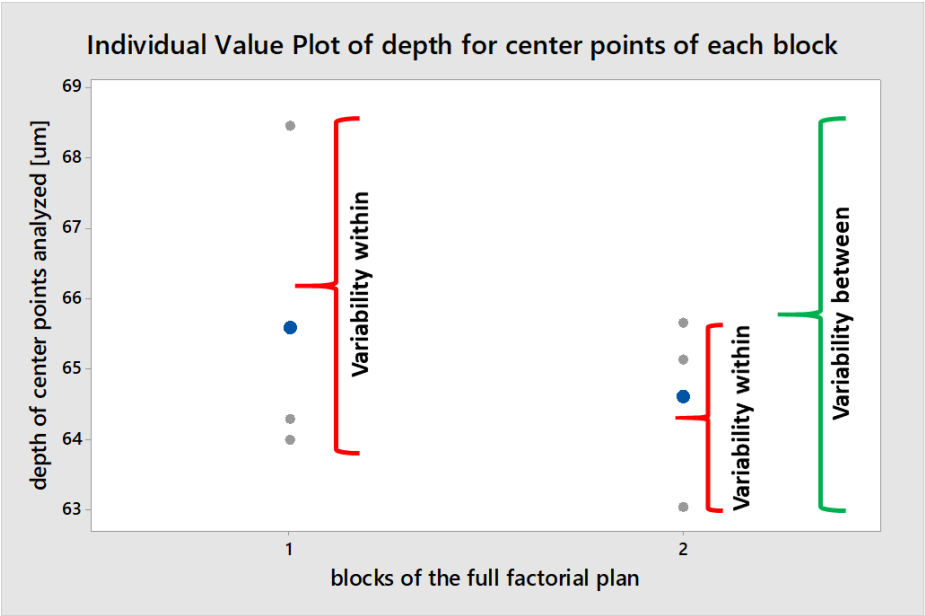


*Figure 4.5: Center points (ct pt) analysis to estimate the within and between variability*

The Figure 4.6 evidences the main factors affecting the response variable depth. As shown in the Main Effect Plot in Figure 4.6 (a), the block is not affecting the response variable, which means that, as seen in Chapter 3 section 3.4.2, the process is not influenced by the day. On the other hand, all the main factors are interested in the process even if, for the Analysis of Variance (see Table 4.3), the pulse energy has an Adjust Sum of Squares (Adj SS) that is significantly higher than the others. The interaction plot confirms the higher influence of the pulse energy on the process. In fact, in Figure 4.6 (b) all the significant interactions involve the pulse energy, i.e. the interactions repetition rate-pulse energy (AB), pulse energy- scanning speed (BC) and pulse energy-hatch distance (BD). Based on these results, a model reduction was operated based on p-value evaluation of the Analysis of Variance as reported in the Table 4.3. In fact, a low p-value suggests that the sample under examination provides enough evidence that the null hypothesis can be rejected for the entire population. The main factors and the significant interactions that will be part of the final reduced prediction regression model can be easily identified. It is worth to mention that the adjusted R-squared of the reduced linear model is 95.07%, which means that the linear model well describes the behaviour of the response variable. A further element that confirms this assumption is the value of the Curvature in the Analysis of Variance (Table 4.3), which presents a p-value of 0.891, which indicates that quadratic effects are negligible.

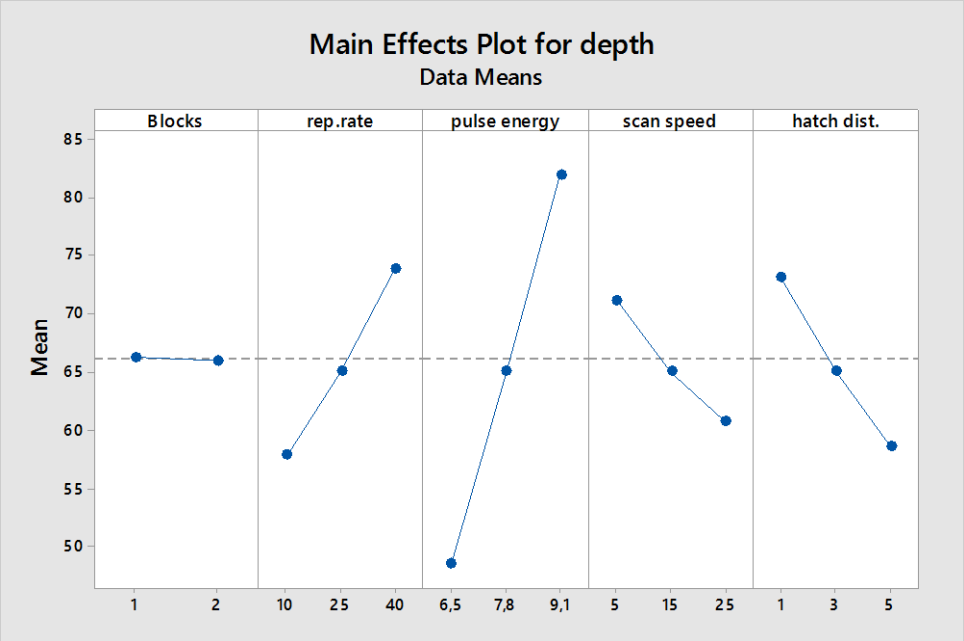


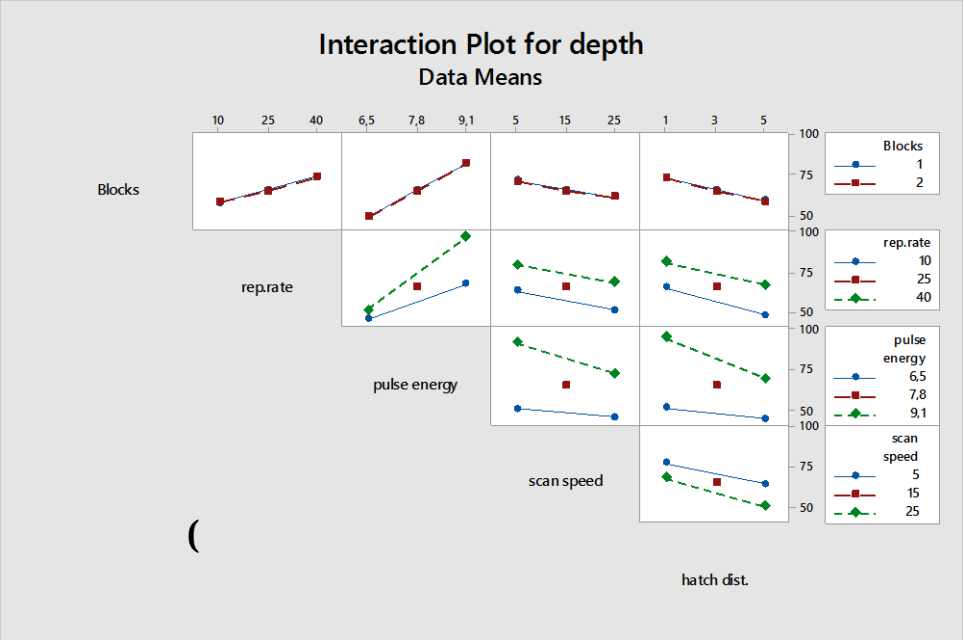


*Figure 4.6: (a) Main effect plot of factors affecting the response variable depth, (b) interaction plot of factors affecting the response variable depth (for units of measurement refer to Table 4.1)*

*Table 4.3: Extract of the Analysis of Variance for the reduced model*

| ***Source*** | DF | Adj SS | Adj MS | F-Value | P-Value |
|---|---|---|---|---|---|
| *Blocks* | 1 | 0,3 | 0,32 | 0,01 | 0,909 |
| *Linear* | 4 | 7102 | 1775,5 | 73,91 | 0,000 |
| ***rep.rate [kHz]*** | 1 | 2313,9 | 2313,86 | 96,32 | 0,000 |
| ***pulse energy [µJ]*** | 1 | 5736,1 | 5736,12 | 238,77 | 0,000 |
| ***scan speed [mm/s]*** | 1 | 1152,3 | 1152,27 | 47,96 | 0,000 |
| ***hatch dist. [µm]*** | 1 | 1804,5 | 1804,52 | 75,11 | 0,000 |
| *2-Way Interactions* | 3 | 1002,6 | 334,2 | 13,91 | 0,000 |
| ***rep.rate* pulse energy*** | 1 | 740,5 | 740,53 | 30,82 | 0,000 |
| ***pulse energy *scan speed*** | 1 | 132,9 | 132,86 | 5,53 | 0,027 |
| ***pulse energy *hatch dist.*** | 1 | 319,5 | 319,49 | 13,3 | 0,001 |
| *Curvature* | 1 | 0,5 | 0,46 | 0,02 | 0,891 |

Finally, in Figure 4.7 it has been verified that the hypothesis of normality (hypothesis that the data come from a normally distributed population) cannot be rejected. Analysing the standardized residuals (Figure 4.7(b)), we can see that all the plots belong to the interval [-3; +3], and no outliers are detected. The test for equal variance indicates that the hypothesis of homogeneity of variances cannot be rejected, as confirmed by the p-value of 0.626 of the Bartlett test (Figure 4.8), which is a test used to verify the homoscedasticity and that is sensitive to deviations from normality [267].

The following Regression Equation, defined in Uncoded Units, has been exploited to predict the milling depth as a function of the process parameters:

$$\text{depth} = -42,6 - 1,401\,A + 14,69\,B + 0,939\,C + 7,20\,D + 0,2613\,AB - 0,2092\,BC - 1.490\,BD + \varepsilon \qquad (4.1)$$

where ε is a value linked to the central point (CtPt) and that is evaluated as +0.79CtPt.

The predictive capabilities of the model of Equation 4.1. are discussed in the next section.

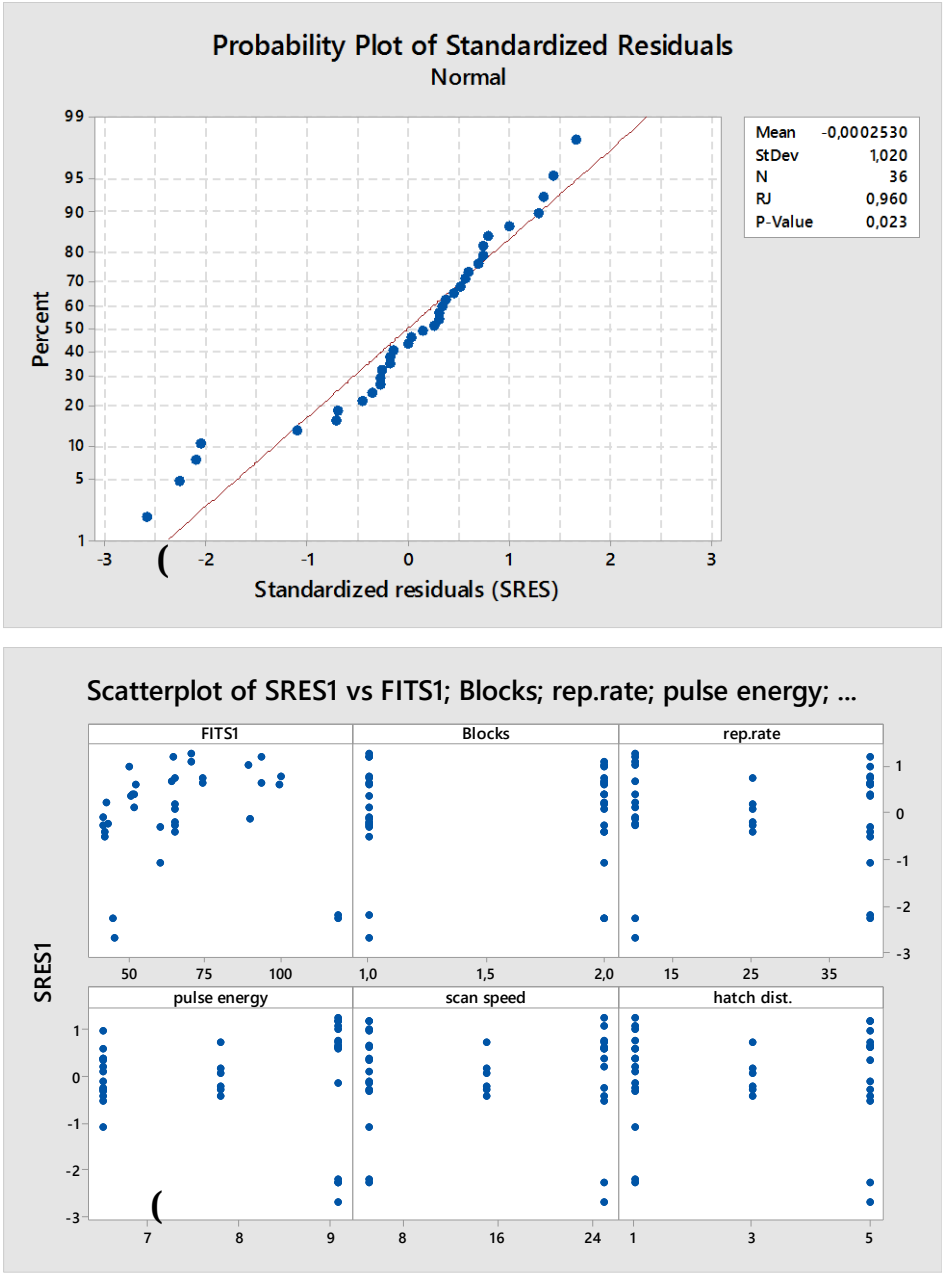


*Figure 4.7: (a) Normal probability plot of standardized residuals, (b) plot of standardized residuals (SRES) versus fits (FITS), block, and main factors (for units of measurement refer to Table 4.1)*

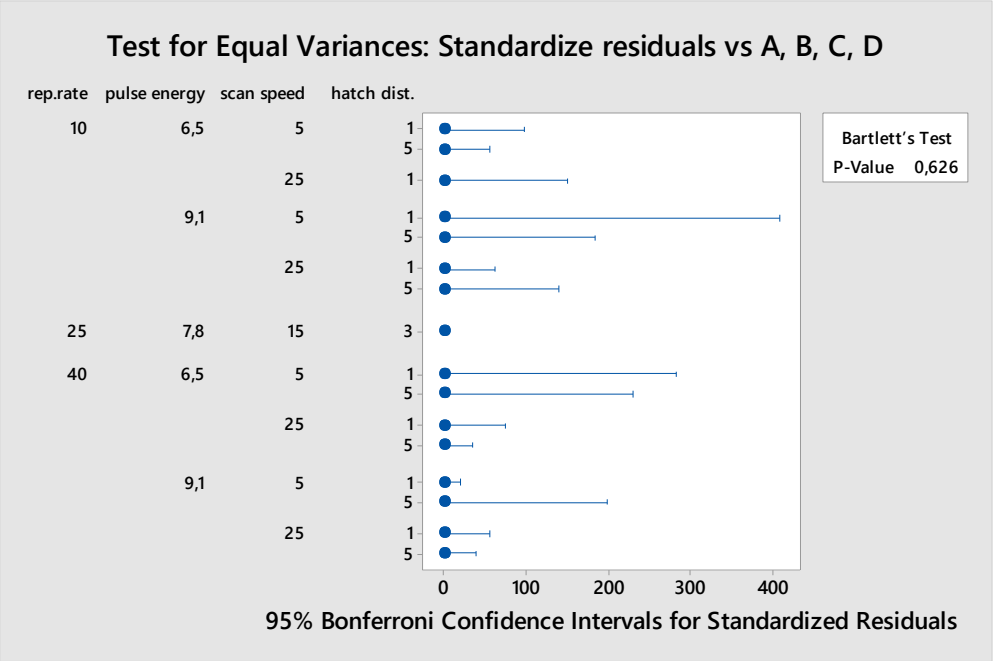


*Figure 4.8: Bartlett test for equal variance (reliable only for normal data). Units of measurement are reported in Table 4.1*

## 4.4.2 Validation of prediction model

The regression model identified in the previous section (see Equation 4.1) has been used to predict the Confidence Interval (CI) and the Prediction Interval (PI) of the milling depth in three points out of the full factorial plan. The CI and PI identified by Minitab are reported in the Table 4.4. An experimentation plan based on 2 trials for each prediction point has been executed and the results of depth measurements are reported in the same Table 4.4 and compared with CI and PI. The depth values of both trials for all the three points fall within the prediction interval (PI). In the case of the second point the measured depth values fall even within the confidence interval (CI), which is more stringent than the prediction interval. Whereas, for points 1 and 2 the related values do not fall in the CI even though they are not so far from its lower limit. Therefore, it can be concluded that the results of the validation test demonstrate the good predictive ability of the regression model for the milling depth.

*Table 4.4: Validation of prediction model based on comparison between experimental trials results and confidence and prediction interval identified with Minitab*

| *Variable* | **Settings of point 1** | | **Settings of point 2** | | **Settings of point 3** | |
|---|---|---|---|---|---|---|
| ***Rep.rate (A) [kHz]*** | 20 | | 30 | | 20 | |
| ***Pulse energy (B) [µJ]*** | 8,9 | | 6,8 | | 7 | |
| ***Scan speed (C) [mm/s]*** | 10 | | 20 | | 5 | |
| ***Hatch dist. (D) [µm]*** | 2 | | 4 | | 2 | |
| *Minitab Prediction of depth values [µm]* | CI | PI | CI | PI | CI | PI |
| | (82; 88) | (74; 95) | (43; 50) | (36; 57) | (56; 63) | (49; 70) |
| *Experimentation* | | | | | | |
| ***Trial 1 depth value [µm]*** | 81 | | 45 | | 53 | |
| ***Trial 2 depth value [µm]*** | 79 | | 44 | | 53 | |

# Chapter 5
# Smart procedure for the femtosecond laser-based fabrication of polymeric lab-on-a-chip for tumor cells capturing

## 5.1 Introduction

In this section, the developing and testing of a new smart procedure for the microfabrication of a PMMA LoC for cells capturing by exploiting fs-laser technology, mechanical micro milling and solvent assisted thermal bonding is described. PMMA is one of the most used polymers in microfluidics because of its optical, mechanical and chemical characteristics, such as transparency, good thermal stability, chemical inertness and high hydrophobicity, as well as for its mechanical stability for use in laser ablation and micro milling processes [268].

Starting from a CAD file, the combination of fs-laser ablation and micro milling manufacturing technologies offers ample adaptability to rapidly create and test different fluidic designs and optimize the cells capturing strategy, taking advantage of the micrometric precision and high flexibility of the ultrashort pulses micromachining but maintaining a sustainable cost per piece.

An easy and cost-effective thermally solvent assisted bonding method for assembling the polymeric chips is also presented. The procedure, established for PMMA-PMMA and based on the use of common solvents, low temperatures and low pressures, makes it possible to obtain strong adhesion and robust devices, without affecting the shape of the fabricated microchannels.

As a proof of application, the device has been used for capturing tumor cells from a mixture containing blood cells. To this aim, after fabrication of serpentine micro-channels, an “in-flow” biological functionalization of their inner walls was performed using Anti-Epcam antibodies, which are able to distinguish cancer from non-cancer cells by recognizing the antigen of the epithelial membrane of the oral carcinoma cells and blocking them on the channel walls. The serpentine shape of the channels allows a prolonged path of the sample helping in maximizing the interactions cells/antibodies.

# 5.2 Fabrication of LOC device

The first step in the realization of the device was the CAD design of its elements which was then transferred in machine-code to the fabrication instruments used. Figure 5.1 (a and b) schematically illustrates the proposed geometry. Some different architectures of the device were designed and tested in order to optimize parameters of fabrication, bonding and final application. Here, the final layout of the device is presented, which is based on a serpentine microchannel with a square cross section of 100 μm per side and a total length of 180 mm to increase the active path and therefore the probability of capturing cells. Two PMMA substrates were used in order to minimize the dimensions of the assembled device and to gain in transparency. The upper substrate (Figure 5.1a) was machined separately on the two faces. On the lower face the serpentine-shaped channel was fabricated by fs-laser ablation and gently removing the material layer-by-layer until reaching the depth designed with micrometric precision. The layer-by-layer milling procedure was performed superimposing two perpendicular scanning patterns. The lateral distance between two parallel scanning lines was 5 μm. A repetition rate of R.R. 50 kHz, a pulse energy of 12 μJ, and a scan speed of 40 mm/s were selected based on the results of the statistical study described in chapter 4.

On the upper face the inlet/outlet drilled holes were micro-milled. The bottom layer was a flat and smooth PMMA substrate with 1mm thickness, just used to seal the bottom of the channel (Figure 5.1a). 1mm thickness was hard enough to seal the device without bending as well as offered a good microscopic imaging.

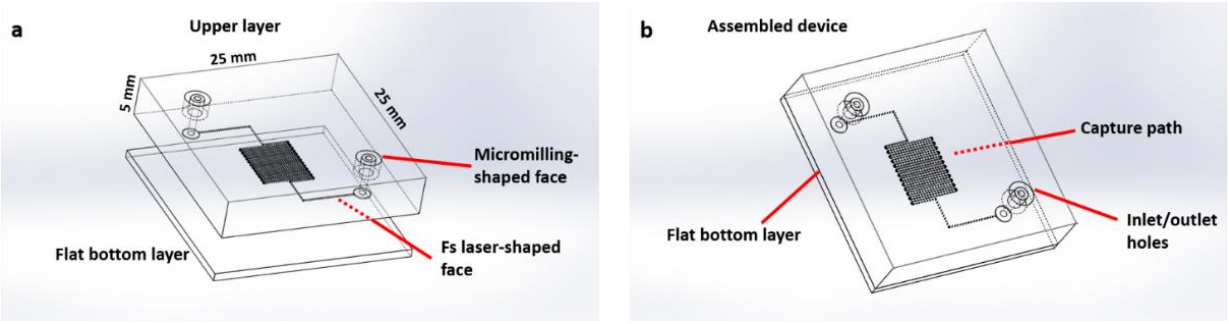


*Figure 5.1: (a) modules of the PMMA device: the upper layer has been milled by both sides to obtain femtosecond pulse-shaped serpentine on the bottom and micro milling machine inlet/outlet holes on the top. A flat slice of PMMA sealed the serpentine channel; (b) architecture of the assembled device.*

The inlet/outlets were obtained through a mechanical micro milling machine mounting a 400 μm tool, after careful alignment with the serpentine ends on the opposite face. The air-cooled milling was accomplished at a feed rate of 100 mm/min and spindle speed of 20.000 RPM according to Reichenbach [142]. Inlet/Outlets were concentric cylinder holes that fit perfectly with the external and internal dimensions of the capillary, therefore making no additional glue or gaskets necessary for the watertight seal. From the center of these cylinders, channels of 600 μm in diameter and 5 mm in length have been realized, which allow the fluids injected from the opposite face to reach the serpentine.

Figure 5.2a shows a stereoscopic image of the micromachined serpentine. In Figure 5.2b a particular of the device is highlighted. The edge of the channel showed no cracks, burrs or recast layers that could hinder the sealing procedure. The bottom part of the channel had a roughness Ra of about 3 μm. This value was negligible compared to the channel height, therefore it did not affect the fluidic transport of the cells.

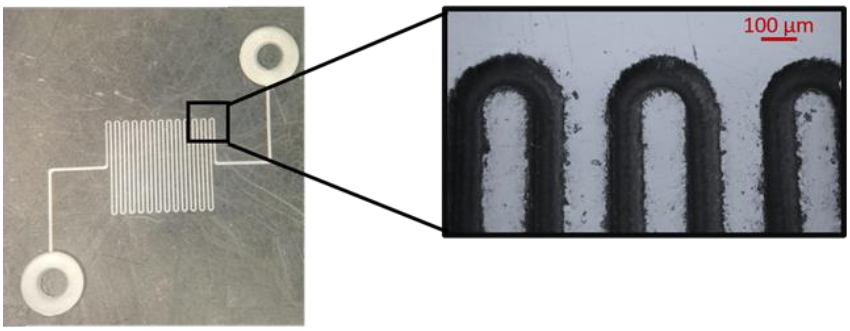


*Figure 5.2: (a) Stereoscopic image of the laser micromachined sample. (b) A microscopic 3D detail of the serpentine channel (magnification 10x).*

# 5.3 Bonding and functionalization of the device

Several cost-effective bonding techniques have been introduced to seal micropatterned PMMA substrates. Among them, SU-8 2010 negative photoresist assisted thermal bonding with glass and direct adhesive bonding using PDMS and plastic cell phone screen protector have been proposed. However, since PDMS was found to detach from the PMMA slice after few days this bonding cannot be considered for commercial purposes. The commercially available cell phone screen protector had a thickness of about 100 µm. When goes for the mass production of the device by injection molding method, it is found to be very difficult to produce mold at this small thickness. While sealing of micropatterned PMMA with glass substrate by photoresist assisted thermal bonding showed leakages at some contacting points thus questioning the bonding strength. In this scenario a cheap, simple, fast and deformation free method for bonding of two PMMA substrates is desirable.

In this work, an isopropyl alcohol assisted thermal bonding method has been developed to assemble the microfluidic device. The hot isopropyl alcohol was deposited in protected environment on the flat substrate. The two PMMA slices were then put together blocking the position with clamps and immediately transferred in oven.

Once the device was assembled it was connected to the micro pumping system by capillary tubes (Figure 5.3a) and the *in-flow* functionalization was performed through the serpentine, followed by optical microscope monitoring (sequence in Figure 5.3b). The complete transparency of the device improved also the reproducibility of the assay and allowed the online monitoring of the flow injection. Sequence of solutions were injected in the serpentine channels starting from Aptes 5% in ethanol. This step resulted in the incorporation of amine functionality and hydrophilization of the PMMA surface. PMMA was grafted by condensation reaction of the surface with sylanol group of Aptes, creating Amine-functionalized PMMA (PMMA-$NH_2$). This made the PMMA channels hydrophilic, allowing the easier flowing of following water-based solutions. After a washing step with water, Glutaraldehyde 0.05% was subsequently injected, which, interacting with the amine-activated group produced PMMA-Glutaraldehyde. The latter underwent, in the following phase, an imine coupling reaction with amine group of the antibody, thus achieving immobilization of the Anti- EpCAM antibody [269][270].

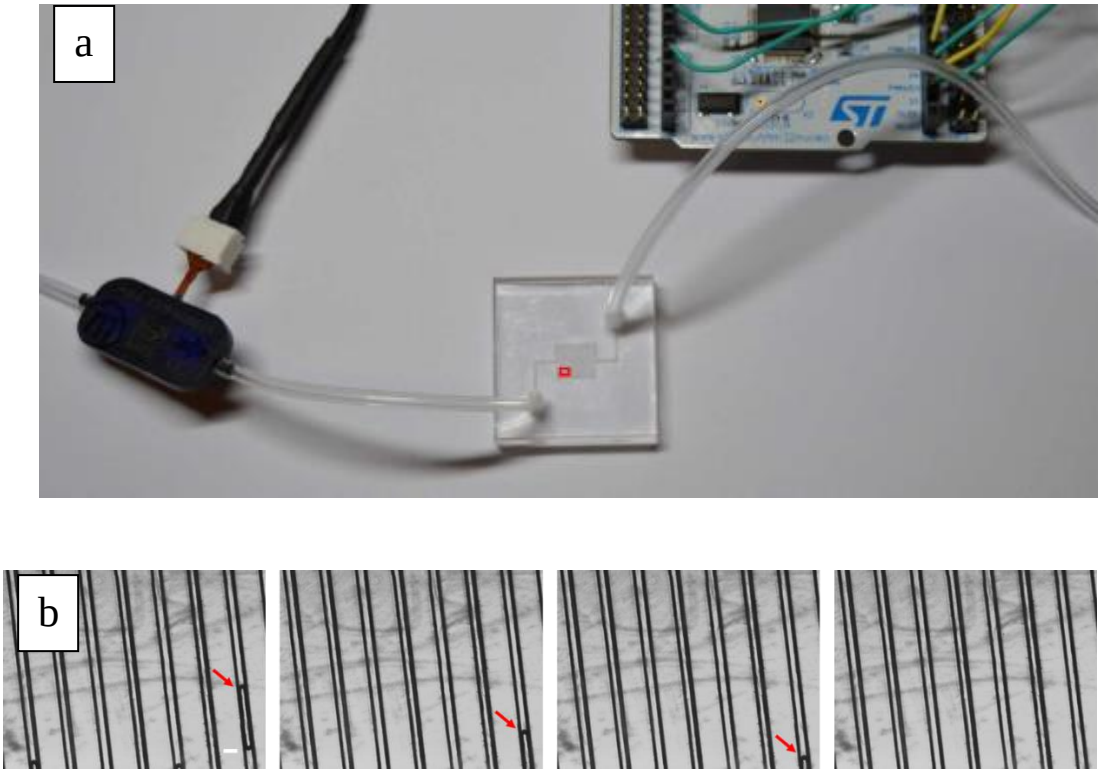


*Figure 5.3: (a) Image of final device with microfluidic connection and micropump. (b) Monitoring of flow into microchannels under optical microscope. The sequence of bubbles generated during injection allows to follow the serpentine channel functionalization. Scale bar: 100 μm.*

# 5.4 CTC capture experiments

The microfluidic device has been tested to capture cancer cells from a mixture of normal and tumor cells. For this reason, in the last step, the Anti-EpCAM antibody has been immobilized, which is able to recognize human EpCAM, a membrane biomarker that is typically present on the surface of epithelial-type cancer cells [271][272]. With a view to demonstrate the effectiveness of the device, the culture medium samples have been spiked with two different population of cells (blood and tumor cells) in order to simulate a complex real sample. In particular, Jurkat cells (blood derived cells) and OECM-1 Human Oral Squamous Carcinoma cell line (Epithelial-like cells from human oral cancer) were used. 5 ml suspensions of cells containing $10^6$ cells/ml from Jurkat line and $10^4$ cells/ml from OECM-1 line have been prepared separately. Cell suspensions were allowed to slowly flow through the serpentine microchannel with a flow rate of 8 μl/min. The low velocity of the fluid, the size of the channel and its serpentine shape have been

optimized to maximize cell interactions with the internal walls, where antibodies fixed on the surface can recognize cells expressing the membrane epithelial antigen.

In the case of Jurkat cells, no or very few cells were identified in the channels after a washing step with PBS solution (Figure 5.4). Jurkat cells indeed did not express EpCAM antigen on the surface of cell membrane, thus they could not be recognized and fixed by antibodies immobilized on channels' walls. In order to demonstrate the presence of Jurkat cells in the serpentine, a hole in the channel was opened during the experiment, where they quickly accumulated, dragged by fluidic forces (Figure 5.5). The hole was introduced in the middle of the channel because the outlet was far and was connected to the tubes. The hole was made before injecting the cells but after the functionalization of the chip and repeated the experiment by cleaned up the debris just to demonstrate the presence of Jurkat cells indeed the hole is not a part of the final chip. Since the Jurkat cells won't attached to the channel, they were flow away.

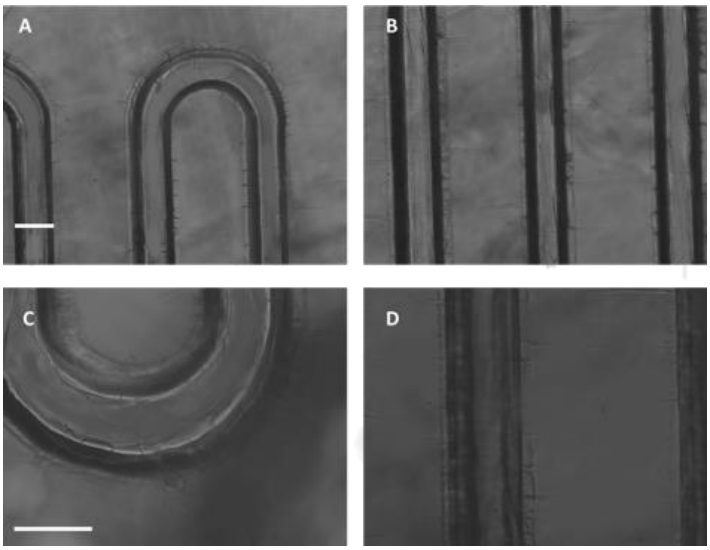


*Figure 5.4: PMMA microchannels after flowing of Jurkat cells and subsequent washing step in PBS. No or few cells are visible into the microchannel. Scale bar: 100 µm*

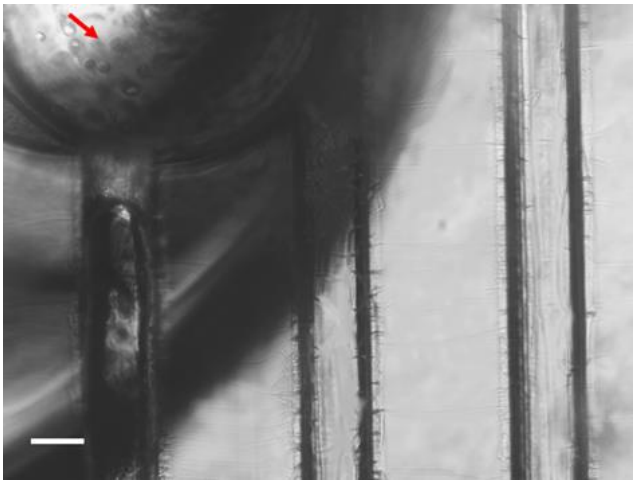

*Figure 5.5: Jurkat cells at the outlet of the device. Scale bar: 100 µm*

In the case of OECM-1 suspension of cells, instead, a high number was captured on the inner walls, adhering to the surface also after a PBS washing step. As demonstrated by Figure 5.6, cells are clearly visible through the transparent PMMA device, confirming the possibility of such a tool to be used as a diagnostic instrument to immobilize and discriminate cancer cells from normal blood cells.

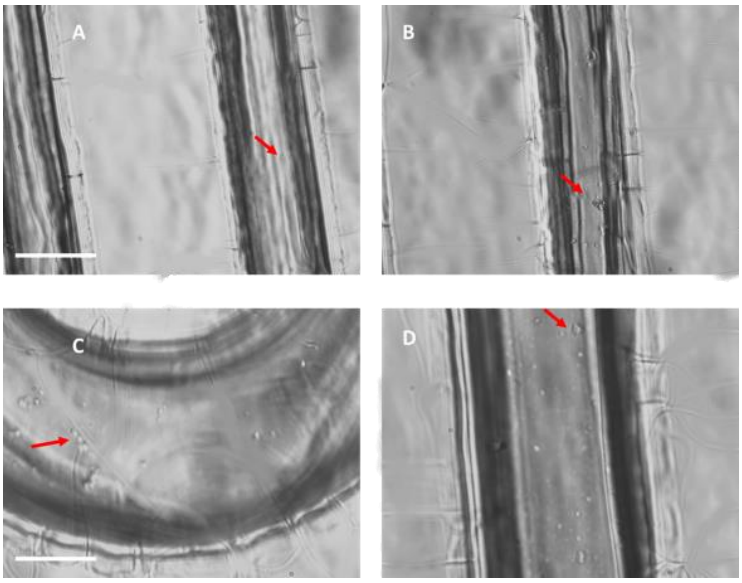


*Figure 5.6: PMMA microchannel after flowing with OECM-1 cells and subsequent washing step with PBS. A high number of cells are captured on the inner surface of channel.*

As it can be seen from high magnification pictures, some wrinkles are evident outside the channel. This is a typical issue occurring with solvent-assisted bonding of thermoplastic materials, and they are probably due to the stress induced by the combination of solvent and temperature treatments, as reported in literature [273]. In

many cases, the presence of cracks is so pronounced that the structure of channels is affected, limiting the applicability of the device. In this case, wrinkles were present only on the surface of the device outside the serpentine, due to the fact that only the flat PMMA substrate was spin-coated with isopropanol and not the upper layer (Figure 5.1a). In this way, the isopropanol never touched the channels during bonding but acted just on the unmodified portions of the milled plate, which were those that supported adhesion.

## 5.5 Discussion

Here, a microfluidic PMMA device has been realized and its capability to capture tumor cells were tested directly in flow. A smart and cost effective fabrication procedure was employed, based on three steps: (i) fabrication of the microfluidic network using an hybrid micro-manufacturing platform which combines fs-laser and mechanical micro milling technologies; (ii) assembly and sealing of the device using a facile and low-cost thermal and solvent-assisted bonding method; (iii) in-flow and on-chip functionalization of the obtained microchannels.

The adoption of this procedure allows to easily prototype devices for many different applications. The whole volume of sample contained in a given moment into the channel was very low (few microliters), but considering the in-flow operation, this configuration is useful for the on-chip collection of rare cells and the enrichment of the sample starting from higher volumes. The same device presented here can be used in a plethora of interesting contexts, as it is a valuable tool not only for the mere study of cells but also for on-site diagnostics, if embedded in a more complex setup.

The hybrid micro-fabrication platform takes advantage from the combination of two advanced manufacturing technologies such as ultrafast laser micromachining and mechanical micro milling that are both extremely flexible and particularly suitable for rapid prototyping of customizable LOCs. While fs-laser ablation, being non-contact, allows fabrication of complex geometrical features with negligible collateral damage of the surrounding material and, in addition, provides micrometric precision thanks to the possibility of focusing the laser radiation in a diffraction limited spot, mechanical micro milling enables to significantly reduce processing times especially when manufacturing larger and simply features, such as holes, that do not require high levels of precision.

An easy and noteworthy low-cost bonding method has been also described, in which neither glues or additional gaskets are required nor a disruptive process with aggressive solvents or temperatures. The choice of PMMA as the material to build the entire device is of strong interest for its feature of being inexpensive and particularly suitable for industrial exploitation. In comparison with other polymers used for the manufacture of microfluidic devices PMMA is stiffer and therefore ensures better mechanical stability, reproducibility and durability of the microfluidic network.

Moreover, the complete transparency of the device has been preserved throughout the fabrication, allowing the perfect alignment during multi-step procedures and the real time monitoring of experiments. This is of crucial importance to check the correct filling of channels and to follow all the steps of experiments under a microscope lens.

As a proof of concept, the assembled device was used as a tool for circulating tumor cells detection. CTC number in blood is highly variable, depending on the stage and aggressivity of a tumor, but their detection at an early stage is considered as a key factor for clinicians' decision-making. This kind of analysis falls within liquid biopsy, aiming at the development of always less invasive methods of analysis and to increase patient's compliance. In order to build up a tool for CTC detection, the microfluidic channel was realized through rapid prototyping methods and functionalized it with Anti-EpCAM antibodies, able to bind a membrane protein highly expressed on the surface of most epithelial malignant tissues [274]. The recognized EpCAM antigen has a regulatory function in cell-cell adhesion strength and tissue plasticity and plays an important role in epithelial cells proliferation and differentiation and is considered as a useful tool for research of epithelial cells, cancer diagnostics and prediction of disease progression [272].

Microfluidics was used to both functionalize and capture human Oral Squamous Carcinoma Cells from spiked suspension of OECM-1 cell culture medium, thus simulating a condition in which a sample may contain few tumor cells into a big amount of blood healthy cells. Blood derived cells flow into serpentine channel without being recognized by capture antibodies able to bind only cancer cells. The starting volume of the sample was 5 ml, thus demonstrating that the device, which contains a total volume of 2 μl, can be used also for the enrichment and concentration of diluted solutions. This result is of high impact in the field of liquid biopsy where this kind of cells are present in

a very low number and collecting them in a little volume or space means the possibility to have consistent biological material for further analysis.

# Chapter 6
# Microfabrication of polymeric lab-on-a-chip for neuronal cell culturing

## 6.1 Introduction

In this section, several microfluidic devices have been fabricated on PMMA to study the primary hippocampal cell culture. The devices have been fabricated exploiting two methods, namely femtosecond laser ablation and hot embossing technique. The design of the device, which is a compartmentalized structure, has been chosen from the previous works [275][276]. Compartmentalized microfluidic devices (CMDs) have been shown (cite) to be highly advantageous to understand the complex network circuit in the Central Nervous System (CNS). More interestingly, it has been used to understand the communication between peripheral neurons and non-neuronal tissues. Communication between neurons and different cell populations is of massive interest to understand how the nervous system controls tissues, both in homeostatic and pathological conditions [277]. Furthermore, CMD design gives more control over the cellular microenvironment with the ability to create distinct regions to mimic in vivo conditions and offers also the possibility to culture different cell types in different compartments.

The growth of the neuronal cells in both fs-laser ablated and hot embossed LOC devices have been realised by staining using immunocytochemistry, particularly primary hippocampal cells were used for culturing.

## 6.2 Fabrication of the device

### 6.2.1 Device design

A compartmentalised microfluidic platform for cell culture is shown in Figure 6.1. It incorporates a physical barrier with embedded microchannels separating two mirror compartments of big channels, that can polarize the growth of central nervous system (CNS) axons into a fluidically isolated environment under the help of hydrostatic pressure.

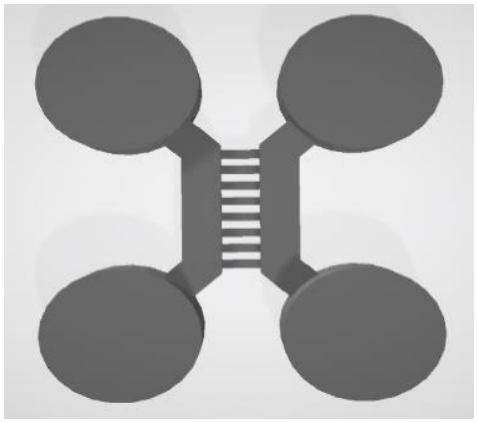

*Figure 6.1: Compartmentalised device design for cell culture*

More precisely, the device consists of two parallel big channels (8 mm long, 2 mm wide and 100 µm deep) which are fed by open inlet and outlet wells at each end of the channels. The area between the two parallel channels is bridged by an array of 100 micro channels (500µm long, 10 µm wide and 8 µm deep) allowing both axons and dendrites to enter and form synapses with the opposing culture.

### 6.2.2 Laser ablated device

The CAD drawing of the previously proposed design was transferred in machine code of the femtosecond laser galvo-scan head to fabricate the device for cell culture (Figure 6.2a). The array of microchannels (Figure 6.2b) were fabricated using the Pharos laser system described in the Chapter 3, section 3.3.1.2. A repetition rate of 0.625 KHz, a pulse energy of 0.017 µJ and a scan speed of 1 mm/s have been chosen as the laser parameters to mill the microchannel arrays after a series of optimization tests. In order to obtain 500 µm long, 8 µm deep and 10 µm wide microchannels the laser beam was focused to the 1 mm thick PMMA substrate through a 2.5 cm focal length convex lens. The two big channels for the cell culture were fabricated using the TruMicro 5050 Femto Edition laser. 8 mm long, 2 mm wide and 100µm deep channels were milled by superimposing two perpendicular scanning patterns with 5µm lateral distance between parallel scan lines. A repetition rate of R.R. 50 kHz, a pulse energy of 12µJ, and a scan speed 40 mm/s were selected as the laser parameters for milling thanks to the statistical study described in chapter 4. Furthermore, 8mm diameter inlet/outlet wells were drilled

at each end of the big channels using the mechanical micro milling machine. The 8 mm dimension was chosen to ensure enough fluid input into the culturing channels.

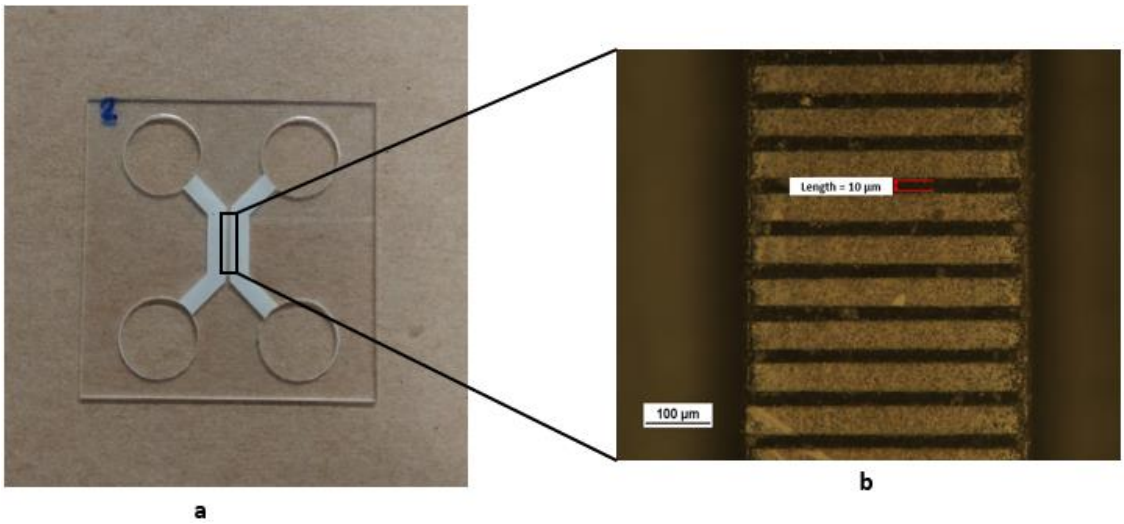


*Figure 6.2: (a) Laser ablated device for neuronal cell culture. (b) microscopic image of the microchannels in between the big cell culture channels.*

## 6.2.3 Hot embossed device

### 6.2.3.1 Master mold preparation

The EpoxyAcast 690 master was prepared from a PDMS mold that was cast from a prepatterned silicon master using soft lithography. A mixture of PDMS and curing agent was prepared in a 10:1 ratio and poured into the micropatterned silicon master, placed in a petri dish. A thorough degassing was applied by using a desiccator to remove the bubbles inside the PDMS cast and put inside a preheated oven for 2 hours and 30 minutes at 80°C. The PDMS was demoulded from the silicon master after the petri dish was cooled down to the room temperature. The PDMS cast obtained was then used as the master mold for EpoxyAcast 690 casting. A mixture of EpoxyAcast 690 and curing agent was prepared in a 7:3 ratio and slowly poured into the PDMS master mold. The degassing was performed to remove any trapped bubbles between uncured EpoxyAcast 690 and PDMS cast and it was left for 48 hours at room temperature (22°C). After 48 hours, a solid cross-linked EpoxyAcast 690 master for hot embossing was obtained by detaching it from the PDMS mold.

### 6.2.3.2 Hot embossing of the device

The previously fabricated micropatterned EpoxyAcast 690 master mold and a 5 mm thick PMMA flat substrate were heated to different loading temperatures $L_T$ (from 130°C to 150°C) above the glass transition temperature of PMMA ($T_g$=120°C) under various pressure loads (loading pressure$L_P$, 0.2 ton to 0.3 ton) for 15 minutes. Afterwards, the loading temperature has been decreased by maintaining the pressure load and leaving the system for 1 hour to reach room temperature (22°C). Once the master-sample set was cooled, the pressure was release by the valve and the sample was picked out from the machine. The imprinted PMMA substrate was demolded from the EpoxyAcast 690 master by hand. Inlet and outlet holes with 4 mm diameters were drilled by a mechanical drill machine. Several types of microchannels (Figure 6.3 a & b) have been realised by changing the channel patterns in the master mold. Figure 6.4 shows a picture of the whole device where the microchannels were 500 µm long, 8 µm deep, while the big channels were 8 mm long, 2 mm wide and 100µm deep.

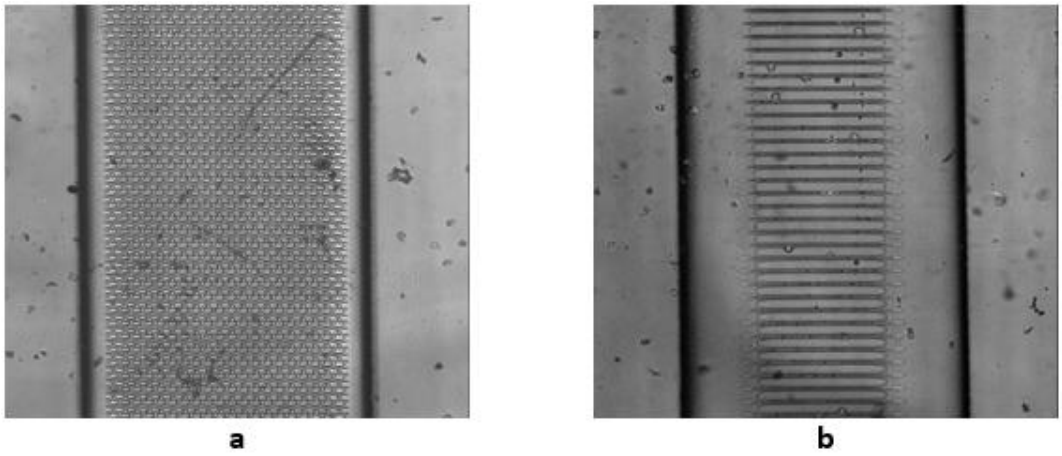


*Figure 6.3: Microscopic image of the different types of hot embossed microchannels in between the 2 big cell culture channels (a) leaf type microchannels (b) straight microchannels*

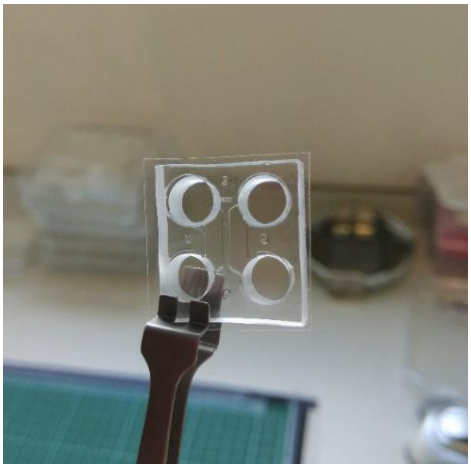

*Figure 6.4: Hot embossed device for neuronal cell culture*

Since EpoxyAcast 690 master mold is reusable it was used numerous times for the replication of the same device.

# 6.3 Preparation for cell culture

Both hot embossed and laser ablated substrates were bonded to a piece of pressure sensitive adhesive film to create complete devices. These were exposed to oxygen plasma to render the surfaces hydrophilic and sterilised, with 70% ethanol added to prevent bubble formation in the channels. Ethanol was removed and the top wells of each device were filled with sterile poly-l-ornithine (PLO). This was left for 3 hours and to improve cells attachment. The PLO was then removed, and channels rinsed using culture medium. Devices were stored in a humidified incubator (37°C, 5% $CO_2$) prior to cell injection. The isolation of the hippocampal cells is described in Chapter 3, section 3.5.2.1.

# 6.4 Results and discussion

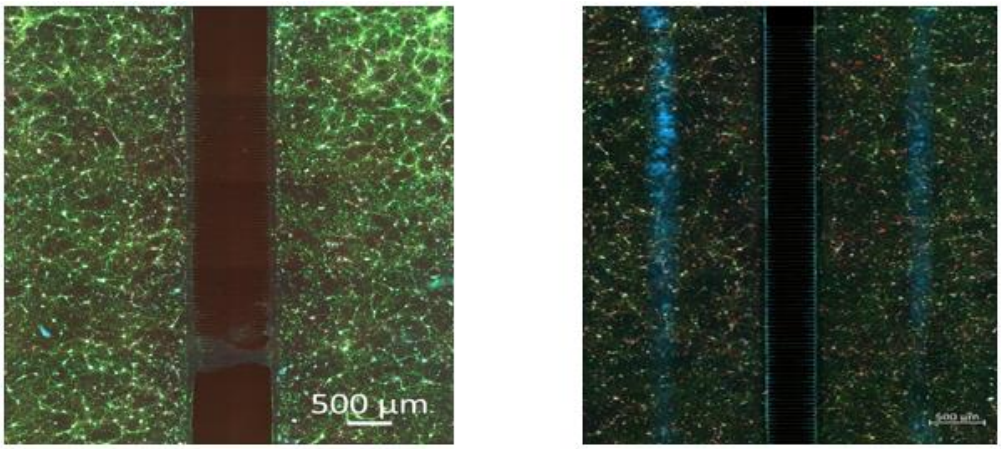


*Figure 6.5: Images taken following immunocytochemical staining after 12-14 days in vitro of primary hippocampal cells cultured in (a) hot embossed and (b) laser ablated PMMA devices. Images are for separate cultures.*

From Figure 6.5a, neuronal staining in hot embossed devices reveals cellular networks formed between neurons, with obvious βIII-tubulin staining (green). This suggests that PMMA does not hamper growth of primary neuronal cultures. However, there are no neurites completely crossing the microchannels and so cells between the two culture channels in this example are not connected.

From Figure 6.5b, neuronal staining in the laser ablated device is less obvious, however these results are from cells isolated separately to those in the hot embossed device. The differences may be due to a number of reasons relating to the culture or staining process, but it is unlikely that laser ablation will have a detrimental impact on the cellular growth. Thus, the poor growth of cells is likely due to other factors such as infection, poor nutrient exchange relating to media refreshing, differences in cell density, or simply with the staining protocol. These factors need to be addressed by further investigation.

Further characterization work is also needed to check whether the hot embossed microchannels are not blocked because of clogging during the embossing process. It was observed that laser ablation renders the PMMA surface not enough transparent because of the increased surface roughness, thus preventing imaging using a light microscope. This implies that cells in big channels cannot be monitored immediately after injection

thus creating a ‘blind’ culture. However, the preliminary observations have shown that primary hippocampal neurons are able to grow and form connections with neighbouring cells and remain functional after 14 days in vitro when cultured in PMMA devices. This represents an alternative to the traditionally used PDMS devices for cell culture applications.

# Conclusions

In this thesis two prototypes of polymeric lab-on-a-chips were designed, fabricated and validated for different biological applications. The rapid prototyping of the LOCs was done by femtosecond laser-based procedures.

In order to avoid a time-consuming trial and error approach for the laser microfabrication, an accurate statistical Design of Experiment (DoE) procedure is defined to estimate the influence of the laser repetition rate, pulse energy, scanning speed, and hatch distance on the fs-laser micro milled depth of the microstructures. Once it was found the model describing the relationship between the response variable depth and the main laser parameters, as the outcome of the research, two different prototypes of polymeric LoCs have been fabricated:

1. A lab-on-a-chip for capturing circulating tumour (CTC) cells.
2. A lab-on-a-chip for neuronal cell culturing.

As part of the fabrication of LoCs a new simple and low-cost bonding technique has been also established.

The CTC capturing device has been realized by a smart microfabrication procedure combining femtosecond laser technology and mechanical micro milling. The microfluidic device was tested to capture cancer cells from a mixture of normal and tumour cells.

The LOC for neuronal cell culturing was realized by a compartmentalized structure and was fabricated by exploiting two microfabrication methods such as femtosecond laser ablation and hot embossing. The growth of the neuronal cells in the polymeric LOC devices was realised by staining using immunocytochemistry.

For all prototypes PMMA was chosen as polymeric substrate. PMMA is a good candidate for the LOC fabrication thanks to its low-cost, biocompatibility, nontoxicity, and transparency. Moreover, the rigidity of PMMA makes it adequate to high pressures applications, where an inflexible structure is to be preferred.

In the statistical Design of Experiment procedure, a two-level full factorial design with resolution V [278] has been defined so that main effects are unconfounded with 3-

factor interactions. Two replicas, as defined by the Power Analysis, based on blocking on the day, have been set to evaluate the influence of the day as possible nuisance factor.

The Factorial design indicated that the pulse energy and its interaction with the other variables are the main factors affecting the depth.

A regression predictive model has been identified and validated in 3 points out of the factorial plan. All the depth values of the trials fall within the prediction interval (PI) and one of them fall within the confidence interval (CI), which is more restricted than the PI, proving the good prediction capability of the regression model.

The CTC capturing device was realized by a smart microfabrication procedure by combining femtosecond laser technology and mechanical micro milling. Even though femtosecond laser technology has lot of advantages, it has also some disadvantages. It is expensive and not good for structuring large area in less time. The hybrid micro-fabrication platform took advantages from both the ultrafast lasers and mechanical micro milling. The serpentine microchannel with micrometric precision was fabricated by femtosecond laser milling with negligible collateral damage of the surrounding material. While the inlet/outlet holes, which do not require high level of precision, were fabricated using mechanical micro milling. The device was assembled and sealed by using a facile and low-cost isopropanol assisted thermal bonding method.

The functionality of the device was tested to capture human Oral Squamous Carcinoma Cells from spiked suspension of OECM-1 cell culture medium. To this purpose Anti-EpCAM antibody was immobilized in the serpentine microchannel, which was able to recognize human EpCAM.

Compartmentalized microfluidic devices for neuronal cell culturing were fabricated by exploiting two microfabrication methods, in particular femtosecond laser ablation and hot embossing. The compartmentalized design consisted of two parallel big channels bridged by an array of microchannels. The ability of fs-laser ablated, and hot embossed LOCs were assessed by immunocytochemistry for primary hippocampal cell culture.

The observations showed that primary hippocampal neurons are able to grow and form connections with neighboring cells and remain functional after 14 days in vitro when cultured in PMMA devices. This represents an alternative to the traditionally used PDMS devices for cell culture applications.

The results presented in this thesis demonstrated that femtosecond laser-based micromachining procedures are very promising for the rapid prototyping of polymeric LOC fabrication. One of its strongest characteristics is the versatility and the great freedom in designing and fabricating complex 3D microfluidic geometries with high precision and reliability. The adoption of hybrid procedures allows to easily prototype devices for many different applications. Furthermore, among the large pool of polymers PMMA is a great candidate for the fabrication LOCs due to plenty of unique characteristics. In particular, the low cost of PMMA opens the door to the mass production and commercialization of polymeric LOCs. In the near future polymeric LOCs are going to be part of daily life for various applications.

# Bibliography


[1] W. Snyder, G. Bilbro, Y. S. Han, R. Whitaker, and S. Pizer, "Image Relaxation: Restoration and Feature Extraction," *IEEE Trans. Pattern Anal. Mach. Intell.*, vol. 17, no. 6, pp. 620–624, 1995, doi: 10.1109/34.387509.

[2] C. Ho and Y. Tai, "MICRO-ELECTRO-MECHANICAL- SYSTEMS ( MEMS ) AND FLUID," pp. 579–612, 1998.

[3] S. G. Kandlikar, "F Lexible M Ethods for," vol. 54, no. 6, pp. 42–48, 2001, doi: 10.1063/1.1387591.

[4] G. M. Walker and D. J. Beebe, "A passive pumping method for microfluidic devices," *Lab Chip*, vol. 2, no. 3, pp. 131–134, 2002, doi: 10.1039/b204381e.

[5] S. H. Lee *et al.*, "Capillary based patterning of cellular communities in laterally open channels," *Anal. Chem.*, vol. 82, no. 7, pp. 2900–2906, 2010, doi: 10.1021/ac902903q.

[6] S. M. Berry, L. J. MacCoux, and D. J. Beebe, "Streamlining immunoassays with immiscible filtrations assisted by surface tension," *Anal. Chem.*, vol. 84, no. 13, pp. 5518–5523, 2012, doi: 10.1021/ac300085m.

[7] S. L. Anna, N. Bontoux, and H. A. Stone, "Formation of dispersions using 'flow focusing' in microchannels," *Appl. Phys. Lett.*, vol. 82, no. 3, pp. 364–366, 2003, doi: 10.1063/1.1537519.

[8] D. Mark, S. Haeberle, G. Roth, F. Von Stetten, and R. Zengerle, "Microfluidic lab-on-a-chip platforms: Requirements, characteristics and applications," *NATO Sci. Peace Secur. Ser. A Chem. Biol.*, no. 3, pp. 305–376, 2010, doi: 10.1007/978-90-481-9029-4-17.

[9] M. Danova, M. Torchio, and G. Mazzini, "Isolation of rare circulating tumor cells in cancer patients: Technical aspects and clinical implications," *Expert Rev. Mol. Diagn.*, vol. 11, no. 5, pp. 473–485, 2011, doi: 10.1586/erm.11.33.

[10] D. C. Colter, I. Sekiya, and D. J. Prockop, "Identification of a subpopulation of rapidly self-renewing and multipotential adult stem cells in colonies of human marrow stromal cells," *Proc. Natl. Acad. Sci. U. S. A.*, vol. 98, no. 14, pp. 7841–7845, 2001, doi: 10.1073/pnas.141221698.

[11] K. Jo, Y. L. Chen, J. J. De Pablo, and D. C. Schwartz, "Elongation and migration of single DNA molecules in microchannels using oscillatory shear flows," *Lab Chip*, vol. 9, no. 16, pp. 2348–2355, 2009, doi: 10.1039/b902292a.

[12] P. Gascoyne, J. Satayavivad, and M. Ruchirawat, "Microfluidic approaches to malaria detection," *Acta Trop.*, vol. 89, no. 3, pp. 357–369, 2004, doi: 10.1016/j.actatropica.2003.11.009.

[13] A. Van De Stolpe, K. Pantel, S. Sleijfer, L. W. Terstappen, and J. M. J. Den Toonder, "Circulating tumor cell isolation and diagnostics: Toward routine clinical use," *Cancer Res.*, vol. 71, no. 18, pp. 5955–5960, 2011, doi: 10.1158/0008-5472.CAN-11-1254.

[14] X. Cheng *et al.*, "A microfluidic device for practical label-free CD4+ T cell counting of HIV-infected subjects," *Lab Chip*, vol. 7, no. 2, pp. 170–178, 2007, doi: 10.1039/b612966h.

[15] J. Den Toonder, “Circulating tumor cells: The Grand Challenge,” *Lab Chip*, vol. 11, no. 3, pp. 375–377, 2011, doi: 10.1039/c0lc90100h.
[16] D. Gänshirt *et al.*, “Enrichment of fetal nucleated red blood cells from the maternal circulation for prenatal diagnosis experiences with triple density gradient and MACS based on more than 600 cases,” *Fetal Diagn. Ther.*, vol. 13, no. 5, pp. 276–286, 1998, doi: 10.1159/000020854.
[17] G. Vona *et al.*, “Isolation by size of epithelial tumor cells: A new method for the immunomorphological and molecular characterization of circulating tumor cells,” *Am. J. Pathol.*, vol. 156, no. 1, pp. 57–63, 2000, doi: 10.1016/S0002-9440(10)64706-2.
[18] D. Vlasselaers *et al.*, “Monitoring blood glucose with microdialysis of interstitial fluid in critically ill children [3],” *Clin. Chem.*, vol. 53, no. 3, pp. 536–537, 2007, doi: 10.1373/clinchem.2006.078089.
[19] H. M. Shapiro, “Pages_from_Practical_Flow_Cytometry.pdf.” .
[20] S. Miltenyi, W. Müller, W. Weichel, and A. Radbruch, “High gradient magnetic cell separation with MACS,” *Cytometry*, vol. 11, no. 2, pp. 231–238, 1990, doi: 10.1002/cyto.990110203.
[21] A. A. S. Bhagat, H. Bow, H. W. Hou, S. J. Tan, J. Han, and C. T. Lim, “Microfluidics for cell separation,” *Med. Biol. Eng. Comput.*, vol. 48, no. 10, pp. 999–1014, 2010, doi: 10.1007/s11517-010-0611-4.
[22] A. H. J. Yang, S. D. Moore, B. S. Schmidt, M. Klug, M. Lipson, and D. Erickson, “Optical manipulation of nanoparticles and biomolecules in sub-wavelength slot waveguides,” *Nature*, vol. 457, no. 7225, pp. 71–75, 2009, doi: 10.1038/nature07593.
[23] A. E. Cohen, “Control of nanoparticles with arbitrary two-dimensional force fields,” *Phys. Rev. Lett.*, vol. 94, no. 11, pp. 1–4, 2005, doi: 10.1103/PhysRevLett.94.118102.
[24] H. Lee, A. M. Purdon, and R. M. Westervelt, “Manipulation of biological cells using a microelectromagnet matrix,” *Appl. Phys. Lett.*, vol. 85, no. 6, pp. 1063–1065, 2004, doi: 10.1063/1.1776339.
[25] M. Evander *et al.*, “Noninvasive acoustic cell trapping in a microfluidic perfusion system for online bioassays,” *Anal. Chem.*, vol. 79, no. 7, pp. 2984–2991, 2007, doi: 10.1021/ac061576v.
[26] R. Dylla-Spears, J. E. Townsend, L. Jen-Jacobson, L. L. Sohn, and S. J. Muller, “Single-molecule sequence detection via microfluidic planar extensional flow at a stagnation point,” *Lab Chip*, vol. 10, no. 12, pp. 1543–1549, 2010, doi: 10.1039/b926847b.
[27] M. Yamada and M. Seki, “Hydrodynamic filtration for on-chip particle concentration and classification utilizing microfluidics,” *Lab Chip*, vol. 5, no. 11, pp. 1233–1239, 2005, doi: 10.1039/b509386d.
[28] C. Jin *et al.*, “Technologies for label-free separation of circulating tumor cells: From historical foundations to recent developments,” *Lab Chip*, vol. 14, no. 1, pp. 32–44, 2014, doi: 10.1039/c3lc50625h.
[29] C. Wyatt Shields Iv, C. D. Reyes, and G. P. López, “Microfluidic cell sorting: A review of the advances in the separation of cells from debulking to rare cell isolation,” *Lab Chip*, vol. 15, no. 5, pp. 1230–1249, 2015, doi: 10.1039/c4lc01246a.
[30] J. McGrath, M. Jimenez, and H. Bridle, “Deterministic lateral displacement for

particle separation: A review," *Lab Chip*, vol. 14, no. 21, pp. 4139–4158, 2014, doi: 10.1039/c4lc00939h.

[31] L. R. Huang, E. C. Cox, R. H. Austin, and J. C. Sturm, "Continuous Particle Separation Through Deterministic Lateral Displacement," *Science (80-. ).*, vol. 304, no. 5673, pp. 987–990, 2004, doi: 10.1126/science.1094567.

[32] M. Yamada, M. Nakashima, and M. Seki, "Pinched flow fractionation: Continuous size separation of particles utilizing a laminar flow profile in a pinched microchannel," *Anal. Chem.*, vol. 76, no. 18, pp. 5465–5471, 2004, doi: 10.1021/ac049863r.

[33] A. Lenshof, C. Magnusson, and T. Laurell, "Acoustofluidics 8: Applications of acoustophoresis in continuous flow microsystems," *Lab Chip*, vol. 12, no. 7, pp. 1210–1223, 2012, doi: 10.1039/c2lc21256k.

[34] Z. R. Gagnon, "Cellular dielectrophoresis: Applications to the characterization, manipulation, separation and patterning of cells," *Electrophoresis*, vol. 32, no. 18, pp. 2466–2487, 2011, doi: 10.1002/elps.201100060.

[35] P. R. C. Gascoyne and J. Vykoukal, "Particle separation by dielectrophoresis," *Electrophoresis*, vol. 23, no. 13, pp. 1973–1983, 2002, doi: 10.1002/1522-2683(200207)23:13<1973::AID-ELPS1973>3.0.CO;2-1.

[36] M. Li, W. H. Li, J. Zhang, G. Alici, and W. Wen, "A review of microfabrication techniques and dielectrophoretic microdevices for particle manipulation and separation," *J. Phys. D. Appl. Phys.*, vol. 47, no. 6, 2014, doi: 10.1088/0022-3727/47/6/063001.

[37] N. Pamme, J. C. T. Eijkel, and A. Manz, "On-chip free-flow magnetophoresis: Separation and detection of mixtures of magnetic particles in continuous flow," *J. Magn. Magn. Mater.*, vol. 307, no. 2, pp. 237–244, 2006, doi: 10.1016/j.jmmm.2006.04.008.

[38] X. Chen, D. Cui, C. Liu, H. Li, and J. Chen, "Continuous flow microfluidic device for cell separation, cell lysis and DNA purification," *Anal. Chim. Acta*, vol. 584, no. 2, pp. 237–243, 2007, doi: 10.1016/j.aca.2006.11.057.

[39] M. Hosokawa *et al.*, "Microcavity array system for size-based enrichment of circulating tumor cells from the blood of patients with small-cell lung cancer," *Anal. Chem.*, vol. 85, no. 12, pp. 5692–5698, 2013, doi: 10.1021/ac400167x.

[40] T. H. Kim *et al.*, "FAST: Size-Selective, clog-free isolation of rare cancer cells from whole blood at a liquid-liquid interface," *Anal. Chem.*, vol. 89, no. 2, pp. 1155–1162, 2017, doi: 10.1021/acs.analchem.6b03534.

[41] N. M. Karabacak *et al.*, "Microfluidic, marker-free isolation of circulating tumor cells from blood samples," *Nat. Protoc.*, vol. 9, no. 3, pp. 694–710, 2014, doi: 10.1038/nprot.2014.044.

[42] M. M. Ferreira, V. C. Ramani, and S. S. Jeffrey, "Circulating tumor cell technologies," *Mol. Oncol.*, vol. 10, no. 3, pp. 374–394, 2016, doi: 10.1016/j.molonc.2016.01.007.

[43] E. Racila *et al.*, "Detection and characterization of carcinoma cells in the blood," *Proc. Natl. Acad. Sci. U. S. A.*, vol. 95, no. 8, pp. 4589–4594, 1998, doi: 10.1073/pnas.95.8.4589.

[44] A. A. Adams *et al.*, "Highly efficient circulating tumor cell isolation from whole blood and label-free enumeration using polymer-based microfluidics with an integrated conductivity sensor," *J. Am. Chem. Soc.*, vol. 130, no. 27, pp. 8633–8641, 2008, doi: 10.1021/ja8015022.

[45] U. Dharmasiri, S. Balamurugan, A. A. Adams, P. I. Okagbare, A. Obubuafo, and S. A. Soper, “Highly efficient capture and enumeration of low abundance prostate cancer cells using prostate-specific membrane antigen aptamers immobilized to a polymeric microfluidic device,” *Electrophoresis*, vol. 30, no. 18, pp. 3289–3300, 2009, doi: 10.1002/elps.200900141.

[46] Y. Ma *et al.*, “A combinatory strategy for detection of live CTCs using microfiltration and a new telomerase-selective adenovirus,” *Mol. Cancer Ther.*, vol. 14, no. 3, pp. 835–843, 2015, doi: 10.1158/1535-7163.MCT-14-0693.

[47] S. Nagrath *et al.*, “Isolation of rare circulating tumour cells in cancer patients by microchip technology,” *Nature*, vol. 450, no. 7173, pp. 1235–1239, 2007, doi: 10.1038/nature06385.

[48] J. P. Gleghorn *et al.*, “Capture of circulating tumor cells from whole blood of prostate cancer patients using geometrically enhanced differential immunocapture (GEDI) and a prostate-specific antibody,” *Lab Chip*, vol. 10, no. 1, pp. 27–29, 2010, doi: 10.1039/b917959c.

[49] R. Edmondson, J. J. Broglie, A. F. Adcock, and L. Yang, “Three-dimensional cell culture systems and their applications in drug discovery and cell-based biosensors,” *Assay Drug Dev. Technol.*, vol. 12, no. 4, pp. 207–218, 2014, doi: 10.1089/adt.2014.573.

[50] J. W. Haycock, “Chapter 1 and Techniques,” *3D Cell Cult. Methods Protoc. Methods Mol. Biol.*, vol. 695, pp. 1–15, 2011, doi: 10.1007/978-1-60761-984-0.

[51] M. Ravi, V. Paramesh, S. R. Kaviya, E. Anuradha, and F. D. Paul Solomon, “3D cell culture systems: Advantages and applications,” *J. Cell. Physiol.*, vol. 230, no. 1, pp. 16–26, 2015, doi: 10.1002/jcp.24683.

[52] D. Huh, G. A. Hamilton, and D. E. Ingber, “From 3D cell culture to organs-on-chips,” *Trends Cell Biol.*, vol. 21, no. 12, pp. 745–754, 2011, doi: 10.1016/j.tcb.2011.09.005.

[53] Y. Fang and R. M. Eglen, “Three-Dimensional Cell Cultures in Drug Discovery and Development,” *SLAS Discov.*, vol. 22, no. 5, pp. 456–472, 2017, doi: 10.1177/1087057117696795.

[54] S. Breslin and L. O’Driscoll, “Three-dimensional cell culture: The missing link in drug discovery,” *Drug Discov. Today*, vol. 18, no. 5–6, pp. 240–249, 2013, doi: 10.1016/j.drudis.2012.10.003.

[55] A. Grosberg, P. W. Alford, M. L. McCain, and K. K. Parker, “Ensembles of engineered cardiac tissues for physiological and pharmacological study: Heart on a chip,” *Lab Chip*, vol. 11, no. 24, pp. 4165–4173, 2011, doi: 10.1039/c1lc20557a.

[56] A. Tourovskaia, M. Fauver, G. Kramer, S. Simonson, and T. Neumann, “Tissue-engineered microenvironment systems for modeling human vasculature,” *Exp. Biol. Med.*, vol. 239, no. 9, pp. 1264–1271, 2014, doi: 10.1177/1535370214539228.

[57] S. Yasotharan, S. Pinto, J. G. Sled, S. S. Bolz, and A. Günther, “Artery-on-a-chip platform for automated, multimodal assessment of cerebral blood vessel structure and function,” *Lab Chip*, vol. 15, no. 12, pp. 2660–2669, 2015, doi: 10.1039/c5lc00021a.

[58] K. Hattori, Y. Munehira, H. Kobayashi, T. Satoh, S. Sugiura, and T. Kanamori, “Microfluidic perfusion culture chip providing different strengths of shear stress for analysis of vascular endothelial function,” *J. Biosci. Bioeng.*, vol. 118, no. 3, pp. 327–332, 2014, doi: 10.1016/j.jbiosc.2014.02.006.

[59] V. M. Dominical, D. M. Vital, F. O'Dowd, S. T. O. Saad, F. F. Costa, and N. Conran, "In vitro microfluidic model for the study of vaso-occlusive processes," *Exp. Hematol.*, vol. 43, no. 3, pp. 223–228, 2015, doi: 10.1016/j.exphem.2014.10.015.

[60] D. G. Harris, P. K. Benipal, X. Cheng, L. Burdorf, A. M. Azimzadeh, and R. N. Pierson, "Four-Dimensional characterization of thrombosis in a live-cell, shear-flow assay: Development and application to xenotransplantation," *PLoS One*, vol. 10, no. 4, pp. 1–16, 2015, doi: 10.1371/journal.pone.0123015.

[61] R. Hu *et al.*, "Microfluidic analysis of pressure drop and flow behavior in hypertensive micro vessels," *Biomed. Microdevices*, vol. 17, no. 3, pp. 1–9, 2015, doi: 10.1007/s10544-015-9959-4.

[62] L. Li, X. Lv, S. Ostrovidov, X. Shi, N. Zhang, and J. Liu, "Biomimetic microfluidic device for in vitro antihypertensive drug evaluation," *Mol. Pharm.*, vol. 11, no. 7, pp. 2009–2015, 2014, doi: 10.1021/mp5000532.

[63] E. S. Hald, K. E. Steucke, J. A. Reeves, Z. Win, and P. W. Alford, "Long-term vascular contractility assay using genipin-modified muscular thin films," *Biofabrication*, vol. 6, no. 4, 2014, doi: 10.1088/1758-5082/6/4/045005.

[64] D. Huh, B. D. Matthews, A. Mammoto, M. Montoya-Zavala, H. Yuan Hsin, and D. E. Ingber, "Reconstituting organ-level lung functions on a chip," *Science (80-. ).*, vol. 328, no. 5986, pp. 1662–1668, 2010, doi: 10.1126/science.1188302.

[65] J. E. Nichols, J. A. Niles, S. P. Vega, L. B. Argueta, A. Eastaway, and J. Cortiella, "Modeling the lung: Design and development of tissue engineered macro- and micro-physiologic lung models for research use," *Exp. Biol. Med.*, vol. 239, no. 9, pp. 1135–1169, 2014, doi: 10.1177/1535370214536679.

[66] E. Li *et al.*, "Continual exposure to cigarette smoke extracts induces tumor-like transformation of human nontumor bronchial epithelial cells in a microfluidic chip," *J. Thorac. Oncol.*, vol. 9, no. 8, pp. 1091–1100, 2014, doi: 10.1097/JTO.0000000000000219.

[67] T. H. Punde *et al.*, "A biologically inspired lung-on-a-chip device for the study of protein-induced lung inflammation," *Integr. Biol. (United Kingdom)*, vol. 7, no. 2, pp. 162–169, 2015, doi: 10.1039/c4ib00239c.

[68] J. Wu *et al.*, "A microfluidic platform for evaluating neutrophil chemotaxis induced by sputum from COPD patients," *PLoS One*, vol. 10, no. 5, pp. 1–13, 2015, doi: 10.1371/journal.pone.0126523.

[69] M. Felder, A. O. Stucki, J. D. Stucki, T. Geiser, and O. T. Guenat, "The potential of microfluidic lung epithelial wounding: Towards in vivo-like alveolar microinjuries," *Integr. Biol. (United Kingdom)*, vol. 6, no. 12, pp. 1132–1140, 2014, doi: 10.1039/c4ib00149d.

[70] H. J. Kim, D. Huh, G. Hamilton, and D. E. Ingber, "Human gut-on-a-chip inhabited by microbial flora that experiences intestinal peristalsis-like motions and flow," *Lab Chip*, vol. 12, no. 12, pp. 2165–2174, 2012, doi: 10.1039/c2lc40074j.

[71] G. Pasirayi, S. M. Scott, M. Islam, L. O'Hare, S. Bateson, and Z. Ali, "Low cost microfluidic cell culture array using normally closed valves for cytotoxicity assay," *Talanta*, vol. 129, pp. 491–498, 2014, doi: 10.1016/j.talanta.2014.06.020.

[72] K. M. Kovach *et al.*, "In vitro evaluation and in vivo demonstration of a biomimetic, hemocompatible, microfluidic artificial lung," *Lab Chip*, vol. 15, no. 5, pp. 1366–1375, 2015, doi: 10.1039/c4lc01284d.

[73] J. Gan, S. M. Greenwood, S. R. Cobb, and T. J. Bushell, "Indirect modulation of

neuronal excitability and synaptic transmission in the hippocampus by activation of proteinase-activated receptor-2," *Br. J. Pharmacol.*, vol. 163, no. 5, pp. 984–994, 2011, doi: 10.1111/j.1476-5381.2011.01293.x.

[74] J. Park, H. Koito, J. Li, and A. Han, "Multi-compartment neuron-glia co-culture platform for localized CNS axon-glia interaction study," *Lab Chip*, vol. 12, no. 18, pp. 3296–3304, 2012, doi: 10.1039/c2lc40303j.

[75] L. Li *et al.*, "Spatiotemporally controlled and multifactor involved assay of neuronal compartment regeneration after chemical injury in an integrated microfluidics," *Anal. Chem.*, vol. 84, no. 15, pp. 6444–6453, 2012, doi: 10.1021/ac3013708.

[76] E. Neto *et al.*, "Sensory neurons and osteoblasts: Close partners in a microfluidic platform," *Integr. Biol. (United Kingdom)*, vol. 6, no. 6, pp. 586–595, 2014, doi: 10.1039/c4ib00035h.

[77] K. A. Southam, A. E. King, C. A. Blizzard, G. H. McCormack, and T. C. Dickson, "Microfluidic primary culture model of the lower motor neuron-neuromuscular junction circuit," *J. Neurosci. Methods*, vol. 218, no. 2, pp. 164–169, 2013, doi: 10.1016/j.jneumeth.2013.06.002.

[78] V. Hessel and H. Löwe, "Microchemical engineering: Components, plant concepts user acceptance - Part I," *Chem. Eng. Technol.*, vol. 26, no. 1, pp. 13–24, 2003, doi: 10.1002/ceat.200390000.

[79] K. F. Lei, "Materials and fabrication techniques for nano-and microfluidic devices," *RSC Detect. Sci.*, vol. 2015-Janua, no. 5, pp. 1–28, 2015.

[80] F. M. Wisser, B. Schumm, G. Mondin, J. Grothe, and S. Kaskel, "Precursor strategies for metallic nano- and micropatterns using soft lithography," *J. Mater. Chem. C*, vol. 3, no. 12, pp. 2717–2731, 2015, doi: 10.1039/c4tc02418d.

[81] M. Hemling *et al.*, "Microfluidics for high school chemistry students," *J. Chem. Educ.*, vol. 91, no. 1, pp. 112–115, 2014, doi: 10.1021/ed4003018.

[82] B. L. Ramos, S. J. Choquette, and N. F. Fell, "Embossable Grating Couplers for Planar Waveguide Optical Sensors," *Anal. Chem.*, vol. 68, no. 7, pp. 1245–1249, 1996, doi: 10.1021/ac950579x.

[83] C. Kawasaki, "Photokilling of T-24 human bladder cancer cell with titanium dioxide molecules," *Yokohama Med. J.*, vol. 46, no. 2, pp. 103–110, 1995.

[84] S. Sarkar, P. K. Biswas, and S. Jana, "Nano silver coated patterned silica thin film by sol-gel based soft lithography technique," *J. Sol-Gel Sci. Technol.*, vol. 61, no. 3, pp. 577–584, 2012, doi: 10.1007/s10971-011-2663-9.

[85] J. H. Moon *et al.*, "Patterned polymer photonic crystals using soft lithography and holographic lithography," *Synth. Met.*, vol. 148, no. 1, pp. 99–102, 2005, doi: 10.1016/j.synthmet.2004.09.019.

[86] M. Abdelgawad, C. Wu, W. Y. Chien, W. R. Geddie, M. A. S. Jewett, and Y. Sun, "A fast and simple method to fabricate circular microchannels in polydimethylsiloxane (PDMS)," *Lab Chip*, vol. 11, no. 3, pp. 545–551, 2011, doi: 10.1039/c0lc00093k.

[87] S. Lakshminarayanan, "Micro/Nano Patterning on Polymers Using Soft Lithography Technique," *Micro/Nanolithography - A Heuristic Asp. Endur. Technol.*, 2018, doi: 10.5772/intechopen.72885.

[88] I. D. Block, L. L. Chan, and B. T. Cunningham, "Large-area submicron replica molding of porous low-k dielectric films and application to photonic crystal biosensor fabrication," *Microelectron. Eng.*, vol. 84, no. 4, pp. 603–608, 2007, doi:

10.1016/j.mee.2006.12.011.
[89] J. T. Borenstein, H. Terai, K. R. King, E. J. Weinberg, M. R. Kaazempur-Mofrad, and J. P. Vacanti, "Microfabrication technology for vascularized tissue engineering," *Biomed. Microdevices*, vol. 4, no. 3, pp. 167–175, 2002, doi: 10.1023/A:1016040212127.
[90] C. J. Bettinger, B. Orrick, A. Misra, R. Langer, and J. T. Borenstein, "Microfabrication of poly (glycerol-sebacate) for contact guidance applications," *Biomaterials*, vol. 27, no. 12, pp. 2558–2565, 2006, doi: 10.1016/j.biomaterials.2005.11.029.
[91] Y. Xia and G. M. Whitesides, "Soft lithography," *Angew. Chemie - Int. Ed.*, vol. 37, no. 5, pp. 550–575, 1998, doi: 10.1002/(sici)1521-3773(19980316)37:5<550::aid-anie550>3.3.co;2-7.
[92] K. Wu, T. C. Bailey, C. G. Willson, and J. G. Ekerdt, "Surface hydration and its effect on fluorinated SAM formation on SiO 2 surfaces," *Langmuir*, vol. 21, no. 25, pp. 11795–11801, 2005, doi: 10.1021/la0516330.
[93] Y. Xu and C. B. Musgrave, "A DFT Study of the Al2O3 Atomic Layer Deposition on SAMs: Effect of SAM Termination," *Chem. Mater.*, vol. 16, no. 4, pp. 646–653, 2004, doi: 10.1021/cm035009p.
[94] D. M. Walba *et al.*, "Self-assembled monolayers for liquid crystal alignment: Simple preparation on glass using alkyltrialkoxysilanes," *Liq. Cryst.*, vol. 31, no. 4, pp. 481–489, 2004, doi: 10.1080/02678290410001666075.
[95] G. J. Kluth, M. M. Sung, and R. Maboudian, "Thermal behavior of alkylsiloxane self-assembled monolayers on the oxidized Si(100) surface," *Langmuir*, vol. 13, no. 14, pp. 3775–3780, 1997, doi: 10.1021/la970135r.
[96] R. N. Orth *et al.*, "Creating Biological Membranes on the Micron Scale: Forming Patterned Lipid Bilayers Using a Polymer Lift-Off Technique," *Biophys. J.*, vol. 85, no. 5, pp. 3066–3073, 2003, doi: 10.1016/S0006-3495(03)74725-0.
[97] M. Mrksich, L. E. Dike, J. Tien, D. E. Ingber, and G. M. Whitesides, "Using microcontact printing to pattern the attachment of mammalian cells to self-assembled monolayers of alkanethiolates on transparent films of gold and silver," *Exp. Cell Res.*, vol. 235, no. 2, pp. 305–313, 1997, doi: 10.1006/excr.1997.3668.
[98] T. Das, S. K. Mallick, D. Paul, S. K. Bhutia, T. K. Bhattacharyya, and T. K. Maiti, "Microcontact printing of Concanavalin A and its effect on mammalian cell morphology," *J. Colloid Interface Sci.*, vol. 314, no. 1, pp. 71–79, 2007, doi: 10.1016/j.jcis.2007.05.017.
[99] G. Vozzi, C. Flaim, A. Ahluwalia, and S. Bhatia, "Fabrication of PLGA scaffolds using soft lithography and microsyringe deposition," *Biomaterials*, vol. 24, no. 14, pp. 2533–2540, 2003, doi: 10.1016/S0142-9612(03)00052-8.
[100] A. Folch, S. Mezzour, M. Düring, O. Hurtado, M. Toner, and R. Müller, "Stacks of microfabricated structures as scaffolds for cell culture and tissue engineering," *Biomed. Microdevices*, vol. 2, no. 3, pp. 207–214, 2000, doi: 10.1023/A:1009932530375.
[101] S. Terane, M. Kobayashi, and T. Ichiki, "Integration of heteromaterial microelements into plastic microfluidic devices by capillary-force-assisted micromolding," *J. Photopolym. Sci. Technol.*, vol. 27, no. 4, pp. 471–476, 2014, doi: 10.2494/photopolymer.27.471.
[102] J.-H. Lee, C.-H. Kim, K. Constant, and K.-M. Ho, "Tailorable 3D microfabrication for photonic applications: two-polymer microtransfer molding," *Photonic Cryst.*

*Mater. Devices IV*, vol. 6128, p. 612805, 2006, doi: 10.1117/12.645303.
[103] K. Muammer and O. Tugrul, "Micro-Manufacturing Design and Manufacturing," *Book*, 2011.
[104] R. Bartolini, W. Hannan, D. Karlsons, and M. Lurie, "HOLOGRAPHY Embossed Hologram Motion Pictures for Television Playback," *Appl. Opt.*, vol. 9, no. 10, p. 2283, 1970, doi: 10.1364/ao.9.002283.
[105] R. Ulrich, H. P. Weber, E. A. Chandross, W. J. Tomlinson, and E. A. Franke, "Embossed optical waveguides," *Appl. Phys. Lett.*, vol. 20, no. 6, pp. 213–215, 1972, doi: 10.1063/1.1654115.
[106] A. Kolew, D. Münch, K. Sikora, and M. Worgull, "Hot embossing of micro and sub-micro structured inserts for polymer replication," *Microsyst. Technol.*, vol. 17, no. 4, pp. 609–618, 2011, doi: 10.1007/s00542-010-1182-x.
[107] C. Liu, J. M. Li, J. S. Liu, and L. D. Wang, "Deformation behavior of solid polymer during hot embossing process," *Microelectron. Eng.*, vol. 87, no. 2, pp. 200–207, 2010, doi: 10.1016/j.mee.2009.07.014.
[108] S. Lan *et al.*, "Experimental and numerical study on the viscoelastic property of polycarbonate near glass transition temperature for micro thermal imprint process," *Mater. Des.*, vol. 30, no. 9, pp. 3879–3884, 2009, doi: 10.1016/j.matdes.2009.03.045.
[109] A. Dubcek, "Rubber Physics," 2007.
[110] M. C. Lin, J. P. Yeh, S. C. Chen, R. Der Chien, and C. L. Hsu, "Study on the replication accuracy of polymer hot embossed microchannels," *Int. Commun. Heat Mass Transf.*, vol. 42, pp. 55–61, 2013, doi: 10.1016/j.icheatmasstransfer.2012.12.008.
[111] C. M. Kiew, W. J. Lin, T. J. Teo, J. L. Tan, W. Lin, and G. Yang, "Finite element analysis of PMMA pattern formation during hot embossing process," *IEEE/ASME Int. Conf. Adv. Intell. Mechatronics, AIM*, pp. 314–319, 2009, doi: 10.1109/AIM.2009.5229996.
[112] H. Taylor, D. Boning, and C. Iliescu, "A razor-blade test of the demolding energy in a thermoplastic embossing process," *J. Micromechanics Microengineering*, vol. 21, no. 6, 2011, doi: 10.1088/0960-1317/21/6/067002.
[113] B. Saha, S. B. Tor, E. Liu, D. E. Hardt, and J. H. Chun, "Hot-embossing performance of silicon micromold coated with self-assembled n-octadecyltrichlorosilane," *Sensors Actuators, B Chem.*, vol. 160, no. 1, pp. 207–214, 2011, doi: 10.1016/j.snb.2011.07.036.
[114] M. H. Dirikolu and E. Akdemir, "Computer aided modelling of flexible forming process," *J. Mater. Process. Technol.*, vol. 148, no. 3, pp. 376–381, 2004, doi: 10.1016/j.jmatprotec.2004.02.049.
[115] P. Nagarajan and D. Yao, "Rubber-assisted micro forming of polymer thin films," *Microsyst. Technol.*, vol. 15, no. 2, pp. 251–257, 2009, doi: 10.1007/s00542-008-0680-6.
[116] S. J. Liu and Y. T. Dung, "Hot embossing precise structure onto plastic plates by ultrasonic vibration," *Polym. Eng. Sci.*, vol. 45, no. 7, pp. 915–925, 2005, doi: 10.1002/pen.20357.
[117] H. Hocheng, T. T. Wen, and S. Y. Yang, "Replication of microlens arrays by gas-assisted hot embossing," *Mater. Manuf. Process.*, vol. 23, no. 3, pp. 261–268, 2008, doi: 10.1080/10426910701860830.
[118] J. T. Wu, S. Y. Yang, W. C. Deng, and W. Y. Chang, "A novel fabrication of

polymer film with tapered sub-wavelength structures for anti-reflection," *Microelectron. Eng.*, vol. 87, no. 10, pp. 1951–1954, 2010, doi: 10.1016/j.mee.2009.12.004.
[119] F. Lazzarino, C. Gourgon, P. Schiavone, and C. Perret, "Mold deformation in nanoimprint lithography," *J. Vac. Sci. Technol. B Microelectron. Nanom. Struct.*, vol. 22, no. 6, p. 3318, 2004, doi: 10.1116/1.1815299.
[120] J. M. GmbH, "No Title," *GmbH www.jenoptik.com/en-optical-systems*.
[121] H. Tan, "Roller nanoimprint lithography," *J. Vac. Sci. Technol. B Microelectron. Nanom. Struct.*, vol. 16, no. 6, p. 3926, 1998, doi: 10.1116/1.590438.
[122] J. J. Dumond and H. Yee Low, "Recent developments and design challenges in continuous roller micro- and nanoimprinting," *J. Vac. Sci. Technol. B, Nanotechnol. Microelectron. Mater. Process. Meas. Phenom.*, vol. 30, no. 1, p. 010801, 2012, doi: 10.1116/1.3661355.
[123] D. Yun *et al.*, "Development of roll-to-roll hot embossing system with induction heater for micro fabrication," *Rev. Sci. Instrum.*, vol. 83, no. 1, pp. 1–8, 2012, doi: 10.1063/1.3675574.
[124] R. Liedert *et al.*, "Disposable roll-to-roll hot embossed electrophoresis chip for detection of antibiotic resistance gene mecA in bacteria," *Lab Chip*, vol. 12, no. 2, pp. 333–339, 2012, doi: 10.1039/c1lc20782b.
[125] T. Mäkelä and T. Haatainen, "Roll-to-roll pilot nanoimprinting process for backlight devices," *Microelectron. Eng.*, vol. 97, pp. 89–91, 2012, doi: 10.1016/j.mee.2012.03.031.
[126] J. Wang and Q. Mao, "Methodology Based on the PVT Behavior of Polymer for Injection Molding," *Adv. Polym. Technol.*, vol. 32, no. 2013, pp. 474–485, 2012, doi: 10.1002/adv.
[127] T. Mäkelä, T. Haatainen, and J. Ahopelto, "Roll-to-roll printed gratings in cellulose acetate web using novel nanoimprinting device," *Microelectron. Eng.*, vol. 88, no. 8, pp. 2045–2047, 2011, doi: 10.1016/j.mee.2011.02.016.
[128] S. H. Ng and Z. F. Wang, "Hot roller embossing for microfluidics: Process and challenges," *Microsyst. Technol.*, vol. 15, no. 8, pp. 1149–1156, 2009, doi: 10.1007/s00542-008-0722-0.
[129] B. K. Lee, J. H. Kim, D. S. Kim, S. S. Chang, and T. H. Kwon, "Microfabrication of a nickel mold insert by a modified deep X-ray lithography process and its application to hot embossing," *Microelectron. Eng.*, vol. 87, no. 12, pp. 2449–2455, 2010, doi: 10.1016/j.mee.2010.04.023.
[130] C. K. Chung, K. L. Sher, Y. J. Syu, and C. C. Cheng, "Fabrication of cone-like microstructure using UV LIGA-like for light guide plate application," *Microsyst. Technol.*, vol. 16, no. 8–9, pp. 1619–1624, 2010, doi: 10.1007/s00542-009-1012-1.
[131] S. Gorelick, J. Vila-Comamala, V. Guzenko, R. Mokso, M. Stampanoni, and C. David, "Direct e-beam writing of high aspect ratio nanostructures in PMMA: A tool for diffractive X-ray optics fabrication," *Microelectron. Eng.*, vol. 87, no. 5–8, pp. 1052–1056, 2010, doi: 10.1016/j.mee.2009.11.091.
[132] C. K. Chung, Y. J. Syu, H. Y. Wang, C. C. Cheng, S. L. Lin, and K. Z. Tu, "Fabrication of flexible light guide plate using CO2 laser LIGA-like technology," *Microsyst. Technol.*, vol. 19, no. 3, pp. 439–443, 2013, doi: 10.1007/s00542-012-1665-z.
[133] T. Wienhold *et al.*, "Diffusion driven optofluidic dye lasers encapsulated into

polymer chips," *Lab Chip*, vol. 12, no. 19, pp. 3734–3739, 2012, doi: 10.1039/c2lc40494j.
[134] L. J. Kricka, P. Fortina, N. J. Panaro, P. Wilding, G. Alonso-Amigo, and H. Becker, "Fabrication of plastic microchips by hot embossing," *Lab Chip*, vol. 2, no. 1, pp. 1–4, 2002, doi: 10.1039/b109775j.
[135] V. N. Goral, Y. C. Hsieh, O. N. Petzold, R. A. Faris, and P. K. Yuen, "Hot embossing of plastic microfluidic devices using poly(dimethylsiloxane) molds," *J. Micromechanics Microengineering*, vol. 21, no. 1, 2011, doi: 10.1088/0960-1317/21/1/017002.
[136] A. L. Vig, T. Mäkelä, P. Majander, V. Lambertini, J. Ahopelto, and A. Kristensen, "Roll-to-roll fabricated lab-on-a-chip devices," *J. Micromechanics Microengineering*, vol. 21, no. 3, 2011, doi: 10.1088/0960-1317/21/3/035006.
[137] 2018 et al., "Rapid and Low-cost Hot-Embossing of Polycaprolactone Microfluidic," *Geophys. Res. Lett.*, vol. in press, pp. 0–31, 2017.
[138] J. Geier and H. Lessmann, *Metalworking fluids*. 2011.
[139] I. Tansel, O. Rodriguez, M. Trujillo, E. Paz, and W. Li, "Micro-end-milling - I. Wear and breakage," *Int. J. Mach. Tools Manuf.*, vol. 38, no. 12, pp. 1419–1436, 1998, doi: 10.1016/S0890-6955(98)00015-7.
[140] D. Dornfeld, S. Min, and Y. Takeuchi, "Recent advances in mechanical micromachining," *CIRP Ann. - Manuf. Technol.*, vol. 55, no. 2, pp. 745–768, 2006, doi: 10.1016/j.cirp.2006.10.006.
[141] M. P. Vogler, R. E. DeVor, and S. G. Kapoor, "On the modeling and analysis of machining performance in micro-endmilling, part i: Surface generation," *J. Manuf. Sci. Eng. Trans. ASME*, vol. 126, no. 4, pp. 685–694, 2004, doi: 10.1115/1.1813470.
[142] I. G. Reichenbach, M. Bohley, F. J. P. Sousa, and J. C. Aurich, "Micromachining of PMMA—manufacturing of burr-free structures with single-edge ultra-small micro end mills," *Int. J. Adv. Manuf. Technol.*, vol. 96, no. 9–12, pp. 3665–3677, 2018, doi: 10.1007/s00170-018-1821-4.
[143] C. R. Friedrich and M. J. Vasile, "Development of the micromilling process for high-aspect-ratio microstructures," *J. Microelectromechanical Syst.*, vol. 5, no. 1, pp. 33–38, 1996, doi: 10.1109/84.485213.
[144] M. E. Wilson *et al.*, "Fabrication of circular microfluidic channels by combining mechanical micromilling and soft lithography," *Lab Chip*, vol. 11, no. 8, pp. 1550–1555, 2011, doi: 10.1039/c0lc00561d.
[145] C. H. Chen, Y. C. Wang, and B. Y. Lee, "The optimal design of micro end mill for milling SKD61 tool steel," *Int. J. Adv. Manuf. Technol.*, vol. 68, no. 1–4, pp. 165–173, 2013, doi: 10.1007/s00170-012-4716-9.
[146] T. Moriwaki, "Multi-functional machine tool," *CIRP Ann. - Manuf. Technol.*, vol. 57, no. 2, pp. 736–749, 2008, doi: 10.1016/j.cirp.2008.09.004.
[147] T. Childs, "Metal Machining," *Met. Mach.*, 2000, doi: 10.1016/c2009-0-23990-0.
[148] A. J. Shih, J. Luo, M. A. Lewis, and J. S. Strenkowski, "Chip morphology and forces in end milling of elastomers," *J. Manuf. Sci. Eng. Trans. ASME*, vol. 126, no. 1, pp. 124–130, 2004, doi: 10.1115/1.1633276.
[149] D. J. Guckenberger, T. E. De Groot, A. M. D. Wan, D. J. Beebe, and E. W. K. Young, "Micromilling: A method for ultra-rapid prototyping of plastic microfluidic devices," *Lab Chip*, vol. 15, no. 11, pp. 2364–2378, 2015, doi: 10.1039/c5lc00234f.

[150] L. N. López De Lacalle, A. Lamikiz, O. Ocerin, D. Díez, and E. Maidagan, "The Denavit and Hartenberg approach applied to evaluate the consequences in the tool tip position of geometrical errors in five-axis milling centres," *Int. J. Adv. Manuf. Technol.*, vol. 37, no. 1–2, pp. 122–139, 2008, doi: 10.1007/s00170-007-0956-5.
[151] J. H. Kim, J. W. Park, and T. J. Ko, "End mill design and machining via cutting simulation," *CAD Comput. Aided Des.*, vol. 40, no. 3, pp. 324–333, 2008, doi: 10.1016/j.cad.2007.11.005.
[152] M. B. G. Jun, X. Liu, R. E. DeVor, and S. G. Kapoor, "Investigation of the dynamics of microend milling - Part I: Model development," *J. Manuf. Sci. Eng. Trans. ASME*, vol. 128, no. 4, pp. 893–900, 2006, doi: 10.1115/1.2193546.
[153] A. Aramcharoen, P. T. Mativenga, S. Yang, K. E. Cooke, and D. G. Teer, "Evaluation and selection of hard coatings for micro milling of hardened tool steel," *Int. J. Mach. Tools Manuf.*, vol. 48, no. 14, pp. 1578–1584, 2008, doi: 10.1016/j.ijmachtools.2008.05.011.
[154] E. Brinksmeier, R. Gläbe, O. Riemer, and S. Twardy, "Potentials of precision machining processes for the manufacture of micro forming molds," *Microsyst. Technol.*, vol. 14, no. 12, pp. 1983–1987, 2008, doi: 10.1007/s00542-008-0656-6.
[155] G. Kiswanto, D. L. Zariatin, and T. J. Ko, "The effect of spindle speed, feed-rate and machining time to the surface roughness and burr formation of Aluminum Alloy 1100 in micro-milling operation," *J. Manuf. Process.*, vol. 16, no. 4, pp. 435–450, 2014, doi: 10.1016/j.jmapro.2014.05.003.
[156] J. Z. Zhang and J. C. Chen, "The development of an in-process surface roughness adaptive control system in end milling operations," *Int. J. Adv. Manuf. Technol.*, vol. 31, no. 9–10, pp. 877–887, 2007, doi: 10.1007/s00170-005-0262-z.
[157] K. Lee and D. A. Dornfeld, "Micro-burr formation and minimization through process control," *Precis. Eng.*, vol. 29, no. 2, pp. 246–252, 2005, doi: 10.1016/j.precisioneng.2004.09.002.
[158] S. Dimov, D. T. Pham, A. Ivanov, K. Popov, and K. Fansen, "Micromilling strategies: Optimization issues," *Proc. Inst. Mech. Eng. Part B J. Eng. Manuf.*, vol. 218, no. 7, pp. 731–736, 2004, doi: 10.1177/095440540421800706.
[159] C. K. Toh, "A study of the effects of cutter path strategies and orientations in milling," *J. Mater. Process. Technol.*, vol. 152, no. 3, pp. 346–356, 2004, doi: 10.1016/j.jmatprotec.2004.04.382.
[160] P. G. Benardos and G. C. Vosniakos, "Prediction of surface roughness in CNC face milling using neural networks and Taguchi's design of experiments," *Robot. Comput. Integr. Manuf.*, vol. 18, no. 5–6, pp. 343–354, 2002, doi: 10.1016/S0736-5845(02)00005-4.
[161] C. H. Chu and D. Dornfeld, "Geometric approaches for reducing burr formation in planar milling by avoiding tool exits," *J. Manuf. Process.*, vol. 7, no. 2, pp. 182–195, 2005, doi: 10.1016/S1526-6125(05)70095-5.
[162] D. P. Yen, Y. Ando, and K. Shen, "A cost-effective micromilling platform for rapid prototyping of microdevices," *Technology*, vol. 04, no. 04, pp. 234–239, 2016, doi: 10.1142/s2339547816200041.
[163] A. Aramcharoen, S. K. C. Sean, and L. Kui, "An experimental study of micromilling of polymer materials for microfluidic applications," *Int. J. Abras. Technol.*, vol. 5, no. 4, pp. 286–298, 2012, doi: 10.1504/IJAT.2012.052037.
[164] R. Lopes *et al.*, "Low cost microfluidic device for partial cell separation: Micromilling approach," *Proc. IEEE Int. Conf. Ind. Technol.*, vol. 2015-June, no.

June, pp. 3347–3350, 2015, doi: 10.1109/ICIT.2015.7125594.
[165] A. Lashkaripour, R. Silva, and D. Densmore, “Desktop micromilled microfluidics,” *Microfluid. Nanofluidics*, vol. 22, no. 3, pp. 1–13, 2018, doi: 10.1007/s10404-018-2048-2.
[166] X. Ku, Z. Zhang, X. Liu, L. Chen, and G. Li, “Low-cost rapid prototyping of glass microfluidic devices using a micromilling technique,” *Microfluid. Nanofluidics*, vol. 22, no. 8, p. 0, 2018, doi: 10.1007/s10404-018-2104-y.
[167] D. Bauerle, *Laser Processing and Chemistry, 2nd ed. Chap. 7, Springer- Verlag, 1996. Title*. 1996.
[168] A. Ancona *et al.*, “High speed laser drilling of metals using a high repetition rate , high average power ultrafast fiber CPA system,” vol. 16, no. 12, pp. 593–596, 2008.
[169] C. Momma, S. Nolte, B. N. Chichkov, F. V. Alvensleben, and A. Tünnermann, “Precise laser ablation with ultrashort pulses,” *Appl. Surf. Sci.*, vol. 109–110, pp. 15–19, 1997, doi: 10.1016/S0169-4332(96)00613-7.
[170] F. Chen and J. R. V. de Aldana, “Optical waveguides in crystalline dielectric materials produced by femtosecond-laser micromachining,” *Laser Photonics Rev.*, vol. 8, no. 2, pp. 251–275, 2014, doi: 10.1002/lpor.201300025.
[171] W. Kautek, J. Krüger, M. Lenzner, S. Sartania, C. Spielmann, and F. Krausz, “Laser ablation of dielectrics with pulse durations between 20 fs and 3 ps,” *Appl. Phys. Lett.*, vol. 69, no. 21, pp. 3146–3148, 1996, doi: 10.1063/1.116810.
[172] D. J. Hwang, C. P. Grigoropoulos, and T. Y. Choi, “Efficiency of silicon micromachining by femtosecond laser pulses in ambient air,” *J. Appl. Phys.*, vol. 99, no. 8, 2006, doi: 10.1063/1.2187196.
[173] D. V. Tran, Y. C. Lam, H. Y. Zheng, V. M. Murukeshan, J. C. Chai, and D. E. Hardt, “Femtosecond laser processing of crystalline silicon,” no. c, 2005, [Online]. Available: http://dspace.mit.edu/handle/1721.1/7449.
[174] A. Volpe *et al.*, “Welding of PMMA by a femtosecond fiber laser,” *Opt. Express*, vol. 23, no. 4, 2015, doi: 10.1364/OE.23.004114.
[175] B. N. Chichkov, C. Momma, S. Nolte, F. Von Alvensleben, and A. Tünnermann, “Femtosecond, picosecond and nanosecond laser ablation of solids,” *Appl. Phys. A Mater. Sci. Process.*, vol. 63, no. 2, pp. 109–115, 1996, doi: 10.1007/BF01567637.
[176] S. Weiler, “High-power pico- and femtosecond lasers enable new applications. Laser Focus World 47:55-61,” in *Laser Focus World*, 2011.
[177] G. Eberhardt, H. Banse, U. Wagner, and T. Peschel, “Structuring of thin film solar cells,” *Laser-based Micro- Nanopackaging Assem. IV*, vol. 7585, no. figure 2, p. 75850P, 2010, doi: 10.1117/12.846821.
[178] D. T. Pham, S. S. Dimov, and P. V. Petkov, “Laser milling of ceramic components,” *Int. J. Mach. Tools Manuf.*, vol. 47, no. 3–4, pp. 618–626, 2007, doi: 10.1016/j.ijmachtools.2006.05.002.
[179] 2013. L. Cerami, E. Mazur, S. Nolte, C.B. Schaffer, R. Thomson, C. Leburn, D. Reid (Eds.), 287-322, “L. Cerami, E. Mazur, S. Nolte, C.B. Schaffer, Femtosecond Laser Micromachining. R. Thomson, C. Leburn, D. Reid (Eds.), Ultrafast NonlinearOptics, Springer-Verlag, Heidelberg 287-322, 2013.,” 2013.
[180] Y. L. Yao, H. Chen, and W. Zhang, “Time scale effects in laser material removal: A review,” *Int. J. Adv. Manuf. Technol.*, vol. 26, no. 5–6, pp. 598–608, 2005, doi: 10.1007/s00170-003-2026-y.

[181] E. G. Gamaly, A. V. Rode, B. Luther-Davies, and V. T. Tikhonchuk, “Ablation of solids by femtosecond lasers: Ablation mechanism and ablation thresholds for metals and dielectrics,” *Phys. Plasmas*, vol. 9, no. 3, p. 949, 2002, doi: 10.1063/1.1447555.
[182] S. Anisimov, B. Kapeliovich, and T. Perel’Man, “Electron emission from metal surfaces exposed to ultrashort laser pulses,” *Sov. J. Exp. Theor. Phys.*, vol. 39, pp. 776–781, 1974.
[183] Sven Döring, “Analysis of the Hole Shape Evolution in Ultrashort Pulse Laser Drilling zur Erlangung des akademischen Grades,” 1983.
[184] N. N. Nedialkov, S. E. Imamova, and P. A. Atanasov, “Ablation of metals by ultrashort laser pulses,” *J. Phys. D. Appl. Phys.*, vol. 37, no. 4, pp. 638–643, 2004, doi: 10.1088/0022-3727/37/4/016.
[185] T. Spotlight, “Femtosecond Laser Processing Overcomes Barriers for Use in Medical Device Manufacturing,” *Adv. Mater. Process.*, no. December, pp. 26–30, 2014.
[186] S. Ameer-Beg, W. Perrie, S. Rathbone, J. Wright, W. Weaver, and H. Champoux, “Femtosecond laser micro structuring of materials,” *Appl. Surf. Sci.*, vol. 127–129, pp. 875–880, 1998, doi: 10.1016/S0169-4332(97)00760-5.
[187] D. Karnakis, G. Rutterford, M. Knowles, T. Dobrev, P. Petkov, and S. Dimov, “High quality laser milling of ceramics, dielectrics and metals using nanosecond and picosecond lasers,” *Phot. Process. Microelectron. Photonics V*, vol. 6106, p. 610604, 2006, doi: 10.1117/12.645711.
[188] A. Ben-Yakar *et al.*, “Morphology of femtosecond-laser-ablated borosilicate glass surfaces,” *Appl. Phys. Lett.*, vol. 83, no. 15, pp. 3030–3032, 2003, doi: 10.1063/1.1619560.
[189] J. Zhao, B. Huettner, and A. Menschig, “Microablation with ultrashort laser pulses,” *Opt. Laser Technol.*, vol. 33, no. 7, pp. 487–491, 2001, doi: 10.1016/S0030-3992(01)00066-4.
[190] A. Malshe, D. Deshpande, E. Stach, K. Rajurkar, and D. Alexander, “Investigation of femtosecond laser-assisted micromachining of lithium niobate,” *CIRP Ann. - Manuf. Technol.*, vol. 53, no. 1, pp. 187–190, 2004, doi: 10.1016/S0007-8506(07)60675-1.
[191] F. Di Niso, C. Gaudiuso, T. Sibillano, F. P. Mezzapesa, A. Ancona, and P. M. Lugarà, “Role of heat accumulation on the incubation effect in multi-shot laser ablation of stainless steel at high repetition rates,” *Opt. Express*, vol. 22, no. 10, p. 12200, 2014, doi: 10.1364/oe.22.012200.
[192] R. Suriano *et al.*, “Femtosecond laser ablation of polymeric substrates for the fabrication of microfluidic channels,” *Appl. Surf. Sci.*, vol. 257, no. 14, pp. 6243–6250, 2011, doi: 10.1016/j.apsusc.2011.02.053.
[193] J. König, S. Nolte, and A. Tünnermann, “Plasma evolution during metal ablation with ultrashort laser pulses,” *Opt. Express*, vol. 13, no. 26, p. 10597, 2005, doi: 10.1364/opex.13.010597.
[194] B. Neuenschwander, B. Jäggi, M. Schmid, U. Hunziker, B. LüEscher, and C. Nocera, “Processing of industrially relevant non metals with laser pulses in the range between 10ps and 50ps,” *30th Int. Congr. Appl. Lasers Electro-Optics, ICALEO 2011*, vol. 783, no. 2011, pp. 783–791, 2011, doi: 10.2351/1.5062327.
[195] A. Ancona *et al.*, “Femtosecond and picosecond laser drilling of metals at high repetition rates and average powers,” *Opt. Lett.*, vol. 34, no. 21, p. 3304, 2009, doi:

10.1364/ol.34.003304.
[196] B. Neuenschwander, B. Jaeggi, M. Schmid, V. Rouffiange, and P.-E. Martin, "Optimization of the volume ablation rate for metals at different laser pulse-durations from ps to fs," *Laser Appl. Microelectron. Optoelectron. Manuf. XVII*, vol. 8243, p. 824307, 2012, doi: 10.1117/12.908583.
[197] J. Lopez, A. Lidolff, M. Delaigue, C. Hönninger, S. Ricaud, and E. Mottay, "Ultrafast laser with high energy and high average power for industrial micromachining: Comparison Ps-Fs," *30th Int. Congr. Appl. Lasers Electro-Optics, ICALEO 2011*, vol. 875, no. 2011, pp. 875–881, 2011, doi: 10.2351/1.5062342.
[198] J. Lopez *et al.*, "Comparison of picosecond and femtosecond laser ablation for surface engraving of metals and semiconductors," *Laser Appl. Microelectron. Optoelectron. Manuf. XVII*, vol. 8243, p. 82430O, 2012, doi: 10.1117/12.907792.
[199] J. Schille *et al.*, "Micro processing of metals using a high repetition rate femtosecond laser: From laser process parameter study to machining examples," *30th Int. Congr. Appl. Lasers Electro-Optics, ICALEO 2011*, vol. 773, pp. 773–782, 2011, doi: 10.2351/1.5062326.
[200] B. Neuenschwander *et al.*, "Processing of dielectric materials and metals with PS laserpulses," *29th Int. Congr. Appl. Lasers Electro-Optics, ICALEO 2010 - Congr. Proc.*, vol. 103, pp. 1079–1083, 2010, doi: 10.2351/1.5062103.
[201] and H. E. J. Schille, R. Ebert, U. Loeschner, L. Schneider, N. Walther, P. Regenfuss, P. Scully, N. Goddard, "An ultrafast femtosecond fibre laser as a new tool in Rapid Microtooling. Proc. of LAMP2009, the 5th Int. Congress on Laser Advanced Materials Processing, Kobe (Japan), 2009.," 2009.
[202] R. Knappe, "Applications of picosecond lasers and pulse-bursts in precision manufacturing," *Laser Appl. Microelectron. Optoelectron. Manuf. XVII*, vol. 8243, p. 82430I, 2012, doi: 10.1117/12.913626.
[203] Y. Cheng, K. Sugioka, and K. Midorikawa, "Microfabrication of 3D hollow structures embedded in glass by femtosecond laser for Lab-on-a-chip applications," *Appl. Surf. Sci.*, vol. 248, no. 1–4, pp. 172–176, 2005, doi: 10.1016/j.apsusc.2005.03.078.
[204] Y. Liao *et al.*, "Rapid prototyping of three-dimensional microfluidic mixers in glass by femtosecond laser direct writing," *Lab Chip*, vol. 12, no. 4, pp. 746–749, 2012, doi: 10.1039/c2lc21015k.
[205] F. Bragheri *et al.*, "Optofluidic integrated cell sorter fabricated by femtosecond lasers," *Lab Chip*, vol. 12, no. 19, pp. 3779–3784, 2012, doi: 10.1039/c2lc40705a.
[206] A. Schaap, Y. Bellouard, and T. Rohrlack, "Optofluidic lab-on-a-chip for rapid algae population screening," *Biomed. Opt. Express*, vol. 2, no. 3, p. 658, 2011, doi: 10.1364/boe.2.000658.
[207] A. Volpe, P. Paiè, A. Ancona, and R. Osellame, "Polymeric fully inertial lab-on-a-chip with enhanced-throughput sorting capabilities," *Microfluid. Nanofluidics*, vol. 23, no. 3, p. 37, 2019, doi: 10.1007/s10404-019-2206-1.
[208] A. Volpe, A. Ancona, G. Trotta, R. Martínez Vázquez, I. Fassi, and R. Osellame, "Fabrication and assembling of a microfluidic optical stretcher polymeric chip combining femtosecond laser and micro injection molding technologies," *Laser-based Micro- Nanoprocessing XI*, vol. 10092, p. 100920F, 2017, doi: 10.1117/12.2251372.
[209] R. Martínez Vázquez, S. M. Eaton, G. Cerullo, R. Ramponi, and R. Osellame,

"Plastic optofluidic chip fabricated by femtosecond laser ablation," *Laser-based Micro- Nanopackaging Assem. VI*, vol. 8244, p. 82440N, 2012, doi: 10.1117/12.907939.
[210] R. M. Vázquez *et al.*, "Rapid prototyping of plastic lab-on-a-chip by femtosecond laser micromachining and removable insert microinjection molding," *Micromachines*, vol. 8, no. 11, 2017, doi: 10.3390/mi8110328.
[211] F. Dang *et al.*, "Replica multichannel polymer chips with a network of sacrificial channels sealed by adhesive printing method," *Lab Chip*, vol. 5, no. 4, pp. 472–478, 2005, doi: 10.1039/b417398h.
[212] C. W. Tsao and D. L. DeVoe, "Bonding of thermoplastic polymer microfluidics," *Microfluid. Nanofluidics*, vol. 6, no. 1, pp. 1–16, 2009, doi: 10.1007/s10404-008-0361-x.
[213] F. C. Huang, Y. F. Chen, and G. Bin Lee, "CE chips fabricated by injection molding and polyethylene/thermoplastic elastomer film packaging methods," *Electrophoresis*, vol. 28, no. 7, pp. 1130–1137, 2007, doi: 10.1002/elps.200600351.
[214] D. Paul, A. Pallandre, S. Miserere, J. Weber, and J. L. Viovy, "Lamination-based rapid prototyping of microfluidic devices using flexible thermoplastic substrates," *Electrophoresis*, vol. 28, no. 7, pp. 1115–1122, 2007, doi: 10.1002/elps.200600503.
[215] P. Abgrall, C. Lattes, V. Conédéra, X. Dollat, S. Colin, and A. M. Gué, "A novel fabrication method of flexible and monolithic 3D microfluidic structures using lamination of SU-8 films," *J. Micromechanics Microengineering*, vol. 16, no. 1, pp. 113–121, 2006, doi: 10.1088/0960-1317/16/1/016.
[216] C. Lucio, H. Dominguez, C. A. Neves, A. Fracassi, and U. De Sa, "A Dry process for Production of Microfluidic Devices Based on the Lamination of Laser-Printed Polyester Films," vol. 75, no. 15, pp. 3853–3858, 2003.
[217] Y. Li, J. S. Buch, F. Rosenberger, D. L. DeVoe, and C. S. Lee, "Integration of Isoelectric Focusing with Parallel Sodium Dodecyl Sulfate Gel Electrophoresis for Multidimensional Protein Separations in a Plastic Microfludic Network," *Anal. Chem.*, vol. 76, no. 3, pp. 742–748, 2004, doi: 10.1021/ac034765b.
[218] H. Y. Tan, W. K. Loke, Y. T. Tan, and N. T. Nguyen, "A lab-on-a-chip for detection of nerve agent sarin in blood," *Lab Chip*, vol. 8, no. 6, pp. 885–891, 2008, doi: 10.1039/b800438b.
[219] C. H. Ahn *et al.*, "Disposable smart lab on a chip for point-of-care clinical diagnostics," *Proc. IEEE*, vol. 92, no. 1, pp. 154–173, 2004, doi: 10.1109/JPROC.2003.820548.
[220] H. Shadpour, H. Musyimi, J. Chen, and S. A. Soper, "Physiochemical properties of various polymer substrates and their effects on microchip electrophoresis performance," *J. Chromatogr. A*, vol. 1111, no. 2, pp. 238–251, 2006, doi: 10.1016/j.chroma.2005.08.083.
[221] L. E. Locascio, C. E. Perso, and C. S. Lee, "Measurement of electroosmotic flow in plastic imprinted microfluid devices and the effect of protein adsorption on flow rate," *J. Chromatogr. A*, vol. 857, no. 1–2, pp. 275–284, 1999, doi: 10.1016/S0021-9673(99)00774-8.
[222] A. Taberham, M. Kraft, M. Mowlem, and H. Morgan, "The fabrication of lab-on-chip devices from fluoropolymers," *J. Micromechanics Microengineering*, vol. 18, no. 6, 2008, doi: 10.1088/0960-1317/18/6/064011.

[223] L. P. Hromada, B. J. Nablo, J. J. Kasianowicz, M. A. Gaitan, and D. L. DeVoe, “Single molecule measurements within individual membrane-bound ion channels using a polymer-based bilayer lipid membrane chip,” *Lab Chip*, vol. 8, no. 4, pp. 602–608, 2008, doi: 10.1039/b716388f.
[224] A. Bhattacharyya and C. M. Klapperich, “Mechanical and chemical analysis of plasma and ultraviolet-ozone surface treatments for thermal bonding of polymeric microfluidic devices,” *Lab Chip*, vol. 7, no. 7, pp. 876–882, 2007, doi: 10.1039/b700442g.
[225] C. K. Fredrickson, Z. Xia, C. Das, R. Ferguson, F. T. Tavares, and Z. H. Fan, “Effects of fabrication process parameters on the properties of cyclic olefin copolymer microfluidic devices,” *J. Microelectromechanical Syst.*, vol. 15, no. 5, pp. 1060–1068, 2006, doi: 10.1109/JMEMS.2006.880352.
[226] Y. Sun, Y. C. Kwok, and N. T. Nguyen, “Low-pressure, high-temperature thermal bonding of polymeric microfluidic devices and their applications for electrophoretic separation,” *J. Micromechanics Microengineering*, vol. 16, no. 8, pp. 1681–1688, 2006, doi: 10.1088/0960-1317/16/8/033.
[227] B. J, “Brydson J (1999) Plastic materials. Butterworth-Heinemann, Oxford.”
[228] J. L. Gardon and J. P. Teas, “Solubility Parameters.,” *Charact Coat, Phys Tech, Pt 2*, no. c, pp. 413–471, 1976.
[229] H. Klank, J. P. Kutter, and O. Geschke, “CO2-laser micromachining and back-end processing for rapid production of PMMA-based microfluidic systems,” *Lab Chip*, vol. 2, no. 4, pp. 242–246, 2002, doi: 10.1039/b206409j.
[230] Y. C. Hsu and T. Y. Chen, “Applying Taguchi methods for solvent-assisted PMMA bonding technique for static and dynamic μ-TAS devices,” *Biomed. Microdevices*, vol. 9, no. 4, pp. 513–522, 2007, doi: 10.1007/s10544-007-9059-1.
[231] X. Sun, B. A. Peeni, W. Yang, H. A. Becerril, and A. T. Woolley, “Rapid prototyping of poly(methyl methacrylate) microfluidic systems using solvent imprinting and bonding,” *J. Chromatogr. A*, vol. 1162, no. 2 SPEC. ISS., pp. 162–166, 2007, doi: 10.1016/j.chroma.2007.04.002.
[232] L. Brown, T. Koerner, J. H. Horton, and R. D. Oleschuk, “Fabrication and characterization of poly(methylmethacrylate) microfluidic devices bonded using surface modifications and solvents,” *Lab Chip*, vol. 6, no. 1, pp. 66–73, 2006, doi: 10.1039/b512179e.
[233] C. H. Lin, L. M. Fu, C. H. Tsai, C. H. Chao, and C. W. Lan, “Low azeotropic solvent sealing of PMMA microfluidic devices,” *Dig. Tech. Pap. - Int. Conf. Solid State Sensors Actuators Microsystems, TRANSDUCERS ’05*, vol. 1, pp. 944–947, 2005, doi: 10.1109/sensor.2005.1496574.
[234] S. AB, “Strong AB (2000) Plastics Materials and Processing. Prentice-Hall, Upper Saddle River.”
[235] R. Truckenmüller, R. Ahrens, Y. Cheng, G. Fischer, and V. Saile, “An ultrasonic welding based process for building up a new class of inert fluidic microsensors and -actuators from polymers,” *Sensors Actuators, A Phys.*, vol. 132, no. 1 SPEC. ISS., pp. 385–392, 2006, doi: 10.1016/j.sna.2006.04.040.
[236] K. F. Lei, S. Ahsan, N. Budraa, W. J. Li, and J. D. Mai, “Microwave bonding of polymer-based substrates for potential encapsulated micro/nanofluidic device fabrication,” *Sensors Actuators, A Phys.*, vol. 114, no. 2–3, pp. 340–346, 2004, doi: 10.1016/j.sna.2003.12.018.
[237] J. Kim and X. Xu, “Excimer laser fabrication of polymer microfluidic devices,” *J.*

*Laser Appl.*, vol. 15, no. 4, pp. 255–260, 2003, doi: 10.2351/1.1585085.
[238] M. Díaz-González and A. Baldi, "Fabrication of biofunctionalized microfluidic structures by low-temperature wax bonding," *Anal. Chem.*, vol. 84, no. 18, pp. 7838–7844, 2012, doi: 10.1021/ac301512f.
[239] W. S, "Wu S (1982) Polymer Interface and Adhesion. Marcel Dekker, New York."
[240] Y. Uyama, K. Kato, and Y. Ikada, "Surface Modification of Polymers by Grafting," *Adv. Polym. Sci.*, vol. 137, 1998, doi: 10.1007/3-540-69685-7_1.
[241] M. Collaud, P. Groening, S. Nowak, and L. Schlapbach, "Plasma treatment of polymers: the effect of the plasma parameters on the chemical, physical, and morphological states of the polymer surface and on the metal-polymer interface," *J. Adhes. Sci. Technol.*, vol. 8, no. 10, pp. 1115–1127, 1994, doi: 10.1163/156856194X00979.
[242] M. J. Shenton, M. C. Lovell-Hoare, and G. C. Stevens, "Adhesion enhancement of polymer," *J. Phys. D Appl. Phys.*, vol. 34, pp. 2754–2760, 2001, doi: 10.1007/s00220-007-0207-5.
[243] M. A. Eddings, M. A. Johnson, and B. K. Gale, "Determining the optimal PDMS-PDMS bonding technique for microfluidic devices," *J. Micromechanics Microengineering*, vol. 18, no. 6, 2008, doi: 10.1088/0960-1317/18/6/067001.
[244] L. Klintberg, M. Svedberg, F. Nikolajeff, and G. Thornell, "Fabrication of a paraffin actuator using hot embossing of polycarbonate," *Sensors Actuators, A Phys.*, vol. 103, no. 3, pp. 307–316, 2003, doi: 10.1016/S0924-4247(02)00403-X.
[245] Z. Wu, N. Xanthopoulos, F. Reymond, J. S. Rossier, and H. H. Girault, "Polymer microchips bonded by O2-plasma activation," *Electrophoresis*, vol. 23, no. 5, pp. 782–790, 2002, doi: 10.1002/1522-2683(200203)23:5<782::AID-ELPS782>3.0.CO;2-K.
[246] B. AL Emanuel NM, "Chemical Physics of Polymer Degradation and Stabilization. VNU Science Press, Utrecht," 1987.
[247] E. M. Allen NS, "Fundamentals of polymer degradation and stabilization. Elsevier, New York," 1992.
[248] M. A. Witek *et al.*, "Cell transport via electromigration in polymer-based microfluidic devices," *Lab Chip*, vol. 4, no. 5, pp. 464–472, 2004, doi: 10.1039/b317093d.
[249] D. S. W. Park *et al.*, "A titer plate-based polymer microfluidic platform for high throughput nucleic acid purification," *Biomed. Microdevices*, vol. 10, no. 1, pp. 21–33, 2008, doi: 10.1007/s10544-007-9106-y.
[250] R. Truckenmüller, P. Henzi, D. Herrmann, V. Saile, and W. K. Schomburg, "A new bonding process for polymer micro- And nanostructures based on near-surface degradation," *Proc. IEEE Int. Conf. Micro Electro Mech. Syst.*, pp. 761–764, 2004, doi: 10.1109/mems.2004.1290696.
[251] C. W. Tsao, L. Hromada, J. Liu, P. Kumar, and D. L. DeVoe, "Low temperature bonding of PMMA and COC microfluidic substrates using UV/ozone surface treatment," *Lab Chip*, vol. 7, no. 4, pp. 499–505, 2007, doi: 10.1039/b618901f.
[252] R. R. Sowell, R. E. Cuthrell, D. M. Mattox, and R. D. Bland, "Surface Cleaning By Ultraviolet Radiation.," *J Vac Sci Technol*, vol. 11, no. 1, pp. 474–475, 1974, doi: 10.1116/1.1318658.
[253] J. Peeling and D. T. Clark, "Surface Ozonation and Photooxidation of Polyethylene Film.," *J. Polym. Sci. A1.*, vol. 21, no. 7, pp. 2047–2055, 1983, doi: 10.1002/pol.1983.170210715.

[254] “Datasheet ZEIIS AXIO CSM 700, http://www.bemo.com.tr/myfiles/AXIO%20CSM%20700.pdf.” .
[255] G. Robertson, T. J. Bushell, and M. Zagnoni, “Chemically induced synaptic activity between mixed primary hippocampal co-cultures in a microfluidic system †,” pp. 636–644, 2014, doi: 10.1039/c3ib40221e.
[256] S. L. Campanelli, A. D. Ludovico, C. Bonserio, P. Cavalluzzi, and M. Cinquepalmi, “Experimental analysis of the laser milling process parameters,” *J. Mater. Process. Technol.*, vol. 191, no. 1–3, pp. 220–223, 2007, doi: 10.1016/j.jmatprotec.2007.03.005.
[257] A. K. Dubey and V. Yadava, “Experimental study of Nd:YAG laser beam machining-An overview,” *J. Mater. Process. Technol.*, vol. 195, no. 1–3, pp. 15–26, 2008, doi: 10.1016/j.jmatprotec.2007.05.041.
[258] D. Teixidor, J. Ciurana, and C. Rodríguez, “Multiobjective optimization of laser milling parameters of microcavities for the manufacturing of des,” *Mater. Manuf. Process.*, vol. 28, no. 12, pp. 1370–1378, 2013, doi: 10.1080/10426914.2013.832307.
[259] C. Leone, S. Genna, F. Tagliaferri, B. Palumbo, and M. Dix, “Experimental investigation on laser milling of aluminium oxide using a 30 W Q-switched Yb:YAG fiber laser,” *Opt. Laser Technol.*, vol. 76, pp. 127–137, 2016, doi: 10.1016/j.optlastec.2015.08.005.
[260] B. N. B. Jaeggi, L. Cangueiro, D. Bruneel, J.A. Ramos de Campos, C. Hairaye, “Micromachining using pulse bursts: influence of the pulse duration and the number of pulses in the burst on the specific removal rate, in: Proceeding of Laser Applications in Microelectronic and Optoelectronic Manufacturing (LAMOM) XXIII, SPIE LASE, 2018,” in *Laser Applications in Microelectronic and Optoelectronic Manufacturing (LAMOM) XXIII, SPIE LASE*, 2018.
[261] R. Osellame, G. Cerullo, and R. Ramponi, *Femtosecond Laser Micromachining: Photonic and Microfluidic Devices in Transparent Materials*, vol. 123. 2012.
[262] D. J. Magagnosc, J. P. Ligda, T. Sano, and B. E. Schuster, “Femtosecond laser machining of micro-tensile specimens for high throughput mechanical testing,” *Conf. Proc. Soc. Exp. Mech. Ser.*, vol. 5, pp. 7–9, 2018, doi: 10.1007/978-3-319-63405-0_2.
[263] G. Trotta, A. Volpe, A. Ancona, and I. Fassi, “Flexible micro manufacturing platform for the fabrication of PMMA microfluidic devices,” *J. Manuf. Process.*, vol. 35, 2018, doi: 10.1016/j.jmapro.2018.07.030.
[264] J. Y. Cheng, C. W. Wei, K. H. Hsu, and T. H. Young, “Direct-write laser micromachining and universal surface modification of PMMA for device development,” *Sensors Actuators, B Chem.*, vol. 99, no. 1, pp. 186–196, 2004, doi: 10.1016/j.snb.2003.10.022.
[265] C. De Marco *et al.*, “Surface properties of femtosecond laser ablated PMMA,” *ACS Appl. Mater. Interfaces*, vol. 2, no. 8, pp. 2377–2384, 2010, doi: 10.1021/am100393e.
[266] D. Gomez, “Femtosecond laser ablation for microfluidics,” *Opt. Eng.*, vol. 44, no. 5, p. 051105, 2005, doi: 10.1117/1.1902783.
[267] D. C. Montgomery, *Design and Analysis of Experiments, eighth ed., Wiley, New York, 2013*. 2013.
[268] U. Ali, K. J. B. A. Karim, and N. A. Buang, “A Review of the Properties and Applications of Poly (Methyl Methacrylate) (PMMA),” *Polym. Rev.*, vol. 55, no.

4, pp. 678–705, 2015, doi: 10.1080/15583724.2015.1031377.
[269] C. Pipatpanukul *et al.*, “Microfluidic PMMA-based microarray sensor chip with imaging analysis for ABO and RhD blood group typing,” *Vox Sang.*, vol. 110, no. 1, pp. 60–69, 2016, doi: 10.1111/vox.12313.
[270] F. Fixe, M. Dufva, P. Telleman, and C. B. Christensen, “Functionalization of poly(methyl methacrylate) (PMMA) as a substrate for DNA microarrays.,” *Nucleic Acids Res.*, vol. 32, no. 1, pp. 1–8, 2004, doi: 10.1093/nar/gng157.
[271] D. Boral *et al.*, “Molecular characterization of breast cancer CTCs associated with brain metastasis,” *Nat. Commun.*, vol. 8, no. 1, 2017, doi: 10.1038/s41467-017-00196-1.
[272] M. J. Winter, I. D. Nagtegaal, J. H. J. M. Van Krieken, and S. V. Litvinov, “The Epithelial Cell Adhesion Molecule (Ep-CAM) as a Morphoregulatory Molecule Is a Tool in Surgical Pathology,” *Am. J. Pathol.*, vol. 163, no. 6, pp. 2139–2148, 2003, doi: 10.1016/S0002-9440(10)63570-5.
[273] C. Matellan and A. E. Del Río Hernández, “Cost-effective rapid prototyping and assembly of poly(methyl methacrylate) microfluidic devices,” *Sci. Rep.*, vol. 8, no. 1, pp. 1–13, 2018, doi: 10.1038/s41598-018-25202-4.
[274] A. Markou *et al.*, “Multiplex gene expression profiling of in vivo isolated circulating tumor cells in high-risk prostate cancer patients,” *Clin. Chem.*, vol. 64, no. 2, pp. 297–306, 2018, doi: 10.1373/clinchem.2017.275503.
[275] G. Robertson, T. J. Bushell, and M. Zagnoni, “Chemically induced synaptic activity between mixed primary hippocampal co-cultures in a microfluidic system,” *Integr. Biol. (United Kingdom)*, vol. 6, no. 6, pp. 636–644, 2014, doi: 10.1039/c3ib40221e.
[276] J. Wang *et al.*, “Microfluidics: A new cosset for neurobiology,” *Lab Chip*, vol. 9, no. 5, pp. 644–652, 2009, doi: 10.1039/b813495b.
[277] E. Neto *et al.*, “Compartmentalized microfluidic platforms: The unrivaled breakthrough of in vitro tools for neurobiological research,” *J. Neurosci.*, vol. 36, no. 46, pp. 11573–11584, 2016, doi: 10.1523/JNEUROSCI.1748-16.2016.
[278] “https://www.itl.nist.gov/div898/handbook/pri/section3/pri3344.htm.” .

# Publications and conferences attendance

## Publications

- Annalisa Volpe, Gianluca Trotta, Udith Krishnan, Antonio Ancona "Prediction model of the depth of the femtosecond laser micro-milling of PMMA". Optics and Laser Technology 120 (2019) 105713. https://doi.org/10.1016/j.optlastec.2019.105713
- Annalisa Volpe, Udith Krishnan, Maria Serena Chiriaco, Elisabetta Primiceri, Antonio Ancona, Francesco Ferrara. "Smart procedure for the femtosecond laser-based fabrication of polymeric lab on a chip for tumor cells capturing". – Accepted in Engineering journal

## Poster presentations

- "Fs-laser based smart procedures for the fabrication of polymeric Lab on a Chip devices" – Science and Industry for environment, Health and Digital Society Technologies; Industrial PhD Day at Università degli Studi di Bari Aldo Moro – 26 June 2019
- Udith Krishnan, Annalisa Volpe, Maria Serena Chiriaco, Elisabetta Primiceri, Antonio Ancona, Francesco Ferrara "Smart procedure for the femtosecond laser-based fabrication of polymeric lab on a chip for tumor cells capturing"- 1st International workshop on Emerging and Disruptive next-GEneration Technologies for POC (EDGE-Tech); 26-30 October 2020

## Conferences

- 21st International Symposium on Laser Precision Microfabrication, 23-26 June 2020 – Dresden, Germany, "Femtosecond laser based smart procedures for the fabrication of polymeric lab-on-a-chip devices"- Oral presentation
- 1st International workshop on Emerging and Disruptive next-GEneration Technologies for POC (EDGE-Tech); 26-30 October 2020

## Summer schools

- International School on Laser Micro/Nanostructuring and Surface Tribology 1-5 October 2018 – Bari, Italy. "Femtosecond laser micro-fabrication of polymeric lab-on-chip for advanced and mini-invasive diagnostics" – Oral presentation

# Acknowledgements

First and foremost, I would like to express a very big thank you to my PhD supervisors Dr. Antonio Ancona, and Dr. Ing. Francesco Ferrara for believing in me and giving me the opportunity to carry out this research work. Their insistence on expressing problems in the most simplistic terms and enthusiastic scientific attitude guided me towards the core and fundamental issues of femtosecond laser technology and micromachining of lab on a chip. I really appreciate the time they had spent with me for academic interaction in between their busy teacher-researcher schedule. It has been a long and hard road, but the end was fruitful. I could not have completed my doctoral studies without the support of a great number of amazing mentors, family, friends, relatives and my dear comrades to whom I dedicate my thesis.

I am grateful to the Programma Operativo Nazionale Ricerca e Innovazione 2014-2020 (CCI 2014IT16M2OP005), Fondo Sociale Europeo, Azione I.1 "Dottorati Innovativi con caratterizzazione Industriale" for giving me this opportunity funded under Dottorati di Ricerca Innovativi a caratterizzazione industriale PON FSE-FESR RI 2014-2020, Azione 11, grant agreement Codice borsa 995, CUP: H96D17000020006.

I would like to wholeheartedly thank Dr. Annalisa Volpe for all the fruitful discussions and immense support she gave over the past years. It has helped me to have an in-depth understanding of the various issues in the lab. Cheers to all the good times and coffee breaks we had.

My sincere thanks to Dr. Michele Zagnoni for providing me the opportunity to work under your guidance during the secondment at University of Strathclyde, Glasgow. Thanks, Daniel Megarity, for helping me understand the invitro investigations in lab on a chip devices. I express my special regards to Dr. Maria Serena Chiriaco for being with me at the zero-dust lab and biological sample experiments at STMicroelectronics and CNR Nanotec Lecce.

I am sincerely thankful to Prof. Giuseppe Iaselli (Coordinator-PhD School), Cinzia Balsamo and all the administrative staffs of Physics department, Uniba. A big thanks to all my colleagues and friends from Bari. You people have always given me a home away from home feeling here.

I would like to gratefully acknowledge all my teachers who have always pushed me to move forward. A massive shout out goes to all my friends for being with me through the thin and thick. Heartfelt thanks to my parents for supporting and guiding me to where I am today and much love to my grandparents, brothers, sisters and other relatives for their unconditional love and care upon me.

Finally, I express my gratitude to Università degli Studi di Bari Aldo Moro for enrolling me in this doctoral program and STMicroelectronics, Lecce for being the industrial partner of this endeavor and University of Strathclyde, Glasgow for accommodating me for the secondment of this PhD program.

Udith Krishnan

La borsa di dottorato è stata cofinanziata con risorse del
Programma Operativo Nazionale Ricerca e Innovazione 2014-2020 (CCI 2014IT16M2OP005),
Fondo Sociale Europeo, Azione I.1 "Dottorati Innovativi con caratterizzazione Industriale"

UNIONE EUROPEA
Fondo Sociale Europeo

Ministero dell'Istruzione, dell'Università e della Ricerca